

PERIDYNAMICS WITH STRAIN GRADIENT ELASTICITY TO ACCOUNT FOR
MICROSTRUCTURAL SIZE EFFECT

by

Cody Aaron Mitts

Copyright © Cody Aaron Mitts 2024

A Dissertation Submitted to the Faculty of the

DEPARTMENT OF AEROSPACE AND MECHANICAL ENGINEERING

In Partial Fulfillment of the Requirements

For the Degree of

DOCTOR OF PHILOSOPHY

WITH A MAJOR IN MECHANICAL ENGINEERING

In the Graduate College

THE UNIVERSITY OF ARIZONA

2024

THE UNIVERSITY OF ARIZONA
GRADUATE COLLEGE

As members of the Dissertation Committee, we certify that we have read the dissertation prepared by: *Cody Aaron Mitts*, titled: *Peridynamics with strain gradient elasticity to account for microstructural size effect*

and recommend that it be accepted as fulfilling the dissertation requirement for the Degree of Doctor of Philosophy.

Erdogan Madenci

Date: Aug 15, 2024

Erdogan Madenci

[Signature]

Olesya Zhupanska (Aug 15, 2024 13:44 PDT)

Date: Aug 15, 2024

Olesya Zhupanska

David Poirier

Date: Aug 16, 2024

David Poirier

Stewart Silling

Stewart Silling (Aug 15, 2024 14:41 MDT)

Date: Aug 15, 2024

Stewart Silling

Final approval and acceptance of this dissertation is contingent upon the candidate's submission of the final copies of the dissertation to the Graduate College.

I hereby certify that I have read this dissertation prepared under my direction and recommend that it be accepted as fulfilling the dissertation requirement.

Erdogan Madenci

Date: Aug 15, 2024

Erdogan Madenci

Dissertation Committee Chair

Department of Aerospace and Mechanical Engineering

ACKNOWLEDGEMENTS

I would like to express my heartfelt gratitude to all those who have supported me throughout my studies. Their encouragement, guidance, and unwavering support have been instrumental in helping me reach this significant milestone in my life.

I am deeply grateful to my advisor, Dr. Erdogan Madenci, for his invaluable guidance throughout my academic journey.

I extend my sincere thanks to each of my committee members: Dr. Olesya Zhupanska, Dr. David Poirier, and Dr. Stewart Silling. I have learned immensely from each of you, whether in the classroom or at conferences and seminars.

A special thanks to Dr. Elias Aifantis for introducing me to his field of study and setting me on this research path. I also owe a debt of gratitude to Dr. Atila Barut for his continuous help and guidance throughout my academic career.

I would also like to thank my close friends at AME: Dr. Ali Can Bekar, Dr. Hamed Malakoutikhah, Dr. Deepak Behera, Dr. Vinod Anicode, and John Fox. I am fortunate to have gotten to know you all, and I am proud to call you my friends.

Finally, I want to express my deepest appreciation to my family for their unwavering love and support, without which I would not be where I am today.

DEDICATION

Dedicated to my family

TABLE OF CONTENTS

LIST OF FIGURES	7
ABSTRACT	10
1. INTRODUCTION	11
1.1 Background and motivation	11
1.2 Brief introduction to strain gradient elasticity	12
1.3 Introduction to peridynamics	14
1.4 Summary	17
1.5 Organization of thesis	17
2. GOVERNING EQUATIONS	19
2.1 Introduction to elastic deformation with gradient elasticity theory	19
2.2 Boundary conditions	20
3. PERIDYNAMIC DIFFERENTIAL OPERATOR	23
3.1 Introduction	23
3.2 Construction of one-dimensional PD derivatives	23
3.3 Construction of two-dimensional PD derivatives	26
3.4 Analytical form of PD derivatives	30
3.5 Investigation of analytical PD functions and derivatives with examples	31
4. ONE-DIMENSIONAL ANALYSIS	34
4.1 PD form of the equation of motion with gradient elasticity	34
4.2 PDSG Dispersion relations	35
4.3 Numerical implementation	37
4.4 Numerical results	40
4.4.1 PDSG model of carbon nanotube under tensile force	40
4.4.2 PDSG model of CNT under dynamic loading	43
5. TWO-DIMENSIONAL ANALYSIS	45
5.1 Ordinary state-based formulation with gradient elasticity	45
5.2 Homogeneous deformation	48
5.2 Numerical implementation	50
5.3 Boundary conditions	50
5.3.1 Displacement boundary conditions	51
5.3.2 Displacement gradient boundary condition	51
5.3.3 Traction boundary condition	55
5.3.4 Double traction boundary condition	56
5.4 Numerical results	64
5.4.1 Quasi-static PDSG model of CNT under tensile force	64
5.4.2 PDSG model of a microscale film under tangential displacement	68
5.4.3 PDSG model of a square nanoscale film with and without a crack	72
6. CONCLUSIONS AND FUTURE WORK	78
6.1 Summary	78
6.2 Future work	79

APPENDICES	81
Appendix A: PDDO for a relative function	81
Appendix B: One-dimensional analytical form of PD functions	84
Appendix C: Two-dimensional analytical form of PD derivatives	86
Appendix D: Lagrange multiplier method for enforcing boundary conditions.....	90
Appendix E: Acronyms	93
 BIBLIOGRAPHY	 94

LIST OF FIGURES

Figure 1. Interaction of PD points, and with arbitrary family sizes for one-dimensional analysis.	24
Figure 2. Symmetric position of points \mathbf{x} and \mathbf{x}' in their interaction domains.	26
Figure 3. Comparison of PD and classical wave frequency dispersions	37
Figure 4. Geometry and boundary condition of a carbon nanotube.....	41
Figure 5. Representative discretization of a carbon nanotube	42
Figure 6. Comparison of the analytical SG solution to the PDSG displacement predictions	43
Figure 7. Comparison of classical SG and PDSG transient solutions of CNT	44
Figure 8. Force density vectors in PD: OSB.....	45
Figure 9. Force density vectors in PD: BB	48
Figure 10. Fictitious PD points, $\tilde{\mathbf{x}}_\alpha$ around the actual PD points, \mathbf{x}_α in the real domain for the imposition of boundary conditions on the boundary point $\bar{\mathbf{x}}_\alpha$ with unit normal \mathbf{n}	51
Figure 11. A set of points in the real and fictitious domains for computing the first order derivatives along the unit normal $\mathbf{n}^T = \{0, \pm 1\}$ in a 2D model.....	53
Figure 12. A set of points in the real and fictitious domains for computing the first order derivatives in a 1D model	53
Figure 13. A set of points in the real and fictitious domains for computing the first order derivatives along the unit normal $\mathbf{n}^T = \{\pm 1, 0\}$ in a 2D model.....	54
Figure 16. A set of points in the real and fictitious domains for approximating the second order derivatives in the direction of unit normal $\mathbf{n}^T = \{0, \pm 1\}$ in a nonlocal sense for a 2D model	58
Figure 17. A set of points in the real and fictitious domains for approximating the second order mixed derivatives in the direction of unit normal $\mathbf{n}^T = \{0, \pm 1\}$ in a nonlocal sense for a 2D model	59

Figure 18. A set of points in the real and fictitious domains for computing the second order derivatives in a nonlocal sense for a 1D model	60
Figure 19. A set of points in the real and fictitious domains for approximating the second order derivatives in the direction of unit normal $\mathbf{n}^T = \{\pm 1, 0\}$ in a nonlocal sense for a 2D model	61
Figure 20. A set of domain and fictitious points for computing the mixed second order derivatives in the direction of unit normal $\mathbf{n}^T = \{\pm 1, 0\}$ in a nonlocal sense for a 2D model.....	62
Figure 21. A set of points in the real and fictitious domains for computing the second order derivatives in a nonlocal sense for a 1D model	63
Figure 22. Carbon nanotube idealization as a nanoscale film for: a) one-dimensional analysis, and b) two-dimensional analysis	65
Figure 23. PD discretization with uniform grid spacing: a) 1D analysis, and b) 2D analysis	66
Figure 24. Comparison of PDSG prediction with analytical solution for horizontal displacement, u_1 for $\ell/\delta = 10.0$ and 40.0 : a) 1D model and, b) 2D model.....	68
Figure 25. A rectangular microscale film subjected to tangential displacement constraint: a) Geometry and boundary conditions, and b) PD discretization	69
Figure 26. PDSG prediction of horizontal displacement (displacements scaled 100x), u_1 : a) $\ell/\delta = 1.11$ and b) $\ell/\delta = 3.32$	71
Figure 27. Comparison of PDSG and analytical solutions for horizontal displacement, $u_1(x_1 = 0.5W, x_2)$ along the x_2 axis for $\ell/\delta = 18$ and 36	72
Figure 28. Geometry and loading of the square film under tension: a) without a crack, and b) with a central crack	73
Figure 29. Discretization of the square film: a) without a crack, and b) with a central crack	73

Figure 30. In the absence of a crack, the vertical displacement along the center line, $x_1 = 5.0\text{nm}$ for varying values of ℓ/δ	75
Figure 31. PDSG predictions of vertical displacement contour variations: a) $\ell/\delta = 0.08$, and b) $\ell/\delta = 0.40$	76
Figure 32. In the presence of a crack, displacement variation as a function of ℓ/δ : $u_2(x_1, x_2 = 5\text{nm})$	76
Figure 33. Reduction in crack opening displacement for increasing value of ℓ/δ	77
Figure 34. Mesh dependence study with constant ℓ/δ ratio.....	77

ABSTRACT

This study proposes the development of a peridynamic (PD) model with strain gradient elasticity (SGE) for size effect on scaling of structural strength. Peridynamic theory introduces damage into the constitutive relations in a natural way. It will enable the investigation of the combined effect of PD and SGE length scale parameters on the stiffness and strength of the material. The primary challenges of general gradient elasticity are the vast number of constitutive parameters. Also, it requires two additional non-classical boundary conditions arising from the presence of fourth order spatial derivatives in the equation of motion. Considering a simplified SGE model with commonly accepted length parameters, the PD form of the equilibrium equations are established for one- and two-dimensional analysis. The PD with SGE (PDSG) equation of motion is without any spatial derivatives and allows for the imposition of displacement constraints and non-zero tractions in the form of a body force density. The PD equations are derived in their bond-based and state-based forms. This derivation presents a novel approach to write the bond-based and ordinary state-based force density vectors for PD and PDSG in terms of the PD functions provided by the Peridynamic differential operator (PDDO). The resulting equations present two length parameters: the horizon of a material point in PD and the characteristic length in SGE theory. The PDSG is first applied to study the deformation response of a single-walled carbon nanotube (SWCNT) subjected to an axial load, and subsequently its longitudinal vibration. To verify the two-dimensional PDSG formulation a thin film is modeled to mimic the one-dimensional SWCNT problem and subsequently compared with the one-dimensional analytical solution. Another benchmark problem of a thin film subjected to tangential displacement is compared to its analytical solution. The dynamic response is compared to a point-wise computational solution with nonclassical boundary conditions. Finally, a plate with and without a crack is modeled to showcase the capability of the PDSG model.

1. INTRODUCTION

1.1 Background and motivation

Advancements in material science, fabrication techniques, experimental characterization, and computational modeling at micro and nanoscales have led to the emergence of materials with significantly improved properties (Greer and De Hosson, 2011). Both intrinsic (microstructural) and extrinsic (dimensional) effects play significant roles in the mechanical response of materials at different length scales (Greer and De Hosson, 2011; Wu et al., 2023; Al-Rub, 2004). The size of the engineered microstructure and the external bulk structure can be considered as additional parameters in the design space.

Experimental observations suggest that structural size can significantly impact the deformation or failure response of materials (Al-Rub and Voyiadjis, 2004; Voyiadjis and Al-Rub, 2005). Materials exhibit increased stiffness when the structure is small, leading to the so-called "size effect," which encompasses various phenomena (Zhu et al., 2008). The size effect can be categorized into two main types: intrinsic and extrinsic. The intrinsic size effect is closely linked to material microstructural heterogeneities, such as soluble alloying elements, second-phase precipitates, and variations in grain size, which play pivotal roles in determining material strength. Conversely, the extrinsic size effect is associated with the physical dimensions of the structure itself. In small structures, fewer sources of dislocations result in increased strength. Greer and Hosson (2011) discuss the interplay between intrinsic and extrinsic size effects, emphasizing the importance of studying the dynamics of moving dislocations in this context.

When observing materials at microscales and nanoscales, they exhibit discrete characteristics, and their size-dependent behavior becomes more pronounced. This is particularly evident in microelectromechanical systems (MEMS) and nanoelectromechanical systems (NEMS) (Al-Rub, 2004), which have recently found widespread applications in medicine and engineering. For example, nanomaterials have been used to treat infectious diseases (Feizi, 2022). Feizi et al. (2022) applied silver nanoparticles (Ag NPs) as an alternative to antibiotics to treat infections caused by antibiotic-resistant bacteria. Damodharan (2021) reviewed the areas where nanomaterials have applications, such as drug

delivery, nano-machinery, antibacterial agents, tissue engineering, and nano-imaging. Environmental science and engineering also benefit from using nanomaterials to detect and restore polluted soils and water (Shan, 2009). These are just a few of the applications for nanomaterials. At micro and nanoscales, size-dependency becomes apparent due to the increased surface-to-volume ratio of grains in polycrystals and the influence of granular materials (Al-Rub, 2004). Additionally, lattice structures introduce a characteristic length scale that further affects the size of the representative volume element.

Ensuring accuracy in material modeling is crucial to effectively characterize and predict the mechanical behavior of these materials. Mathematical and computational models with a length scale parameter become essential to capture the size effect for structures. Classical continuum mechanics (CCM) operates under the assumption that the typical size of material constituents, such as grains or imperfections, is significantly smaller than the representative volume to which the principles of averaging apply. There exists no length scale in the constitutive description of the material within CCM. Studies have shown that standard models lack the precision needed to adequately capture the unique bending behaviors occurring in beams at both micrometer and nanometer dimensions (Chen et al., 2006; Lam et al., 2003; Liebold and Müller, 2015). Similarly, these models also fall short when trying to accurately represent wave transmissions within materials possessing a hexagonal microstructure (Rosi and Auffray, 2016). As materials and structures with microarchitecture grow more complex across length scales, there is a rising need for modeling techniques that go beyond what classical continuum theory offers to predict and simulate the mechanical responses of a broad array of both natural and engineered materials. The introduction of a length scale parameter in material modeling has become important for material development, particularly considering the swift advancements in manufacturing technologies such as additive manufacturing.

1.2 Brief introduction to strain gradient elasticity

The strain gradient (SG) theory, initially introduced by Mindlin (1964) and further developed by Mindlin and Eshel (1968), incorporates material length scales into continuum models. By introducing higher-order gradients with multiple characteristic length scales, Mindlin distinguished between micro-scale and macro-scale quantities. The first-order SG theory includes the first gradient of

strains in the strain energy density (SED) function, introducing five higher-order material coefficients in addition to the classical material moduli. Mindlin extended the theory by incorporating the second gradient of strains, resulting in a total of eighteen material constants (Mindlin, 1964, 1965). To simplify this theory, Mindlin derived specific forms of the equations of motion, the simplest of which employs only three additional length scales related to stiffness and inertia. This form can be further simplified by disregarding the inertial length scale and equating the stiffness-related length scale parameters, linking the parameter to the material microstructure.

Aifantis (1992) proposed a linear elastic constitutive relationship incorporating the Laplacian of strain multiplied by a length scale parameter. This model is appealing due to its simplicity, introducing only one additional parameter and resulting in a fourth-order partial differential equation (PDE) that necessitates nonclassical boundary conditions (Askes et al., 2008). Altan and Aifantis (1992) and Ru and Aifantis (1993) demonstrated that the SG theory effectively eliminates strain singularities. Special techniques, such as splitting the fourth-order equilibrium equation into two second-order equations, can be used to construct solutions (Ru and Aifantis, 1993). Askes and Aifantis (2002) provided solutions using the Element-Free Galerkin method, assuming derivatives of strain vanish on the boundary. Niiranen et al. (2016) examined the strong and weak forms of the governing equations for simple structural components, employing the isogeometric Galerkin method to capture the stiffening effect in a bar for an increasing length scale parameter.

Although identifying length scale parameters poses significant challenges and complexities, they can be estimated through a reverse methodology combining empirical observations with theoretical models. Maranganti and Sharma (2007) provided SG elasticity values for various materials relevant to nanotechnology, based on an atomistic perspective. Additionally, it can be approximated by comparing the dispersion charts of Rayleigh waves generated by the SG theory with those obtained from lattice dynamics computations (Gourgiotis et al., 2004; Gourgiotis and Georgiadis, 2009).

There is a wide range of applications for SG models in materials science and engineering. Several studies, such as those by Vardoulakis et al. (1996), Lazar et al. (2006), Deng et al. (2007), Gao

and Park (2007), Khakalo and Niiranen (2017), Zhang and Sharma (2005), Gao and Ma (2010), and Liu and Gao (2013), employ SG models to avoid stress singularities arising from the presence of cracks. Other studies, such as those by Lam et al. (2003), Liebold and Müller (2016), and Reddy et al. (2013), applied SG models to simulate nanostructures and microstructures, accounting for size and scale influences on material behavior in various microscale and nanoscale devices. Polyzos and Fotiadis (2012) applied SG models to investigate granular materials exhibiting complex behavior due to interactions between individual grains. Additionally, Alibert et al. (2003), Askes and Metrikine (2005), Madeo et al. (2014), Seppecher et al. (2011), Dell'Isola et al. (2015), and Rahali et al. (2015) demonstrated the adoption of SG models during the design of metamaterials.

The trade-offs of including strain gradients in material models are the increase in computational complexity and cost. Strain gradient theories require the computation of higher-order spatial derivatives, which can be numerically challenging and expensive. Additionally, although strain gradient theories have existed for a while, the experimental validation of these theories can be challenging due to difficulties in measuring higher-order strain gradients. This can lead to skepticism about the practical utility and physical relevance of these models. The additional material parameters are difficult to measure or calibrate, limiting their predictive capabilities. In some cases, simpler theories without strain gradients might be "good enough" for practical engineering purposes, following the principle of parsimony that the simplest model fitting the data is usually the best. Strain gradient effects are usually significant at microscales and nanoscales. For problems at larger scales, the inclusion of strain gradients might not be necessary or might lead to insignificant corrections.

1.3 Introduction to peridynamics

Within the realm of CCM, solving the equation of motion with SG theory, which appear as PDEs, requires smoothness. The undefined derivatives of displacement components in the presence of discontinuities such as cracks pose mathematical and computational challenges. Introduced by Silling (2000) and Silling et al. (2007), the PD theory with an internal length parameter (horizon of a material point) removes such challenges, allowing for interactions of material points within their horizons. The PD horizon can be viewed as an internal length parameter of a continuum model, facilitating

information exchange between material points beyond immediate neighbors, which is advantageous for handling field discontinuities. The choice of the PD horizon is often a function of grid spacing, and the degree of nonlocality can be adjusted depending on the application. Due to the nature of the PD horizon, there is a tradeoff between computational cost and the degree of nonlocality, which may limit its ability to accommodate size-dependent effects.

Recent efforts have aimed to capture size effects using PD. Bazilevs et al. (2022) introduced the Microplane model (M7) of concrete into the non-ordinary state-based PD formulation. This constitutive model provides additional parameters to account for the complex mechanical behavior of concrete and can capture size effect. Hobbs et al. (2022) introduced the bond-based PD model with a damage parameter to capture the structural size effect of notched and unnotched concrete beams. The damage model introduces additional parameters that need to be calibrated against experiments, indicating that the length scale parameter (horizon) introduced in PD is a computational cut-off parameter and not related to the material. Nonetheless, the addition of an internal or characteristic length scale is necessary to capture the size-dependent behaviors across different length scales (Bažant, 1999).

The PDDO based on the concept of PD interactions enables recasting any PDE in its nonlocal integral form (Madenci et al., 2016; Madenci et al., 2019). The PDDO is used to directly implement SG theory into the nonlocal PD framework. In the context of PD with SGE, the model incorporates the effects of both nonlocal interactions and strain gradients. The internal length scale parameter(s) introduced by SG theory invokes the effect of material microstructure.

Towards this goal, Chen and Chan (2020) and Chan and Chen (2023) developed a higher-order PD material correspondence model using the SG theory. This introduces a micron or sub-micron material length parameter in addition to the PD horizon. They specifically state that the imposition of nonclassical boundary conditions in PD is challenging and requires further investigation. This model captures the reference solutions corresponding to the classical SG equation. To remove the singular stress field at the dislocation core, Ritter and Zaiser (2024) combined bond-based PD and SG elasticity

to construct a two-scale structure model of a dislocation for correct modeling of surface boundary conditions.

This study presents a PD model coupled with SG theory to capture the size effect on the strength of nanoscale and microscale structures. Therefore, the present approach combines the effects of PD and SG length scale parameters on the stiffness and strength of the material. The resulting equations present two length parameters: the horizon of a material point in PD and the characteristic length in SG theory. The PDSG equation of motion is free of spatial derivatives, thus allowing for failure initiation and growth without smoothness. Furthermore, it presents approaches to enforce classical and nonclassical boundary conditions. The coupled PD with SG offers a new computational approach to predict deformation and damage under general loading conditions while capturing size effects.

Both PD and SG aim to address the limitations of classical local theories, though they do so through different mechanisms. In PD, the material points interact with each other over finite distances through integral equations rather than differential equations. The PD horizon represents a fixed interaction distance that does not vary with local structural features of the material, which may limit its ability to capture detailed size-dependent effects. Gradient elasticity extends classical elasticity by incorporating higher-order spatial derivatives of the strain field into the constitutive equations. The SG internal length parameter directly influences how strain gradients affect material behavior, allowing the theory to naturally account for size effects. This is crucial in capturing phenomena such as size-dependent stiffness, hardening, and softening, which are observed in materials when the characteristic dimensions of the specimen or the microstructural features are comparable to the internal length scale. Therefore, gradient elasticity can accurately describe how the behavior of a material changes with size, something that Peridynamics, with its horizon, cannot do as effectively. The union of these two theories allows PD to be used for its robust handling of discontinuities and crack propagation, while gradient elasticity can be applied to capture detailed size effects and localized material behaviors. Their combined use can enhance the accuracy and robustness of simulations, providing a powerful tool for the design and analysis of advanced next-generation materials.

1.4 Summary

In summary, advancements in material science, fabrication techniques, experimental characterization, and computational modeling have significantly improved the properties of materials at micro and nanoscales. Both intrinsic and extrinsic size effects are crucial in understanding and predicting the mechanical behavior of materials. The integration of SG and PD theories presents a comprehensive approach to accurately model and simulate the size-dependent behaviors of advanced materials, offering new possibilities for the design and development of next-generation materials.

1.5 Organization of thesis

The proposed research integrates PD theory with Strain Gradient Elasticity (SGE), introducing two length scale parameters: the horizon of a material point in PD and the characteristic length in SGE. This thesis is organized to explore this integration and its implications.

Chapter 1 provides the background and motivation for the research, emphasizing the importance and potential applications of combining PD with SGE.

Chapter 2 presents the Governing Equations, introducing the foundational concepts of elastic deformation within the framework of gradient elasticity theory. This chapter sets the stage for the detailed formulations and analyses that follow.

Chapter 3 introduces the Peridynamic Differential Operator (PDDO) and highlights its significance. The chapter then delves into the construction of one-dimensional and two-dimensional PD derivatives, presenting their numerical and analytical forms. It concludes with an investigation of these analytical PD functions and their derivatives through practical examples, illustrating their applicability and effectiveness.

Chapter 4 addresses the one-dimensional analysis. It starts with formulating the PD version of the equation of motion that incorporates strain gradient terms. The chapter then explores the wave dispersion relations in the PDSG model and discusses the numerical implementation methods used. The numerical results are presented in detail, including the PDSG model of CNT under tensile forces and dynamic loading conditions.

Chapter 5 extends the analysis to two-dimensional problems. It begins with developing a two-dimensional PD formulation that includes strain gradient effects. The chapter covers homogeneous deformation scenarios and the numerical implementation methods employed. A detailed discussion on various boundary conditions follows, including displacement boundary conditions, displacement gradient boundary conditions, traction boundary conditions, and double traction boundary conditions. Numerical results are then presented for two-dimensional cases, including a quasi-static PDSG model of CNT under tensile forces and simple shear as well as a PDSG model of a square nanoscale film, with and without cracks.

Chapter 6 presents the conclusions and future work. This chapter summarizes the initial findings and draws conclusions based on the research. It also discusses plans for future work, outlining potential directions and further investigations that can build upon the outcomes of this study.

Appendices provides essential mathematical and technical details supporting the main content. It begins with the PDDO for a relative function. This is followed by the one-dimensional analytical form of the PD functions and 2D analytical form of PD derivatives. The chapter also includes the Lagrange multiplier method for enforcing boundary conditions, which describes a technique to impose constraints in numerical simulations. Finally, a list of acronyms is provided for quick reference to the abbreviations used throughout the text.

2. GOVERNING EQUATIONS

2.1 Introduction to elastic deformation with gradient elasticity theory

The classical equation of motion is of the form

$$\rho \ddot{\mathbf{u}}(\mathbf{x}, t) = \nabla \cdot \boldsymbol{\sigma}(\mathbf{x}, t) + \mathbf{b}(\mathbf{x}, t) \quad \text{for } \mathbf{x} \in \Omega \quad (2.1)$$

where the variable ρ represents density and \mathbf{b} is the body force vector. For isotropic linear materials, the first and second strain gradient elasticity models introduce, respectively, five and sixteen additional material moduli, which essentially complicate the methods for finding the new material constants Mindlin and Eshel (1968). The Cauchy stress tensor, $\boldsymbol{\sigma}$ with a SG model can be expressed as

$$\boldsymbol{\sigma} = \boldsymbol{\sigma}_c - \ell^2 \boldsymbol{\sigma}_{nc} \quad (2.2)$$

in which ℓ is the internal length parameter introduced by Aifantis (1992). The gradient elastic stress-strain relations include only one additional gradient coefficient, ℓ with the dimension of length squared. For a linear isotropic material, the classical and nonclassical parts of the stress tensor are defined as

$$\boldsymbol{\sigma}_c = \mathbf{C} : \boldsymbol{\varepsilon} \quad (2.3a)$$

and

$$\boldsymbol{\sigma}_{nc} = \nabla^2 \boldsymbol{\sigma}_c = \mathbf{C} : \nabla^2 \boldsymbol{\varepsilon} \quad (2.3b)$$

where \mathbf{C} is the 4th order material property tensor and $\boldsymbol{\varepsilon}$ is the linear strain tensor. The subscripts c and nc denote the classical and nonclassical parts of the stress-strain relations. For a two-dimensional analysis, these expressions can be rewritten in component form as

$$\begin{Bmatrix} \sigma_{c11} \\ \sigma_{c22} \\ \sigma_{c12} \end{Bmatrix} = \begin{bmatrix} D_{11} & D_{12} & 0 \\ D_{12} & D_{22} & 0 \\ 0 & 0 & D_{33} \end{bmatrix} \begin{Bmatrix} \varepsilon_{11} \\ \varepsilon_{22} \\ \varepsilon_{12} \end{Bmatrix} \quad (2.4a)$$

and

$$\begin{cases} \sigma_{nc11} \\ \sigma_{nc22} \\ \sigma_{nc12} \end{cases} = \begin{bmatrix} D_{11} & D_{12} & 0 \\ D_{12} & D_{22} & 0 \\ 0 & 0 & D_{33} \end{bmatrix} \nabla^2 \begin{cases} \varepsilon_{11} \\ \varepsilon_{22} \\ \varepsilon_{12} \end{cases} \quad (2.4b)$$

in which the coefficients are defined as $D_{11} = D_{22} = E(1-\nu)/[(1+\nu)(1-2\nu)]$, $D_{12} = E\nu/[(1+\nu)(1-2\nu)]$ and $D_{33} = E/(1+\nu)$ for plane strain conditions, and $D_{11} = D_{22} = E/(1-\nu)^2$, $D_{12} = E\nu/(1-\nu)^2$ and $D_{33} = E/(1+\nu)$ for plane stress conditions. Where E and ν are the Young's modulus and Poisson's ratio, respectively. The components of the strain tensor are denoted as $\varepsilon_{\alpha\beta}$ with $\alpha, \beta = 1, 2$.

2.2 Boundary conditions

The associated boundary conditions on the surface $\partial\Omega$ with a unit normal vector \mathbf{n} and unit tangent vector \mathbf{s} to the boundary can be specified as Niiranen (2016).

$$\boldsymbol{\sigma}\mathbf{n} - \ell^2 \frac{\partial((\nabla\boldsymbol{\sigma}_c)\mathbf{n})\mathbf{s}}{\partial s} - \frac{\partial\mathbf{s}}{\partial s} \ell^2 ((\nabla\boldsymbol{\sigma}_c)\mathbf{n}) = \mathbf{T}^* \quad \text{or} \quad \mathbf{u} = \mathbf{u}^* \quad \text{for} \quad \mathbf{x} \in \partial\Omega \quad (2.5)$$

and

$$(\nabla\mathbf{u})\mathbf{n} = \bar{\mathbf{u}}^* \quad \text{or} \quad \ell^2 ((\nabla\boldsymbol{\sigma}_c)\mathbf{n})\mathbf{n} = \bar{\mathbf{T}}^* \quad \text{for} \quad \mathbf{x} \in \partial\Omega \quad (2.6)$$

where \mathbf{T}^* is the specified traction vector, $\bar{\mathbf{T}}^*$ is the specified double traction vector, \mathbf{u} represents the displacement vector, \mathbf{u}^* is the specified displacement vector, and $\bar{\mathbf{u}}^*$ is the specified displacement gradient normal to the boundary. The stress tensor can also be written in terms of displacement

$$\boldsymbol{\sigma} = (1 - \ell^2 \nabla^2) \left(\lambda (\nabla \cdot \mathbf{u}) \mathbf{I} + \mu (\nabla \mathbf{u} + (\nabla \mathbf{u})^T) \right) \quad (2.7)$$

where λ and μ are the Lamé material constants, and δ_{ij} is the Kronecker delta, \mathbf{I} is the identity matrix, and ∇ , $\nabla \cdot$, and ∇^2 are, respectively, the gradient, divergence and Laplacian operators.

Substituting for the stress tensor, $\boldsymbol{\sigma}$ leads to the Navier-like displacement equation in the form

$$\begin{aligned} \rho \ddot{\mathbf{u}}(\mathbf{x}, t) = & \left(a \nabla \theta(\mathbf{x}, t) + \mu (\nabla^2 \mathbf{u}(\mathbf{x}, t) + 2 \nabla \nabla \cdot \mathbf{u}(\mathbf{x}, t)) \right) \\ & - \ell^2 \left(a \nabla \nabla^2 \theta + \mu (\nabla^4 \mathbf{u}(\mathbf{x}, t) + 2 \nabla \nabla^2 (\nabla \cdot \mathbf{u}(\mathbf{x}, t))) \right) + \mathbf{b}(\mathbf{x}, t) \end{aligned} \quad (2.8)$$

in which θ represents dilatation and is expressed as

$$\theta(\mathbf{x}, t) = \nabla \cdot \mathbf{u}(\mathbf{x}, t) \quad (2.9)$$

The parameter a is defined as

$$a = \begin{cases} \mu \left(\frac{4\nu - 1}{1 - 2\nu} \right) & \text{3D and plane strain} \\ \mu \left(\frac{3\nu - 1}{1 - 2\nu} \right) & \text{plane stress} \end{cases} \quad (2.10)$$

The equation of motion can be rewritten as

$$\rho \ddot{\mathbf{u}}(\mathbf{x}, t) = \mathbf{M}(\mathbf{x}, t) - \ell^2 \mathbf{N}(\mathbf{x}, t) + \mathbf{b}(\mathbf{x}, t) \quad (2.11)$$

where the internal force vectors \mathbf{M} and \mathbf{N} are defined as

$$\mathbf{M}(\mathbf{x}, t) = a \nabla \theta(\mathbf{x}, t) + \mu (\nabla^2 \mathbf{u}(\mathbf{x}, t) + 2 \nabla \nabla \cdot \mathbf{u}(\mathbf{x}, t)) \quad (2.12)$$

and

$$\mathbf{N}(\mathbf{x}, t) = a \nabla \nabla^2 \theta(\mathbf{x}, t) + \mu (\nabla^4 \mathbf{u}(\mathbf{x}, t) + 2 \nabla \nabla^2 (\nabla \cdot \mathbf{u}(\mathbf{x}, t))) \quad (2.13)$$

This equation of motion presents fourth order spatial derivatives; therefore, its solution requires additional non-classical boundary conditions, and their physical interpretation are unclear. Also, its solution suffers from mathematical inconsistency when the material fractures because the spatial derivatives of displacements are not defined across discontinuities. Hence, it is not suitable for the initiation and propagation of damage. To this end, PD theory is used due to its reformulation of the equilibrium equations in the form of an integro-differential equation in time and space Silling (2000). It is a non-local theory that provides a robust theoretical framework that includes failure behavior of

materials. It defines material behavior at a point in a continuum body as an integral equation of the surrounding displacement. The governing equations of PD theory are free of spatial derivatives, and crack initiation and growth is intrinsic to the constitutive relations. No additional assumptions or techniques are required for modeling damage and fracture. Also, boundary traction does not appear in the PD equation of motion. Furthermore, constraint conditions are, in general, not necessary for the solution of an integro-differential equation. Physically meaningful boundary conditions can be imposed on displacement and velocity fields and the external loads can be applied as body force density (Madenci et al., 2013). Also, the PD theory captures the dispersion characteristics of the continuum (Eringen, 1972). The dispersive nature of waves is the feature of real materials as a result of long-range forces. The second length parameter appearing in SGE for propagation characteristics of the higher wave numbers is not necessary (Askes et al., 2006).

3. PERIDYNAMIC DIFFERENTIAL OPERATOR

3.1 Introduction

The PD concept includes nonlocal interactions between a point \mathbf{x} with other points in its domain of interaction, \mathbf{x}' . Each point has its own family of points dictated by its domain of interaction, H_x . These points, also called material points, occupy an infinitesimally small volume, area, or distance depending on the dimension of the analysis. The horizon denoted as δ , truncates the domain of interaction limiting \mathbf{x} and \mathbf{x}' to only interact with other points of their respective families, H_x and $H_{x'}$. The initial relative position vector can be expressed as $\xi = \mathbf{x} - \mathbf{x}'$. This framework allows for symmetric or nonsymmetric domains of interaction and each point to have its own unique family with an arbitrary position. The family size and its shape influence the degree of nonlocality. As the family size decreases, the more local the interactions become. The degree of interaction of material points within a family is dictated by introducing a weight function, $w(|\xi|)$. Although commonly specified to be the same for each point, the weight function can be different. The PD form of the PDEs can be derived by employing the PDDO (Madenci et al., 2016 and Madenci et al., 2019). The PDDO converts local differentiation into a nonlocal integral form by using the PD functions. They are determined directly by constructing them as orthogonal to each term in the Taylor Series Expansion (TSE).

3.2 Construction of one-dimensional PD derivatives

Since the governing equations require up to fourth-order derivatives the one-dimensional TSE can be expressed as

$$f(x + \xi) - f(x) = \xi \frac{\partial f(x)}{\partial x} + \frac{1}{2!} \xi^2 \frac{\partial^2 f(x)}{\partial x^2} + \frac{1}{3!} \xi^3 \frac{\partial^3 f(x)}{\partial x^3} + \frac{1}{4!} \xi^4 \frac{\partial^4 f(x)}{\partial x^4} + R_4(x) \quad (3.1)$$

As shown in Fig. 1, a point x interacts with and is influenced by other points, x' within its horizon, H_x . The relative distance between these two points is defined as $\xi = x' - x$. The function $f(x)$ is treated as known to evaluate the relative change in the function $f(x + \xi) - f(x)$. Each term in the

TSE is multiplied by the PD functions g_4^p where the subscript and superscript represent the order of the TSE and the order of the derivative, respectively as

$$\int_{H_x} (f(x+\xi) - f(x)) g_4^p(\xi) dV_{x'} = \frac{\partial f(x)}{\partial x} \int_{H_x} \xi g_4^p(\xi) dV_{x'} + \frac{\partial^2 f(x)}{\partial x^2} \int_{H_x} \frac{1}{2!} \xi^2 g_4^p(\xi) dV_{x'} + \frac{\partial^3 f(x)}{\partial x^3} \int_{H_x} \frac{1}{3!} \xi^3 g_4^p(\xi) dV_{x'} + \frac{\partial^4 f(x)}{\partial x^4} \int_{H_x} \frac{1}{4!} \xi^4 g_4^p(\xi) dV_{x'} \quad (3.2)$$

Where $V_{x'}$ is the volume at point x' . All terms except the desired PD function corresponding to the order of derivative must be orthogonal to the remaining terms in the TSE as

$$\frac{1}{n!} \int_{H_x} \xi^n g_4^p(\xi) dV_{x'} = \delta_{np} \quad (3.3)$$

with $n, p = 0, 1, 2, 3, 4$ and δ_{np} is the Kronecker delta symbol. Enforcing orthogonality results in the PD form of the derivatives as

$$\begin{pmatrix} \frac{\partial f(x)}{\partial x} \\ \frac{\partial^2 f(x)}{\partial x^2} \\ \frac{\partial^3 f(x)}{\partial x^3} \\ \frac{\partial^4 f(x)}{\partial x^4} \end{pmatrix} = \int_{H_x} (f(x+\xi) - u(x)) \begin{pmatrix} g_4^1(\xi) \\ g_4^2(\xi) \\ g_4^3(\xi) \\ g_4^4(\xi) \end{pmatrix} dV_{x'} \quad (3.4)$$

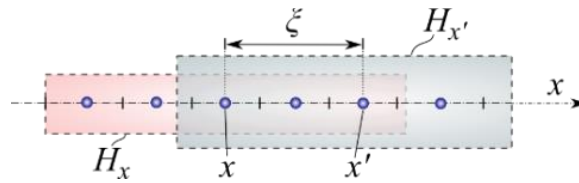


Figure 1. Interaction of PD points, and with arbitrary family sizes for one-dimensional analysis.

By employing the PDDO the nonlocal form of the derivatives at point x with a complete horizon,

$H_x = \{x' \in [-\delta, \delta]\}$ where $x' = x + \xi$ can be expressed as

$$\frac{\partial^2 u(x)}{\partial x^2} = \frac{2}{A\delta^2} \int_{-\delta}^{\delta} \frac{u(x+\xi) - u(x)}{|\xi|} dV_x. \quad (3.5)$$

and

$$\frac{\partial^4 u(x)}{\partial x^4} = \int_{-\delta}^{\delta} \frac{u(x+\xi) - u(x)}{|\xi|} \frac{144}{A|\xi|^2} \left(-\frac{\xi^2}{\delta^4} + 2\frac{\xi^4}{\delta^6} \right) dV_x. \quad (3.6)$$

Equations (3.5) and (3.6) are derived with a specific weight function, $w_2(|\xi|) = w_4(|\xi|) = \frac{\delta^3}{|\xi|^3}$. A

detailed explanation for the derivation of the one-dimensional PD form of the derivatives can be found in Appendix A. For a point with an incomplete horizon, these expressions can be expressed as

$$\frac{\partial^2 u(x)}{\partial x^2} = \int_{H_x} (u(x') - u(x)) \bar{g}_2^2(\xi) dV_x. \quad (3.7)$$

and

$$\frac{\partial^4 u(x)}{\partial x^4} = \int_{H_x} (u(x') - u(x)) \bar{g}_4^4(\xi) dV_x. \quad (3.8)$$

The PD functions $\bar{g}_2^2(\xi)$ and $\bar{g}_4^4(\xi)$ are defined in terms of the PD functions g_2^2 and g_4^4 as derived in Appendix A. They are defined as the average between the two PD functions connected by a bond between the point of interest and one of its family members.

$$\bar{g}_2^2(\xi) = \frac{g_2^2(\xi) + g_2^2(-\xi)}{2} \quad (3.9)$$

and

$$\bar{g}_4^4(\xi) = \frac{g_4^4(\xi) + g_4^4(-\xi)}{2} \quad (3.10)$$

3.3 Construction of two-dimensional PD derivatives

The addition of a spatial dimension increases the complexity. As shown in Fig. 2 the interaction of material point \mathbf{x} with a family member \mathbf{x}' .

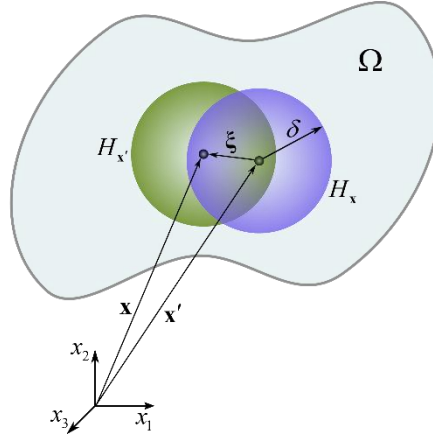


Figure 2. Symmetric position of points \mathbf{x} and \mathbf{x}' in their interaction domains.

Each term of the equation of motion Eq. 2.5 can be written in terms of the analytical PD functions. The gradient enriched equation of motion requires first, second, third, fourth and certain mixed order derivatives. The derivation of the two-dimensional derivatives up to fourth order is shown in Appendix C. The two-dimensional TSE for a relative function can be written as

$$\begin{aligned}
 f(\mathbf{x} + \boldsymbol{\xi}) - f(\mathbf{x}) &= \xi_1 \frac{\partial f(\mathbf{x})}{\partial x_1} + \xi_2 \frac{\partial f(\mathbf{x})}{\partial x_2} + \frac{1}{2!} \xi_1^2 \frac{\partial^2 f(\mathbf{x})}{\partial x_1^2} + \frac{1}{2!} \xi_2^2 \frac{\partial^2 f(\mathbf{x})}{\partial x_2^2} + \xi_1 \xi_2 \frac{\partial^2 f(\mathbf{x})}{\partial x_1 \partial x_2} \\
 &+ \frac{1}{3!} \xi_1^3 \frac{\partial^3 f(\mathbf{x})}{\partial x_1^3} + \frac{1}{3!} \xi_2^3 \frac{\partial^3 f(\mathbf{x})}{\partial x_2^3} + \frac{1}{2!} \xi_1^2 \xi_2 \frac{\partial^3 f(\mathbf{x})}{\partial x_1^2 \partial x_2} + \frac{1}{2!} \xi_1 \xi_2^2 \frac{\partial^3 f(\mathbf{x})}{\partial x_1 \partial x_2^2} \\
 &+ \frac{1}{4!} \xi_1^4 \frac{\partial^4 f(\mathbf{x})}{\partial x_1^4} + \frac{1}{4!} \xi_2^4 \frac{\partial^4 f(\mathbf{x})}{\partial x_2^4} + \frac{1}{3!} \xi_1^3 \xi_2 \frac{\partial^4 f(\mathbf{x})}{\partial x_1^3 \partial x_2} + \frac{1}{3!} \xi_1 \xi_2^3 \frac{\partial^4 f(\mathbf{x})}{\partial x_1 \partial x_2^3} + \frac{1}{2!2!} \xi_1^2 \xi_2^2 \frac{\partial^4 f(\mathbf{x})}{\partial x_1^2 \partial x_2^2} + R_4(\mathbf{x})
 \end{aligned} \tag{3.11}$$

where $f(\mathbf{x})$ is an arbitrary function, the position vector between points \mathbf{x}' and \mathbf{x} is defined as

$$\boldsymbol{\xi} = \mathbf{x}' - \mathbf{x}.$$

$$\begin{aligned}
& \int_{H_x} (f(\mathbf{x} + \xi) - f(\mathbf{x})) g_4^{p_1 p_2}(\xi) dA_{x'} = \frac{\partial f(\mathbf{x})}{\partial \mathbf{x}_1} \int_{H_x} \xi_1 g_4^{p_1 p_2}(\xi) dA_{x'} + \frac{\partial f(\mathbf{x})}{\partial \mathbf{x}_2} \int_{H_x} \xi_2 g_4^{p_1 p_2}(\xi) dA_{x'} \\
& + \frac{1}{2!} \frac{\partial^2 f(\mathbf{x})}{\partial \mathbf{x}_1^2} \int_{H_x} \xi_1^2 g_4^{p_1 p_2}(\xi) dA_{x'} + \frac{1}{2!} \frac{\partial^2 f(\mathbf{x})}{\partial \mathbf{x}_2^2} \int_{H_x} \xi_2^2 g_4^{p_1 p_2}(\xi) dA_{x'} + \frac{\partial^2 f(\mathbf{x})}{\partial \mathbf{x}_1 \partial \mathbf{x}_2} \int_{H_x} \xi_1 \xi_2 g_4^{p_1 p_2}(\xi) dA_{x'} \\
& + \frac{1}{3!} \frac{\partial^3 f(\mathbf{x})}{\partial \mathbf{x}_1^3} \int_{H_x} \xi_1^3 g_4^{p_1 p_2}(\xi) dA_{x'} + \frac{1}{3!} \frac{\partial^3 f(\mathbf{x})}{\partial \mathbf{x}_2^3} \int_{H_x} \xi_2^3 g_4^{p_1 p_2}(\xi) dA_{x'} \\
& + \frac{1}{2!} \frac{\partial^3 f(\mathbf{x})}{\partial \mathbf{x}_1^2 \partial \mathbf{x}_2} \int_{H_x} \xi_1^2 \xi_2 g_4^{p_1 p_2}(\xi) dA_{x'} + \frac{1}{2!} \frac{\partial^3 f(\mathbf{x})}{\partial \mathbf{x}_1 \partial \mathbf{x}_2^2} \int_{H_x} \xi_1 \xi_2^2 g_4^{p_1 p_2}(\xi) dA_{x'} \\
& + \frac{1}{4!} \frac{\partial^4 f(\mathbf{x})}{\partial \mathbf{x}_1^4} \int_{H_x} \xi_1^4 g_4^{p_1 p_2}(\xi) dA_{x'} + \frac{1}{4!} \frac{\partial^4 f(\mathbf{x})}{\partial \mathbf{x}_2^4} \int_{H_x} \xi_2^4 g_4^{p_1 p_2}(\xi) dA_{x'} + \frac{1}{3!} \frac{\partial^4 f(\mathbf{x})}{\partial \mathbf{x}_1^3 \partial \mathbf{x}_2} \int_{H_x} \xi_1^3 \xi_2 g_4^{p_1 p_2}(\xi) dA_{x'} \\
& + \frac{1}{3!} \frac{\partial^4 f(\mathbf{x})}{\partial \mathbf{x}_1 \partial \mathbf{x}_2^3} \int_{H_x} \xi_1 \xi_2^3 g_4^{p_1 p_2}(\xi) dA_{x'} + \frac{1}{2! 2!} \frac{\partial^4 f(\mathbf{x})}{\partial \mathbf{x}_1^2 \partial \mathbf{x}_2^2} \int_{H_x} \xi_1^2 \xi_2^2 g_4^{p_1 p_2}(\xi) dA_{x'} + R_4(\mathbf{x})
\end{aligned} \tag{3.12}$$

Where $A_{x'}$ is the area at point x' . To extract the desired derivative, the PD functions must be orthogonal to the remaining terms in the TSE as

$$\frac{1}{n_1! n_2!} \int_{H_x} \xi_1^{n_1} \xi_2^{n_2} g_4^{p_1 p_2}(\xi) dA_{x'} = \delta_{n_1 p_1} \delta_{n_2 p_2} \tag{3.13}$$

The two-dimensional derivative representations in terms of the PD functions can be written as

$$\begin{pmatrix} \frac{\partial f(\mathbf{x})}{\partial x_1} \\ \frac{\partial f(\mathbf{x})}{\partial x_2} \end{pmatrix} = \int_{H_x} \begin{bmatrix} g_2^{10} & 0 \\ 0 & g_2^{01} \end{bmatrix} (f(\mathbf{x}') - f(\mathbf{x})) dA_{x'} \tag{3.14}$$

and

$$\begin{pmatrix} \frac{\partial^2 f(\mathbf{x})}{\partial x_1^2} \\ \frac{\partial^2 f(\mathbf{x})}{\partial x_2^2} \\ \frac{\partial^2 f(\mathbf{x})}{\partial x_1 \partial x_2} \end{pmatrix} = \int_{H_x} \begin{bmatrix} g_2^{20} & 0 & 0 \\ 0 & g_2^{02} & 0 \\ 0 & 0 & g_2^{11} \end{bmatrix} (f(\mathbf{x}') - f(\mathbf{x})) dA_{x'} \tag{3.15}$$

and

$$\left\{ \begin{array}{l} \frac{\partial^3 f(\mathbf{x})}{\partial x_1^3} \\ \frac{\partial^3 f(\mathbf{x})}{\partial x_2^3} \\ \frac{\partial^3 f(\mathbf{x})}{\partial x_1^2 \partial x_2} \\ \frac{\partial^3 f(\mathbf{x})}{\partial x_2^2 \partial x_1} \end{array} \right\} = \int_{H_x} \begin{bmatrix} g_4^{30} & 0 & 0 & 0 \\ 0 & g_4^{03} & 0 & 0 \\ 0 & 0 & g_4^{21} & 0 \\ 0 & 0 & 0 & g_4^{12} \end{bmatrix} (f(\mathbf{x}') - f(\mathbf{x})) dA_{\mathbf{x}'} \quad (3.16)$$

and

$$\left\{ \begin{array}{l} \frac{\partial^4 f(\mathbf{x})}{\partial x_1^4} \\ \frac{\partial^4 f(\mathbf{x})}{\partial x_2^4} \\ \frac{\partial^4 f(\mathbf{x})}{\partial x_1^3 \partial x_2} \\ \frac{\partial^4 f(\mathbf{x})}{\partial x_2^3 \partial x_1} \\ \frac{\partial^4 f(\mathbf{x})}{\partial x_1^2 \partial x_2^2} \end{array} \right\} = \int_{H_x} \begin{bmatrix} g_4^{40} & 0 & 0 & 0 & 0 \\ 0 & g_4^{04} & 0 & 0 & 0 \\ 0 & 0 & g_4^{31} & 0 & 0 \\ 0 & 0 & 0 & g_4^{13} & 0 \\ 0 & 0 & 0 & 0 & g_4^{22} \end{bmatrix} (f(\mathbf{x} + \xi) - f(\mathbf{x})) dA_{\mathbf{x}'} \quad (3.17)$$

It should be noted that the TSE may be truncated for PD functions of first and second order (e.g. g_4^{01} represents the first order derivative in the x_2 direction).

The gradient, Laplacian, and the gradient of the Laplacian of a function $f(\mathbf{x})$ are expressed as

$$\nabla f(\mathbf{x}) = \int_{H_x} (f(\mathbf{x} + \xi) - f(\mathbf{x})) \mathbf{g}_2(\mathbf{x}, \xi) dA_{\mathbf{x}'} \quad (3.18)$$

and

$$\nabla^2 f(\mathbf{x}) = \int_{H_x} \text{tr} \mathbf{G}_2(\mathbf{x}, \xi) (f(\mathbf{x} + \xi) - f(\mathbf{x})) dA_{\mathbf{x}'} \quad (3.19)$$

and

$$\nabla(\nabla^2 f(\mathbf{x})) = \int_{H_x} (f(\mathbf{x} + \xi) - f(\mathbf{x})) \mathbf{g}_3(\mathbf{x}, \xi) dA_x \quad (3.20)$$

Similarly, the PD form of the gradient of divergence, the Laplacian, the biharmonic operator, and the gradient of the Laplacian of the divergence of a vector field, $\mathbf{u}(\mathbf{x})$ are expressed as

$$\nabla \nabla \cdot \mathbf{u} = \int_{H_x} \mathbf{G}_2(\mathbf{x}, \xi) (\mathbf{u}(\mathbf{x}') - \mathbf{u}(\mathbf{x})) dA_x \quad (3.21)$$

and

$$\nabla^2 \mathbf{u} = \int_{H_x} \text{tr} \mathbf{G}_2(\mathbf{x}, \xi) (\mathbf{u}(\mathbf{x}') - \mathbf{u}(\mathbf{x})) dA_x \quad (3.22)$$

and

$$\nabla^4 \mathbf{u} = \int_{H_x} (\text{tr} \mathbf{G}_4(\mathbf{x}, \xi) \mathbf{I}) (\mathbf{u}(\mathbf{x} + \xi) - \mathbf{u}(\mathbf{x})) dA_x \quad (3.23)$$

and

$$\nabla \nabla^2 (\nabla \cdot \mathbf{u}) = \int_{H_x} \mathbf{G}_4(\mathbf{x}, \xi) (\mathbf{u}(\mathbf{x} + \xi) - \mathbf{u}(\mathbf{x})) dA_x \quad (3.24)$$

The PD vectors comprised of first and third order PD functions are defined as

$$\mathbf{g}_2(\mathbf{x}, \xi) = \begin{Bmatrix} g_2^{10}(\mathbf{x}, \xi) \\ g_2^{01}(\mathbf{x}, \xi) \end{Bmatrix} \quad (3.25)$$

and

$$\mathbf{g}_3(\mathbf{x}, \xi) = \begin{bmatrix} g_4^{30}(\mathbf{x}, \xi) + g_4^{03}(\mathbf{x}, \xi) \\ g_4^{21}(\mathbf{x}, \xi) + g_4^{12}(\mathbf{x}, \xi) \end{bmatrix} \quad (3.26)$$

The PD matrix comprised of second and fourth order PD function are defined as

$$\mathbf{G}_2(\mathbf{x}, \xi) = \begin{bmatrix} g_2^{20}(\mathbf{x}, \xi) & g_2^{11}(\mathbf{x}, \xi) \\ g_2^{11}(\mathbf{x}, \xi) & g_2^{02}(\mathbf{x}, \xi) \end{bmatrix} \quad (3.27)$$

and

$$\mathbf{G}_4(\mathbf{x}, \xi) = \begin{bmatrix} g_4^{40}(\mathbf{x}, \xi) + g_4^{22}(\mathbf{x}, \xi) & g_4^{31}(\mathbf{x}, \xi) + g_4^{13}(\mathbf{x}, \xi) \\ g_4^{31}(\mathbf{x}, \xi) + g_4^{13}(\mathbf{x}, \xi) & g_4^{04}(\mathbf{x}, \xi) + g_4^{22}(\mathbf{x}, \xi) \end{bmatrix} \quad (3.28)$$

For a point, \mathbf{x} , located in the bulk domain and that has a point, \mathbf{x}' , in its family, the following relationships are established as

$$\mathbf{g}_2(\mathbf{x}, \xi) = -\mathbf{g}_2(\mathbf{x}', \xi') \quad (3.29)$$

and

$$\mathbf{g}_3(\mathbf{x}, \xi) = -\mathbf{g}_3(\mathbf{x}', \xi') \quad (3.30)$$

and

$$\mathbf{G}_2(\mathbf{x}, \xi) = \mathbf{G}_2(\mathbf{x}', \xi') \quad (3.31)$$

and

$$\mathbf{G}_4(\mathbf{x}, \xi) = \mathbf{G}_4(\mathbf{x}', \xi') \quad (3.32)$$

3.4 Analytical form of PD derivatives

When the weight functions used to construct the PD derivatives are specifically chosen, an analytical form of the derivatives can be determined. For case of second order TSE as shown in Madenci et al. (2022) the following forms of the gradient of a function, gradient of the divergence of a vector, and the Laplacian of a vector as

$$\nabla f(x) = \frac{2}{\pi\delta^4} \int_{H_x} w_1(|\xi|) (f(x+\xi) - f(x)) \xi dA_x. \quad (3.33)$$

$$\nabla \nabla \cdot \mathbf{u} = -\frac{3}{\pi\delta^6} \int_{H_x} w_2(|\xi|) (\xi \cdot \xi) (\mathbf{u}(x+\xi) - \mathbf{u}(x)) dA_x + \frac{12}{\pi\delta^6} \int_{H_x} w_2(|\xi|) [\xi \cdot (\mathbf{u}(x+\xi) - \mathbf{u}(x))] \xi dA_x. \quad (3.34)$$

$$\nabla^2 \mathbf{u} = \frac{6}{\pi \delta^6} \int_{H_x} w_2(|\xi|) (\xi \cdot \xi) (\mathbf{u}(\mathbf{x} + \xi) - \mathbf{u}(\mathbf{x})) dA_x. \quad (3.35)$$

Similarly, the analytical representation for higher order derivatives required in the SG contribution can be shown to be

$$\nabla(\nabla^2 \theta) = \int_H \left(-\frac{32}{\pi \delta^6} w_1(|\xi|) + \frac{64}{\pi \delta^8} w_3(|\xi|) (\xi \cdot \xi) \right) (\theta(\mathbf{x} + \xi) - \theta(\mathbf{x})) \xi dA_x. \quad (3.36)$$

$$\nabla \nabla^2 (\nabla \cdot \mathbf{u}) = \int_{H_x} \left(\begin{array}{c} -\frac{36 \times 10}{\pi \delta^8} w_2(|\xi|) (\xi \otimes \xi) + \frac{6 \times 10}{\pi \delta^8} w_2(|\xi|) (\xi \cdot \xi) + \\ \frac{60 \times 10}{\pi \delta^{10}} w_4(|\xi|) (\xi \cdot \xi) (\xi \otimes \xi) - \frac{10 \times 10}{\pi \delta^{10}} w_4(|\xi|) (\xi \cdot \xi)^2 \end{array} \right) (\mathbf{u}(\mathbf{x} + \xi) - \mathbf{u}(\mathbf{x})) dA_x. \quad (3.37)$$

and

$$\nabla^4 \mathbf{u}(\mathbf{x}, \xi) = \int_{H_x} \left(\frac{-240}{\pi \delta^8} w_2(|\xi|) (\xi \cdot \xi) + \frac{400}{\pi \delta^{10}} w_4(|\xi|) (\xi \cdot \xi)^2 \right) (\mathbf{u}(\mathbf{x} + \xi) - \mathbf{u}(\mathbf{x})) dA_x. \quad (3.38)$$

With weight functions $w_n(|\xi|) = \frac{\delta^{n+1}}{|\xi|^{n+1}}$, with $n = 1, 2, 3, 4$. The derivation of these analytical derivatives

can be found in Appendix C.

3.5 Investigation of analytical PD functions and derivatives with examples

The capability of the PDDO to accurately recover analytical derivatives is essential for effectively converting local differential equations into their nonlocal integral forms. For this transformation to be successful, the PDDO must precisely replicate the analytical derivatives, ensuring that the resulting nonlocal integral equations preserve the fundamental properties of the original equations. By incorporating the influence of neighboring points, the PDDO captures spatial variations and interactions to compute the derivatives. A detailed derivation of the one-dimensional PD functions can be found in Appendix B. The analytical PD functions are determined to be

$$g_4^0(\xi) = \frac{225}{128\delta} - \frac{525}{64\delta^3} \xi^2 + \frac{945}{128\delta^5} \xi^4 \quad (3.39a)$$

$$g_4^1(\xi) = \frac{75}{8\delta^3}\xi - \frac{105}{8\delta^5}\xi^3 \quad (3.39b)$$

$$g_4^2(\xi) = -\frac{525}{32\delta^3} + \frac{2205}{16\delta^5}\xi^2 - \frac{4725}{32\delta^7}\xi^4 \quad (3.39c)$$

$$g_4^3(\xi) = -\frac{315}{4\delta^5}\xi + \frac{525}{4\delta^7}\xi^3 \quad (3.39d)$$

$$g_4^4(\xi) = \frac{2835}{16\delta^5} - \frac{14175}{8\delta^7}\xi^2 + \frac{33075}{16\delta^9}\xi^4 \quad (3.39e)$$

Multiplying the PD function by an arbitrary function $f(x+\xi)$ and integrating over the family will result in the corresponding derivative, p , in the limit of $\delta \rightarrow 0$. For example $f(x+\xi) = \sin(x+\xi)$ the original function, first, second, third, and fourth order analytical derivatives can be recovered as

$$\begin{aligned} \sin(x) &= \lim_{\delta \rightarrow 0} \int_{-\delta}^{\delta} g_4^0(\xi) \sin(x+\xi) d\xi \\ &= \lim_{\delta \rightarrow 0} \frac{15 \sin(x) (7\delta(-27+2\delta^2) \cos(\delta) + (189-77\delta^2+\delta^4) \sin(\delta))}{8\delta^5} = \sin(x) \end{aligned} \quad (3.40a)$$

$$\begin{aligned} \frac{\partial \sin(x)}{\partial x} &= \lim_{\delta \rightarrow 0} \int_{-\delta}^{\delta} g_4^1(\xi) \sin(x+\xi) d\xi \\ &= \lim_{\delta \rightarrow 0} \frac{15 \cos(x) (\delta(-21+\delta^2) \cos(\delta) + (21-8\delta^2) \sin(\delta))}{2\delta^5} = \cos(x) \end{aligned} \quad (3.40b)$$

$$\begin{aligned} \frac{\partial^2 \sin(x)}{\partial x^2} &= \lim_{\delta \rightarrow 0} \int_{-\delta}^{\delta} g_4^2(\xi) \sin(x+\xi) d\xi \\ &= \lim_{\delta \rightarrow 0} \frac{105 \sin(x) (3\delta(-45+4\delta^2) \cos(\delta) + (135-57\delta^2+\delta^4) \sin(\delta))}{2\delta^7} = -\sin(x) \end{aligned} \quad (3.40c)$$

$$\begin{aligned} \frac{\partial^3 \sin(x)}{\partial x^3} &= \lim_{\delta \rightarrow 0} \int_{-\delta}^{\delta} g_4^3(\xi) \sin(x+\xi) d\xi \\ &= \lim_{\delta \rightarrow 0} \frac{105 \cos(x) (\delta(-15+\delta^2) \cos(\delta) + 3(5-2\delta^2) \sin(\delta))}{\delta^7} = -\cos(x) \end{aligned} \quad (3.40d)$$

$$\begin{aligned}
\frac{\partial^4 \sin(x)}{\partial x^4} &= \lim_{\delta \rightarrow 0} \int_{-\delta}^{\delta} g_4^4(\xi) \sin(x + \xi) d\xi \\
&= \lim_{\delta \rightarrow 0} \frac{945 \sin(x) (5\delta (-21 + 2\delta^2) \cos(\delta) + (105 - 45\delta^2 + \delta^4) \sin(\delta))}{\delta^9} = \sin(x)
\end{aligned} \tag{3.40e}$$

As the horizon approaches zero, the PDDO recovers local differentiation in the example above. When these integrals are calculated numerically using analytical PD functions, there may be difficulties in achieving accurate differentiation. Therefore, it is recommended to use numerical PD functions specifically computed for the discretized domain.

4. ONE-DIMENSIONAL ANALYSIS

4.1 PD form of the equation of motion with gradient elasticity

For one-dimensional analysis with $u_1 = u(x)$, $b_1 = b(x)$ and $u_2 = u_3 = 0$, and noting that $\mu = E/2$ and $\lambda = 0$, Eq. (2.8) reduces to

$$\rho \frac{\partial^2 u}{\partial t^2} = E \frac{\partial^2 u}{\partial x^2} - \ell^2 E \frac{\partial^4 u}{\partial x^4} + b \quad (4.1)$$

Substituting for the local derivatives from Eqs. (3.5) and (3.6) in this equation results in the nonlocal PD form as

$$\rho \ddot{u}(x) = \int_{-\delta}^{\delta} \left[c(\xi) - \left(\frac{\ell}{\delta} \right)^2 c_\ell(\xi) \right] \frac{u(x+\xi) - u(x)}{|\xi|} dV + b(x) \quad (4.2)$$

or

$$\rho \frac{\partial^2 u(x)}{\partial t^2} = \int_{H_x} E \left[\bar{g}_2^2(\xi)(u(x') - u(x)) - \ell^2 \bar{g}_4^4(\xi)(u(x') - u(x)) \right] dV_{x'} + b(x) \quad (4.3)$$

where the PD micromoduli, $c(\xi)$ and $c_\ell(\xi)$ are defined as

$$c(\xi) = \frac{2E}{A\delta^2} \quad (4.4)$$

and

$$c_\ell(\xi) = \frac{144E}{A\delta^2} \left(2 \frac{\xi^2}{\delta^2} - 1 \right) \quad (4.5)$$

The resulting PD equation of motion is an integro-differential equation in time and space. It does not contain any spatial derivatives of displacements. Therefore, constraint conditions are, in general, not necessary for the solution of an integro-differential equation. Construction of its solution involves time and spatial integrations while being subject to constraints and/or loading conditions on the boundary of the material region and initial conditions on the displacement and velocity fields.

4.2 PDSG Dispersion relations

In the derivation of the dispersion relations, the wave number, the wave frequency and phase velocity of the wave are denoted by κ , ω , and ν , respectively. The relationship among these parameters is $\omega = \kappa\nu$. The wave number is related to the half-wavelength, Γ , by the relationship $\kappa = \pi/\Gamma$. In the absence of a body load, the PD equation of motion for a one-dimensional bar with cross sectional area, A , can be written as

$$\rho \ddot{u}(x) = \int_{-\delta}^{\delta} \frac{2E}{A\delta^2} \left[1 - 72 \frac{\ell^2}{\delta^2} \left(2 \frac{\xi^2}{\delta^2} - 1 \right) \right] \frac{u(x') - u(x)}{|\xi|} dV_{x'} \quad (4.6)$$

Dispersion relations are determined by considering a wave propagating in the x-direction. Therefore, wave solutions for material points located at x and x' can be expressed as

$$u(x, t) = u_0 e^{i(\kappa x - \omega t)} \quad \text{and} \quad u(x', t) = u_0 e^{i(\kappa x' - \omega t + \text{sgn}(x' - x)\kappa\xi)} \quad (4.7)$$

in which $\kappa\xi$ is the phase difference between material points located at x and x' , and u_0 represents the amplitudes of these waves. Substituting these wave solutions into the Bond-Based (BB) PD equation of motion leads to

$$-\rho u_0 \omega^2 e^{i(\kappa x - \omega t)} = \frac{4E}{\delta^2} \int_0^{\delta} \left[1 - 72 \frac{\ell^2}{\delta^2} \left(2 \frac{\xi^2}{\delta^2} - 1 \right) \right] \frac{u_0 e^{i(\kappa(x+\xi) - \omega t)} - u_0 e^{i(\kappa x - \omega t)}}{\xi} d\xi \quad (4.8)$$

or

$$\omega^2 = \frac{4E}{\rho\delta^2} \int_0^{\delta} \left[1 - 72 \left(\frac{\ell}{\delta} \right)^2 \left(2 \frac{\xi^2}{\delta^2} - 1 \right) \right] \frac{1}{\xi} (1 - \cos(\kappa\xi)) d\xi \quad (4.9)$$

This expression is dependent on the phase difference, PD horizon and the SGE length parameter. As indicated by Silling (2000), in the limit of a long wavelength, Γ or for a very small wave number ($\kappa \rightarrow 0$), the integral can be analytically evaluated by considering the first three terms of the TSE of the cosine function as

$$\cos(k\xi) = 1 - \frac{(k\xi)^2}{2!} + \frac{(k\xi)^4}{4!} - \dots \quad (4.10)$$

Invoking this approximation into Eq. (4.9) and performing integration results in

$$\omega^2 = \frac{E}{\rho} \left(1 - 72 \frac{\ell^2}{\delta^2} \right) \left(\kappa^2 - \frac{\delta^2}{24} \kappa^4 + \dots \right) \quad (4.11)$$

The wave dispersion relation for long wavelength, i.e., $\kappa < 1$, this expression can be approximated as

$$\omega_{PD SG} = \pm \sqrt{\frac{E}{\rho} \left(1 - 72 \frac{\ell^2}{\delta^2} \right)} \kappa \quad (4.12)$$

For $\ell = 0$, it reduces to

$$\omega_{PD} = \pm \sqrt{\frac{E}{\rho}} \kappa \quad (4.13)$$

For specified values of $E = 200$ GPa, $\rho = 7850$ kg/m³, and a horizon size, $\delta = 0.03$ m, the evaluation of Eq. 4.9 without any simplification leads to the variation of the wave frequency, ω , as a function of the wave number, κ as shown in Fig. 3. The wave dispersions level off as the wave number increases which is a well-known behavior observed in experimental studies (Eringen, 1972). The wave frequency always increases linearly according to the classical theory.

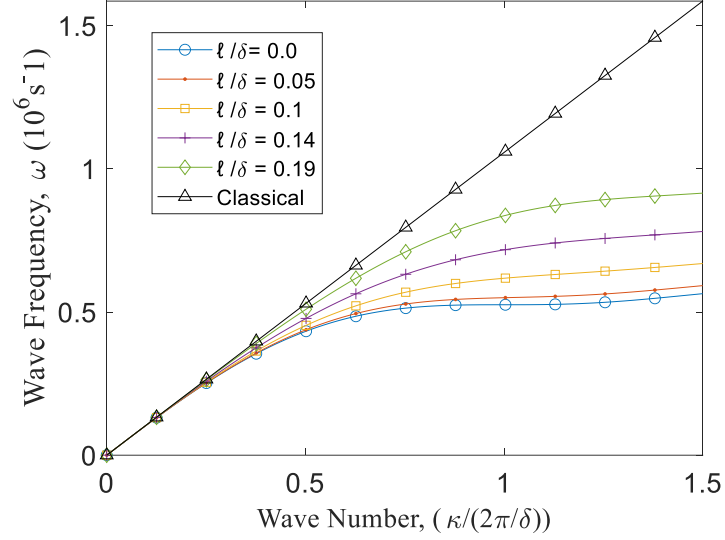


Figure 3. Comparison of PD and classical wave frequency dispersions

4.3 Numerical implementation

For spatial integration, the equation of motion, Eq. (4.1) can be discretized as

$$\rho \frac{\partial^2 \mathbf{u}_{(k)}}{\partial t^2} = EA \sum_{j=1}^{N_{(k)}} \left[\bar{g}_2^2(\xi_{(k)(j)}, \xi_{(j)(k)}) - \ell^2 \bar{g}_4^4(\xi_{(k)(j)}, \xi_{(j)(k)}) \right] (\mathbf{u}_{(j)} - \mathbf{u}_{(k)}) \Delta_{(j)} + \mathbf{b}_{(k)} \quad \text{for } k=1, \dots, M \quad (4.14)$$

where $\mathbf{u}_{(j)}$ is the displacement at point j belonging to the family of point k with $N_{(k)}$ denoting number of its family members and M is the total number of points in the discretization. The relative distance between these points is $\xi_{(k)(j)} = x_{(j)} - x_{(k)}$ and $\Delta_{(j)}$ represents the incremental length associated with point j . The PD functions denoted as \bar{g}_2^2 and \bar{g}_4^4 are the averaged PD functions corresponding to the interaction (bond) between two material points as

$$\bar{g}_2^2(\xi_{(k)(j)}, \xi_{(j)(k)}) = \frac{g_2^2(\xi_{(k)(j)}) + g_2^2(\xi_{(j)(k)})}{2} \quad (4.15)$$

and

$$\bar{g}_4^4(\xi_{(k)(j)}, \xi_{(j)(k)}) = \frac{g_4^4(\xi_{(k)(j)}) + g_4^4(\xi_{(j)(k)})}{2} \quad (4.16)$$

For a point with a symmetric horizon, $\bar{g}_2^2(\xi_{(k)(j)}, \xi_{(j)(k)}) = g_2^2(\xi_{(k)(j)}) = g_2^2(\xi_{(j)(k)})$ and $\bar{g}_4^4(\xi_{(k)(j)}, \xi_{(j)(k)}) = g_4^4(\xi_{(k)(j)}) = g_4^4(\xi_{(j)(k)})$. The determination of the PD functions, $g_2^2(\xi_{(k)(j)})$ and $g_4^4(\xi_{(k)(j)})$ are explained in Appendix A.

For time integration, a central difference scheme can be employed as

$$\rho \frac{u_{(k)}^{n-1} - 2u_{(k)}^n + u_{(k)}^{n+1}}{\Delta t^2} = \frac{2E}{A\delta^2} \sum_{j=1}^{N_{(k)}} \left[1 - 72 \frac{\ell^2}{\delta^2} \left(2 \frac{\xi_{(k)(j)}^2}{\delta^2} - 1 \right) \right] \frac{(u_{(j)}^n - u_{(k)}^n)}{|\xi_{(k)(j)}|} V_{(j)} + b_{(k)} \quad \text{for } k=1, \dots, M \quad (4.17)$$

and

$$\rho \frac{u_{(k)}^{n-1} - 2u_{(k)}^n + u_{(k)}^{n+1}}{\Delta t^2} = EA \sum_{j=1}^{N_{(k)}} \left[\bar{g}_2^2(\xi_{(k)(j)}, \xi_{(j)(k)}) - \ell^2 \bar{g}_4^4(\xi_{(k)(j)}, \xi_{(j)(k)}) \right] (u_{(j)}^n - u_{(k)}^n) \Delta_{(j)} + b_{(k)} \quad (4.18)$$

where $u_{(k)}^n = u_{(k)}(t = n\Delta t)$ is the solution at the n -th time step of Δt (i.e., $t = n\Delta t$). From this equation, $u_{(k)}^{n+1}$ can be evaluated as

$$u_{(k)}^{n+1} = \frac{\Delta t^2}{\rho} \left[EA \sum_{j=1}^{N_{(k)}} \left[\bar{g}_2^2 - \ell^2 \bar{g}_4^4 \right] (u_{(j)}^n - u_{(k)}^n) \Delta_{(j)} + b_{(k)} \right] - u_{(k)}^{n-1} + 2u_{(k)}^n \quad \text{for } n=1, 2, \dots, N \quad (4.19)$$

in which $u_{(k)}^0 = u_{(k)}(t=0)$ and $u_{(k)}^1 = u_{(k)}(t=0)$ represent the initial condition.

Equation (4.19) provides the displacement field at the next time step by simply marching in time. Although the explicit time integration scheme is straightforward, it is only conditionally stable. Therefore, a stability condition is necessary to ensure convergence in results. A stability condition for the critical time step size, Δt , can be derived as (Madenci et al. 2014).

$$\Delta t < \sqrt{\frac{2\rho_{(k)}}{\frac{2E}{A\delta^2} \sum_{j=1}^{N_{(k)}} \left[1 - 72 \frac{\ell^2}{\delta^2} \left(2 \frac{\xi_{(k)(j)}^2}{\delta^2} - 1 \right) \right] \frac{1}{|\xi_{(k)(j)}|} V_{(j)}}}}. \quad (4.20)$$

The use of a safety factor that has a value of less than unity is recommended as it makes the analysis more stable. It is also worth noting that the stable time step size is dependent on the horizon size and SGE parameter.

This time step size is not feasible to obtain the steady-state solution to the equation of motion under quasi-static loading conditions. The Adaptive Dynamic Relaxation (ADR) method by Kilic and Madenci (2010) introduces adaptive artificial damping at each iteration step. This guides the solution to the steady-state solution. The magnitude of the damping term affects the rate of convergence. Therefore, its magnitude is determined at each time step.

According to the ADR method, the PD equation of motion, Eq. (4.14) is written as a set of ordinary differential equations for all material points in the bar. The ADR method replaces the acceleration term with a fictitious diagonal density matrix, Λ and damping matrix, $c\Lambda$ (proportional to the density matrix) and casts the equation of motion as

$$\Lambda\ddot{\mathbf{U}}(\mathbf{X},t) + c\Lambda\dot{\mathbf{U}}(\mathbf{X},t) = \mathbf{F}(\mathbf{U},\mathbf{U}',\mathbf{X},\mathbf{X}') \quad (4.21)$$

The vectors \mathbf{X} and \mathbf{U} contain the initial position and displacement of the points, respectively, and they can be expressed as

$$\mathbf{X}^T = \{x_{(1)}, x_{(2)}, \dots, x_{(M)}\} \quad (4.22)$$

$$\mathbf{U}^T = \{u_{(1)}, u_{(2)}, \dots, u_{(M)}\} \quad (4.23)$$

and

$$\mathbf{F}^T = \{F_{(1)}, F_{(2)}, \dots, F_{(M)}\} \quad (4.24)$$

where M is the total number of material points in the bar. The force vector, \mathbf{F} , can be expressed as

$$F_{(k)} = EA \sum_{j=1}^{N_{(k)}} [\bar{g}_2^2 - \ell^2 \bar{g}_4^4] (u_{(j)}^n - u_{(k)}^n) \Delta_{(j)} + b_{(k)} \quad (4.25)$$

Based on the Velocity-Verlet difference scheme, the velocity and displacement at the k -th point for the next time step can be evaluated as

$$\dot{\mathbf{U}}^{n+1/2} = \frac{\left((2 - c^n \Delta t) \dot{\mathbf{U}}^{n-1/2} - 2\Delta t \Lambda^{-1} \mathbf{F}^n \right)}{(2 + c^n \Delta t)} \quad (4.26)$$

and

$$\mathbf{U}^{n+1} = \mathbf{U}^n + \Delta t \dot{\mathbf{U}}^{n+1/2} \quad (4.27)$$

where n indicates the n -th iteration. Although, Eq. (4.26) cannot be used to start the iteration process due to an unknown velocity field at $t^{-1/2}$, it can be assumed that $\mathbf{U}^0 \neq 0$ and $\dot{\mathbf{U}} = 0$. Therefore, the integration can start with

$$\dot{\mathbf{U}}^{1/2} = -\frac{\Delta t \Lambda^{-1} \mathbf{F}^0}{2} \quad (4.28)$$

Note that the only physical term in this algorithm is the force vector, \mathbf{F}^n . The density matrix, Λ , damping coefficient, c^n , and time step size, $\Delta t = 1$, do not have to be physical quantities. Thus, their values can be chosen to obtain faster convergence. The damping term c^n is evaluated by the procedure described by Kilic and Madenci (2010).

4.4 Numerical results

4.4.1 PDSG model of carbon nanotube under tensile force

As shown in Fig. 4, the CNT is clamped at the left end and subjected to an axial tensile force, F on the right end. Its geometry is described by a length of $L = 10$ nm and annular cross-sectional area $A = \pi(r_o^2 - r_i^2)$ with $r_o = 1.17$ nm, $r_i = 1$ nm. The Young's modulus, Poisson's ratio, and mass density are specified as $E = 1$. TPa, $\nu = 0$, and $\rho = 1,370$ kg/m³, respectively (Limkatanyu et al., 2022). The SGE length parameter, ℓ is specified to be 0.5 and 2 nm. The quasi-static solution is reached when the difference between two consecutive displacement norms is below 1×10^{-9} .

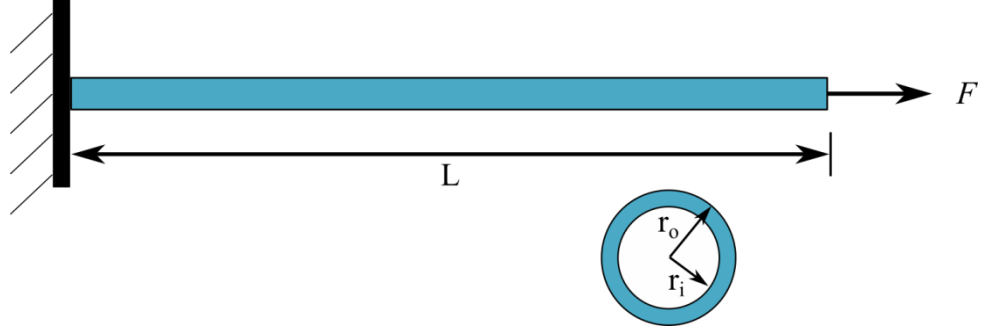


Figure 4. Geometry and boundary condition of a carbon nanotube

The classical and nonclassical boundary conditions can be specified as (Limkatanyu et al., 2022)

$$u(x=0) = 0 \quad (4.29)$$

$$\sigma(x=L) = E \left[\frac{\partial u(x=L)}{\partial x} - \ell^2 \frac{\partial^3 u(x=L)}{\partial x^3} \right] = \frac{F}{A} \quad (4.30)$$

$$\frac{\partial u(x=L)}{\partial x} = 0 \quad (4.31)$$

$$E\ell^2 \frac{\partial^2 u(x=0)}{\partial x^2} = 0 \quad (4.32)$$

Figure 5 shows the PD discretization of the CNT. The point of interest, $x_{(k)}$ is shown in green and the red points, $x_{(j)}$ are its family members. The analysis domain is split into three sections: the fictitious, PDDO, and BB PD regions. Two fictitious points have been added outside of the real domain to facilitate the imposition of boundary conditions. These points are $x_{(-1)}$ and $x_{(K+1)}$ on the left and right edges of the bar, respectively. The pointwise PDDO region has a length of a single material point and starts from the edges. The PDDO region uses the standard PDDO functions for the analysis Appendix A. The bond wise BB PD region is the largest region, and each point is computed by averaging the PD functions, Eq. (4.15) and (4.16). The grid spacing is specified as $\Delta x = 0.01$ nm with

horizon size $\delta = 5.015\Delta x$ for $k = 1, \dots, K = 1000$. The ADR analysis is completed once the difference between subsequent displacement results is below the tolerance of 1×10^{-9} .

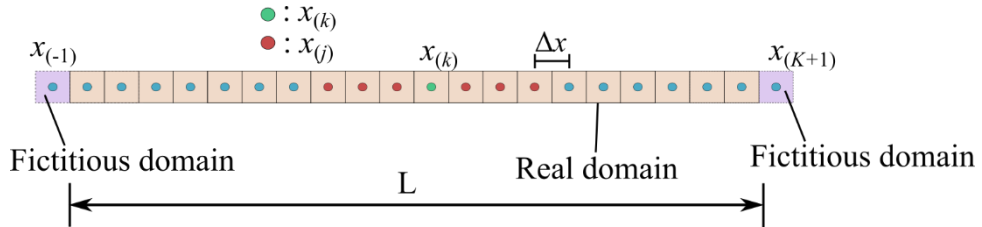


Figure 5. Representative discretization of a carbon nanotube

The primary challenge is the enforcement of boundary conditions. Each of the four boundary conditions is enforced iteratively by using Lagrange multipliers at each time step (Carpenter et al., 1991). Dirichlet type boundary conditions can be enforced directly without the need for special treatment. The details of computing the Lagrange multipliers and enforcing higher-order boundary conditions, Eqs. (4.30), (4.31) and (4.32) are explained in Appendix D. The displacement constraint, Eq. (4.29) is enforced directly as

$$u_{(-1)}(x_{(-1)}, t + \Delta t) = 0 \quad (4.33)$$

Figure 6 shows a comparison of the quasi-static response of the CNT based on the PDSG and analytical SGE solutions. The analytical solution is generated using Mathematica (2022). The predictions are in close agreement for the two different specified ℓ values. Both solution methods indicate an increased stiffening effect along the length of the tube.

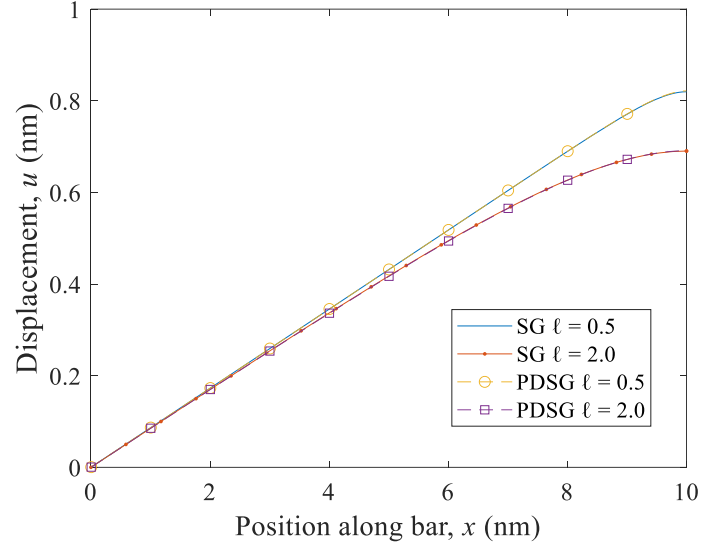


Figure 6. Comparison of the analytical SG solution to the PDSG displacement predictions

4.4.2 PDSG model of CNT under dynamic loading

The CNT shown in Fig. 4 is free of tensile loading, i.e., $F = 0$. The boundary conditions are enforced in the same way as the quasi-static case. The procedure for enforcing the boundary conditions is explained in Appendix D. The CNT is subjected to an initial displacement field of

$$u(x, t = 0) = \frac{0.001x^5 - x^3 + 250x}{1600} \quad (4.34)$$

There is no initial time dependence; therefore, the initial velocity is specified as

$$\frac{\partial u(x, t = 0)}{\partial t} = 0 \quad (4.35)$$

The grid spacing is specified as $\Delta x = 0.1$ nm with horizon size $\delta = 5.015\Delta x$ for $k = 1, \dots, K = 100$. The spatial discretization is the same as that of described in Fig. 5. The time integration is performed with a stable time step, Δt obtained from Eq. (4.20) for $\ell = 0.5$ nm. The initial displacement fields are applied as

$$u_{(k)}^0 = u_{(k)}^{-1} = \frac{0.001x_{(k)}^5 - x_{(k)}^3 + 250x_{(k)}}{1600} \quad \text{for } k = 1, \dots, K = 100 \quad (4.36)$$

Figure 7 shows the comparison of the classical SG and PDSG vibrational response of a CNT. The displacement of almost the midpoint of the bar is plotted over time. The results indicate close agreement between the PDSG and SG predictions.

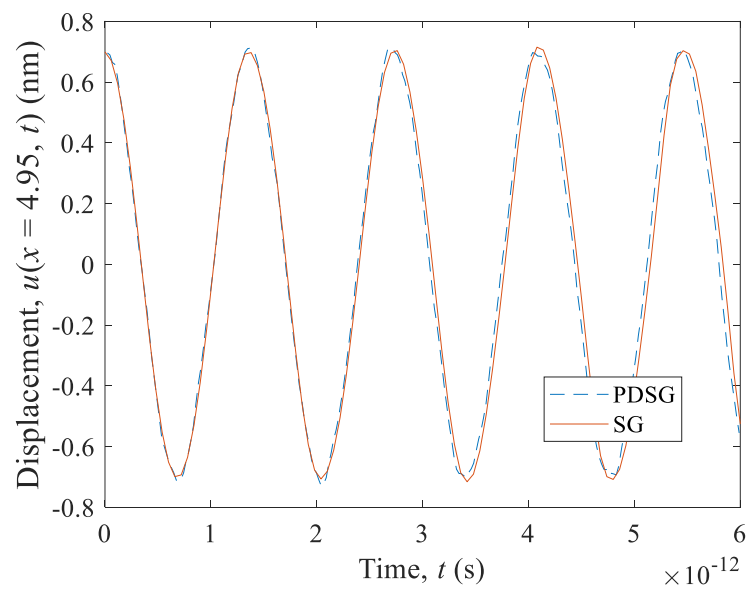


Figure 7. Comparison of classical SG and PDSG transient solutions of CNT

5. TWO-DIMENSIONAL ANALYSIS

5.1 Ordinary state-based formulation with gradient elasticity

To avoid the limitations of one-dimensional analysis and the values of Poisson's ratio related to the PD bond-based formulation, the Ordinary State-Based (OSB) formulation for strain gradient is developed. The force density vectors corresponding to the OSB formulation are depicted in Fig. 8.

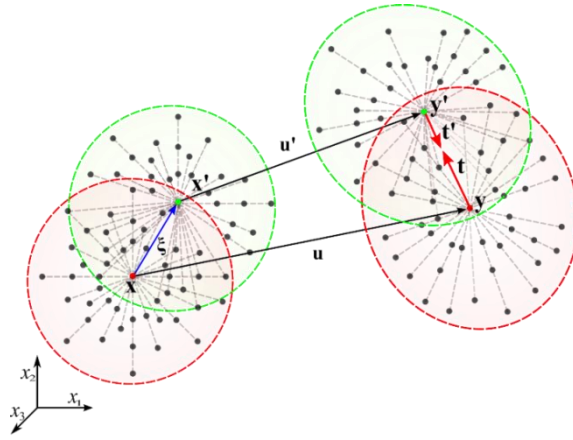


Figure 8. Force density vectors in PD: OSB

For two-dimensional analysis with $u_3 = 0$, substituting for the local derivatives from Eqs. (3.18), (3.19), (3.20), (3.21), (3.22), (3.23), and (3.24) into the internal force vectors \mathbf{M} and \mathbf{N} , their PD form can be obtained as

$$\mathbf{M}^{PD} = \int_{H_x} (a(\theta(\mathbf{x}') + \theta(\mathbf{x}))\mathbf{g}_2(\mathbf{x}, \xi) + \mu(\mathbf{S}(\mathbf{x}, \xi))(\mathbf{u}(\mathbf{x}') - \mathbf{u}(\mathbf{x})))dA_x \quad (5.1)$$

and

$$\mathbf{N}^{PD}(\mathbf{x}) = \int_{H_x} (a\mathbf{g}_3(\mathbf{x}, \xi)(\theta(\mathbf{x}') + \theta(\mathbf{x})) + \mu(\mathbf{Q}(\mathbf{x}, \xi))) (\mathbf{u}(\mathbf{x}') - \mathbf{u}(\mathbf{x}))dA_x \quad (5.2)$$

where $\mathbf{S}(\mathbf{x}, \xi) = \text{tr}\mathbf{G}_2(\mathbf{x}, \xi)\mathbf{I} + 2\mathbf{G}_2(\mathbf{x}, \xi)$ and $\mathbf{Q}(\mathbf{x}, \xi) = (\text{tr}\mathbf{G}_4(\mathbf{x}, \xi)\mathbf{I} + 2\mathbf{G}_4(\mathbf{x}, \xi))$ and $\mathbf{g}_2, \mathbf{g}_3, \mathbf{G}_2,$ and \mathbf{G}_4 are defined in section 3.3. As suggested by Silling et al. (2010), the PD form of the equilibrium equation can be written as

$$\rho \frac{\partial^2 \mathbf{u}}{\partial t^2} = \int_{H_x} (\mathbf{t}(\mathbf{x}) - \mathbf{t}(\mathbf{x}')) dV_{x'} + \mathbf{b} \quad (5.3)$$

in which the force density vectors, $\mathbf{t} = \mathbf{t}(\mathbf{x}, t)$ and $\mathbf{t}' = \mathbf{t}(\mathbf{x}', t)$ contain the constitutive information and describe the interaction between the material points. Comparison of Eqs. (5.3) and Eq. (2.11) reveals that

$$\mathbf{L}^{PD} = \int_{H_x} (\mathbf{t}(\mathbf{x}) - \mathbf{t}(\mathbf{x}')) dV_{x'} = \mathbf{M}^{PD} - \ell^2 \mathbf{N}^{PD} \quad (5.4)$$

Substituting for the expressions for $\mathbf{M}^{PD}(\mathbf{x})$ and $\mathbf{N}^{PD}(\mathbf{x})$ leads to

$$\begin{aligned} \mathbf{L}^{PD} = & \int_{H_x} \left(a(\theta(\mathbf{x}') + \theta(\mathbf{x})) \mathbf{g}_2(\mathbf{x}, \xi) + \mu \mathbf{S}(\mathbf{x}, \xi) (\mathbf{u}(\mathbf{x}') - \mathbf{u}(\mathbf{x})) \right. \\ & \left. - \ell^2 \left(a \mathbf{g}_3(\mathbf{x}, \xi) (\theta(\mathbf{x} + \xi) + \theta(\mathbf{x})) + \mu \mathbf{Q}(\mathbf{x}, \xi) (\mathbf{u}(\mathbf{x}') - \mathbf{u}(\mathbf{x})) \right) \right) dA_{x'} \end{aligned} \quad (5.5)$$

The force density vectors can then be extracted from the internal force representation as

$$\mathbf{t}(\mathbf{x}, \xi) = \hat{\mu}(\mathbf{x}' - \mathbf{x}) \left[\begin{array}{l} \int_{H_x} a \theta(\mathbf{x}) \mathbf{g}_2(\mathbf{x}, \xi) + \frac{1}{2} \mu \mathbf{S}(\mathbf{x}, \xi) (\mathbf{u}(\mathbf{x}') - \mathbf{u}(\mathbf{x})) \\ - \ell^2 \left(a \mathbf{g}_3(\mathbf{x}, \xi) \theta(\mathbf{x}) \mathbf{g}_3(\mathbf{x}, \xi) + \frac{1}{2} \mu \mathbf{Q}(\mathbf{x}, \xi) (\mathbf{u}(\mathbf{x}') - \mathbf{u}(\mathbf{x})) \right) dA_{x'} \end{array} \right] \quad (5.6)$$

and

$$\mathbf{t}(\mathbf{x}', \xi') = \hat{\mu}(\mathbf{x} - \mathbf{x}') \left[\begin{array}{l} \int_{H_x} a \theta(\mathbf{x}') \mathbf{g}_2(\mathbf{x}', \xi') + \frac{1}{2} \mu \mathbf{S}(\mathbf{x}', \xi') (\mathbf{u}(\mathbf{x}) - \mathbf{u}(\mathbf{x}')) \\ + \ell^2 \left(a \theta(\mathbf{x}') \mathbf{g}_3(\mathbf{x}', \xi') + \frac{1}{2} \mu \mathbf{Q}(\mathbf{x}', \xi') (\mathbf{u}(\mathbf{x}) - \mathbf{u}(\mathbf{x}')) \right) dA_{x'} \end{array} \right] \quad (5.7)$$

The force density vectors are written in terms of only the PD functions. It should be noted for certain weight functions the analytical form of these PD functions can be constructed and used to derive the PD equations derived by Silling (2000) and Silling et al. (2007). The status parameter, $\hat{\mu}(\mathbf{x}' - \mathbf{x})$ of a bond connecting point \mathbf{x} and \mathbf{x}' is defined as Silling et al. (2005)

$$\hat{\mu}(\mathbf{x}' - \mathbf{x}) = \begin{cases} 1, & s \leq s_c \\ 0, & s \geq s_c \end{cases} \quad (5.8)$$

in which s_c is the critical stretch. Therefore, it facilitates the removal of force density vectors from the equilibrium equations when the bond stretch, s exceeds the critical value.

Similarly, the expressions for dilatation at points \mathbf{x} and \mathbf{x}' become

$$\theta(\mathbf{x}) = \int_{H_x} \hat{\mu}(\mathbf{x}' - \mathbf{x}) (\mathbf{u}(\mathbf{x}') - \mathbf{u}(\mathbf{x})) \cdot \mathbf{g}_2(\mathbf{x}' - \mathbf{x}) dV_{x'} \quad (5.9)$$

and

$$\theta(\mathbf{x}') = \int_{H_{x'}} \hat{\mu}(\mathbf{x}' - \mathbf{x}') (\mathbf{u}(\mathbf{x}') - \mathbf{u}(\mathbf{x}')) \cdot \mathbf{g}_2(\mathbf{x}' - \mathbf{x}') dV_{x'} \quad (5.10)$$

Thus, the PD internal force vector becomes

$$\mathbf{L}^{PD} = \int_{H_x} \hat{\mu}(\mathbf{x}' - \mathbf{x}) \left\{ \begin{aligned} & \left(a(\theta(\mathbf{x}) - \theta(\mathbf{x}')) \mathbf{g}_2(\mathbf{x}, \xi) + \mu \bar{\mathbf{S}}(\mathbf{x}, \xi) (\mathbf{u}(\mathbf{x}') - \mathbf{u}(\mathbf{x})) \right) \\ & - \ell^2 \left(a(\theta(\mathbf{x}) - \theta(\mathbf{x}')) \mathbf{g}_3(\mathbf{x}, \xi) + \mu \bar{\mathbf{Q}}(\mathbf{x}, \xi) (\mathbf{u}(\mathbf{x}') - \mathbf{u}(\mathbf{x})) \right) \end{aligned} \right\} dA_{x'} \quad (5.11)$$

with

$$\bar{\mathbf{S}}(\mathbf{x}, \mathbf{x}') = \frac{\mathbf{S}(\xi) + \mathbf{S}(-\xi)}{2} \quad (5.12)$$

and

$$\bar{\mathbf{Q}}(\mathbf{x}, \mathbf{x}') = \frac{\mathbf{Q}(\xi) + \mathbf{Q}(-\xi)}{2} \quad (5.13)$$

It is worth noting that $\bar{\mathbf{S}}(\mathbf{x}, \mathbf{x}') = \mathbf{S}(\xi) = \mathbf{S}(-\xi)$ and $\bar{\mathbf{Q}}(\mathbf{x}, \mathbf{x}') = \mathbf{Q}(\xi) = \mathbf{Q}(-\xi)$ for a material point with a complete horizon. This internal force vector at material points with incomplete horizons does not require any surface correction. Under plane strain and plane stress conditions with a Poisson's ratio of 1/4 and 1/3, respectively, the PD internal force vector reduces to

$$\mathbf{L}^{PD} = \int_{H_x} (\mathbf{t}(\mathbf{x}) - \mathbf{t}(\mathbf{x}')) dV_{x'} = \int_{H_x} \hat{\mu}(\mathbf{x}' - \mathbf{x}) \mu (\bar{\mathbf{S}}(\mathbf{x}, \mathbf{x}') - \ell^2 \bar{\mathbf{Q}}(\mathbf{x}, \mathbf{x}')) (\mathbf{u}(\mathbf{x}') - \mathbf{u}(\mathbf{x})) dV_{x'} \quad (5.14)$$

The bond force $\mathbf{f}(\mathbf{x}) = \mathbf{t}(\mathbf{x}) - \mathbf{t}(\mathbf{x}')$ can be expressed as

$$\mathbf{f}(\mathbf{u}' - \mathbf{u}, \mathbf{x}' - \mathbf{x}) = \hat{\mu}(\mathbf{x}' - \mathbf{x}) \mu (\bar{\mathbf{S}}(\mathbf{x}, \mathbf{x}') - \ell^2 \bar{\mathbf{Q}}(\mathbf{x}, \mathbf{x}')) (\mathbf{u}(\mathbf{x}') - \mathbf{u}(\mathbf{x})) \quad (5.15)$$

The bond force vector for bond-based PD is depicted in Fig. 9.

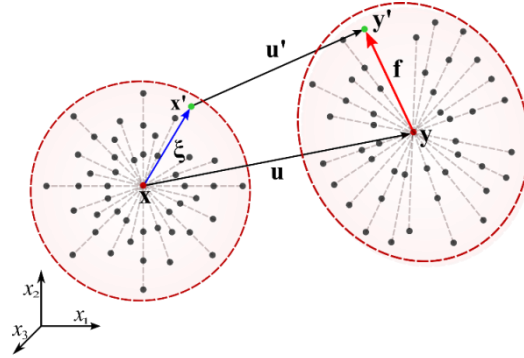


Figure 9. Force density vectors in PD: BB

5.2 Homogeneous deformation

Under homogeneous deformation, the internal force vector should be zero in the bulk region. This condition arises because, in a homogeneously deformed material, every part of the bulk region experiences uniform strain and stress distributions, leading to a state of internal equilibrium. In this state, the forces between neighboring particles or points balance out perfectly, resulting in no net internal force within the bulk. This equilibrium condition is a fundamental aspect of continuum mechanics and ensures that the material remains stable and behaves predictably under uniform deformation conditions. Thus, the requirement for the internal force vector to be zero in the bulk region under homogeneous deformation is a crucial factor in validating the consistency and accuracy of any mechanical model, including those using PD theory.

The analytical derivatives in Eqs. (3.36), (3.37), and (3.38) can be substituted into Eq. (2.13) to construct the SG contribution to the governing equation for a material point with a symmetric

domain of interaction. The bond force vector for the bond-based formulation ($a=0$) can then be determined to be

$$\mathbf{f}^{BBSG} = \mu \ell^2 \left(\frac{480}{h\pi\delta^5} \frac{(\boldsymbol{\xi} \otimes \boldsymbol{\xi})}{|\boldsymbol{\xi}|^2} (\mathbf{u}(\mathbf{x}') - \mathbf{u}(\mathbf{x})) \frac{\boldsymbol{\xi}}{|\boldsymbol{\xi}|} + \frac{80}{h\pi\delta^5} (\mathbf{u}(\mathbf{x}') - \mathbf{u}(\mathbf{x})) \frac{\boldsymbol{\xi}}{|\boldsymbol{\xi}|} \right) \quad (5.16)$$

For homogeneous deformation

$$(\mathbf{u}(\mathbf{x}') - \mathbf{u}(\mathbf{x})) = s_0 \boldsymbol{\xi} \quad (5.17)$$

where s_0 is the stretch. Simplifying using the identity $(\mathbf{a} \otimes \mathbf{b})\mathbf{c} = (\mathbf{b} \cdot \mathbf{c})\mathbf{a}$ leads to

$$\mathbf{f}^{BBSG} = \mu \ell^2 \frac{560}{h\pi\delta^5} s_0 \frac{\boldsymbol{\xi}}{|\boldsymbol{\xi}|} \quad (5.18)$$

Integrating \mathbf{f} over the symmetric domain of interaction leads to the internal force vector as

$$\mathbf{L}^{BBSG}(\mathbf{x}) = \int_{H_x} \mu \ell^2 \frac{560}{h\pi\delta^5} s_0 \frac{\boldsymbol{\xi}}{|\boldsymbol{\xi}|} dV_x. \quad (5.19)$$

Switching to polar coordinates with $\boldsymbol{\xi} = |\boldsymbol{\xi}| \begin{bmatrix} \cos \theta \\ \sin \theta \end{bmatrix}$ allows the integration to be carried out as

$$\mathbf{L}^{BBSG}(\mathbf{x}) = \mu \ell^2 \frac{560}{h\pi\delta^5} s_0 \int_0^\delta \int_0^{2\pi} |\boldsymbol{\xi}| \begin{bmatrix} \cos \theta \\ \sin \theta \end{bmatrix} d\theta d|\boldsymbol{\xi}| = \begin{bmatrix} 0 \\ 0 \end{bmatrix} \quad (5.20)$$

The force density vectors, $\mathbf{t}(\mathbf{x})$ and $\mathbf{t}(\mathbf{x}')$ for the OSB formulation can be shown to be

$$\mathbf{t}^{OSBSG}(\mathbf{x}) = \left(a \frac{32}{h\pi\delta^4} \frac{1}{|\boldsymbol{\xi}|} \theta(\mathbf{x}) \frac{\boldsymbol{\xi}}{|\boldsymbol{\xi}|} + \mu \left(\frac{240}{h\pi\delta^5} \frac{(\boldsymbol{\xi} \otimes \boldsymbol{\xi})}{|\boldsymbol{\xi}|^2} \frac{(\mathbf{u}(\mathbf{x}') - \mathbf{u}(\mathbf{x}))}{|\boldsymbol{\xi}|} + \frac{40}{h\pi\delta^5} \frac{(\mathbf{u}(\mathbf{x}') - \mathbf{u}(\mathbf{x}))}{|\boldsymbol{\xi}|} \right) \right) \quad (5.21a)$$

and

$$\mathbf{t}^{OSBSG}(\mathbf{x}') = \left(a \frac{32}{h\pi\delta^4} \frac{1}{|\boldsymbol{\xi}|} \theta(\mathbf{x}') \frac{\boldsymbol{\xi}'}{|\boldsymbol{\xi}'|} + \mu \left(\frac{240}{h\pi\delta^5} \frac{(\boldsymbol{\xi} \otimes \boldsymbol{\xi})}{|\boldsymbol{\xi}|^2} \frac{(\mathbf{u}(\mathbf{x}) - \mathbf{u}(\mathbf{x}'))}{|\boldsymbol{\xi}|} + \frac{40}{h\pi\delta^5} \frac{(\mathbf{u}(\mathbf{x}) - \mathbf{u}(\mathbf{x}'))}{|\boldsymbol{\xi}|} \right) \right) \quad (5.21b)$$

When subjected to a homogeneous deformation

$$\theta(\mathbf{x}') = \theta(\mathbf{x}) = 2s_0 \quad \text{for 2D} \quad (5.22)$$

The difference between the force density vectors can be simplified to

$$\mathbf{t}^{OSBSG}(\mathbf{x}) - \mathbf{t}^{OSBSG}(\mathbf{x}') = a \frac{128}{h\pi\delta^4} \frac{1}{|\xi|} s_0 \frac{\xi}{|\xi|} + \mu\ell^2 \frac{560}{h\pi\delta^5} s_0 \frac{\xi}{|\xi|} \quad (5.23)$$

Integrating over a symmetric domain of interaction in polar coordinates results in the internal force vector as

$$\mathbf{L}^{OSBSG}(\mathbf{x}) = a\ell^2 s_0 \frac{128}{h\pi\delta^4} \int_0^\delta \int_0^{2\pi} \begin{bmatrix} \cos\theta \\ \sin\theta \end{bmatrix} d\theta d|\xi| + \mu\ell^2 \frac{560}{h\pi\delta^5} s_0 \int_0^\delta \int_0^{2\pi} \begin{bmatrix} \cos\theta \\ \sin\theta \end{bmatrix} d\theta d|\xi| = \begin{bmatrix} 0 \\ 0 \end{bmatrix} \quad (5.24)$$

The derivation of the force density vectors can be found in Appendix C.

5.2 Numerical implementation

The domain Ω is discretized uniformly with K number of PD points. The position of PD point k is denoted by $\mathbf{x}_{(k)}$ and its corresponding volume is denoted by $V_{(k)}$. The discrete form of PD equilibrium equations, i.e., Eq. (2.1) at point $\mathbf{x}_{(k)} \in \Omega$ can be expressed as

$$\rho\ddot{\mathbf{u}}_{(k)} = \mathbf{L}_{(k)} + \mathbf{b}_{(k)} = \sum_{j=1}^K (\mathbf{t}_{(k)(j)} - \mathbf{t}_{(j)(k)}) V_{(j)} + \mathbf{b}_{(k)} \quad \text{with } \mathbf{x}_{(k)} \in \Omega \quad \text{and } k = 1, \dots, K \quad (5.25)$$

5.3 Boundary conditions

In order to impose the boundary conditions expressed in Eq. (2.5) in the PD framework, a fictitious domain $\tilde{\Omega}$ of width δ is introduced around the actual domain Ω and is discretized with K_j PD points. As shown in Fig.10, the position of a PD point in the real domain is denoted by \mathbf{x}_α with $\alpha = k, j, p$ and q . Its projection on the boundary, $\partial\Omega$ is denoted by $\bar{\mathbf{x}}_\alpha$ and its reflection about the boundary in the fictitious domain is denoted by $\tilde{\mathbf{x}}_\alpha$ with $\alpha = k, j, p$ and q . The boundary conditions on the displacements are applied by enforcing the known values on points $\tilde{\mathbf{x}}_\alpha$ in the fictitious domain.

The boundary conditions on displacement gradients are applied in a nonlocal sense by introducing a constraint equation involving a set of points close to the boundary in the real and fictitious domains. It should be noted that this method is different than the Lagrange multiplier method explained in section 4.3. This strategy to enforce the boundary conditions includes extra layers of material points. Both methods are suitable for one- and two- dimensional studies.

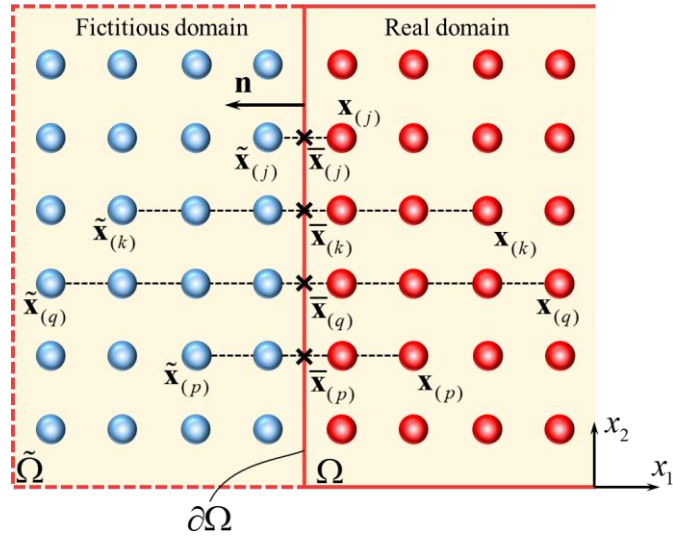


Figure 10. Fictitious PD points, $\tilde{\mathbf{x}}_\alpha$ around the actual PD points, \mathbf{x}_α in the real domain for the imposition of boundary conditions on the boundary point $\bar{\mathbf{x}}_\alpha$ with unit normal \mathbf{n}

5.3.1 Displacement boundary conditions

The applied displacement, $\mathbf{u}^*(\bar{\mathbf{x}}_\alpha, t)$ on the boundary is enforced by considering points $\tilde{\mathbf{x}}_\alpha$ in the fictitious region close to the boundary as

$$\mathbf{u}(\tilde{\mathbf{x}}_\alpha, t) = \mathbf{u}^*(\bar{\mathbf{x}}_\alpha, t) \quad (5.26)$$

5.3.2 Displacement gradient boundary condition

At a point $\bar{\mathbf{x}}_\alpha$ on the boundary, with unit normal vector, \mathbf{n} , the applied displacement gradient, $\bar{\mathbf{u}}^*(\bar{\mathbf{x}}_\alpha, t)$ is enforced as

$$\left(\nabla \mathbf{u}(\bar{\mathbf{x}}_{(k)}, t)\right) \mathbf{n} = \bar{\mathbf{u}}^*(\bar{\mathbf{x}}_k, t) \quad (5.27)$$

For a 2D analysis, this equation can be expressed in component form as

$$\begin{bmatrix} u_{1,1} & u_{1,2} \\ u_{2,1} & u_{2,2} \end{bmatrix} \begin{Bmatrix} n_1 \\ n_2 \end{Bmatrix} = \begin{Bmatrix} u_{1,1}n_1 + u_{1,2}n_2 \\ u_{2,1}n_1 + u_{2,2}n_2 \end{Bmatrix} = \begin{Bmatrix} \bar{u}_1^* \\ \bar{u}_2^* \end{Bmatrix} \quad (5.28)$$

Using the forward difference scheme, the first order derivative of displacement components in Eq. (5.28) can be approximated by considering the displacement components of points, \mathbf{x}_k and $\tilde{\mathbf{x}}_k$ in the real and fictitious regions, respectively, close to the boundary. Thus, the displacement gradient boundary condition is enforced in a nonlocal sense through the constraint equations as

$$\left\{ \begin{array}{l} \frac{u_1(\tilde{\mathbf{x}}_\alpha, t) - u_1(\mathbf{x}_\alpha, t)}{\Delta x_{1\alpha}} n_1 + \frac{u_1(\tilde{\mathbf{x}}_\alpha, t) - u_1(\mathbf{x}_\alpha, t)}{\Delta x_{2\alpha}} n_2 \\ \frac{u_2(\tilde{\mathbf{x}}_\alpha, t) - u_2(\mathbf{x}_\alpha, t)}{\Delta x_{1\alpha}} n_1 + \frac{u_2(\tilde{\mathbf{x}}_\alpha, t) - u_2(\mathbf{x}_\alpha, t)}{\Delta x_{2\alpha}} n_2 \end{array} \right\} = \begin{Bmatrix} \bar{u}_1^* \\ \bar{u}_2^* \end{Bmatrix} \quad (5.29)$$

with $\Delta x_{1\alpha} = \tilde{x}_{1\alpha} - x_{1\alpha}$, $\Delta x_{2\alpha} = \tilde{x}_{2\alpha} - x_{2\alpha}$ and $\alpha = k, k-1, k-2, k-3$. For a boundary with a unit normal $\mathbf{n}^T = \{0, \pm 1\}$ as shown in Fig. 11, Eq. (5.29) simplifies to

$$\pm \left\{ \begin{array}{l} \frac{u_1(\tilde{\mathbf{x}}_\alpha, t) - u_1(\mathbf{x}_\alpha, t)}{\Delta x_{2\alpha}} \\ \frac{u_2(\tilde{\mathbf{x}}_\alpha, t) - u_2(\mathbf{x}_\alpha, t)}{\Delta x_{2\alpha}} \end{array} \right\} = \begin{Bmatrix} \bar{u}_1^* \\ \bar{u}_2^* \end{Bmatrix} \quad \text{with } \alpha = k, k-1, k-2, k-3, k-4 \quad (5.30)$$

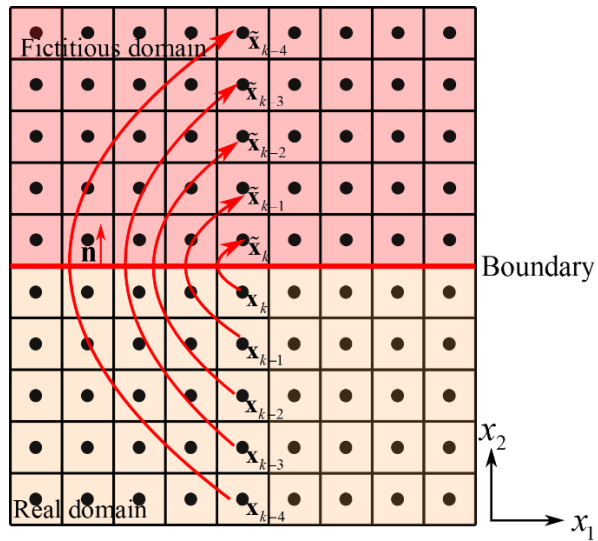


Figure 11. A set of points in the real and fictitious domains for computing the first order derivatives along the unit normal $\mathbf{n}^T = \{0, \pm 1\}$ in a 2D model

For a 1D model with $u_1 = 0$ as shown in Fig. 12, Eq. (5.30) reduces to

$$\pm \frac{u_2(\tilde{\mathbf{x}}_\alpha, t) - u_2(\mathbf{x}_\alpha, t)}{\Delta x_{2\alpha}} = \bar{u}_2^* \quad \text{with } \alpha = k, k-1, k-2, k-3 \tag{5.31}$$

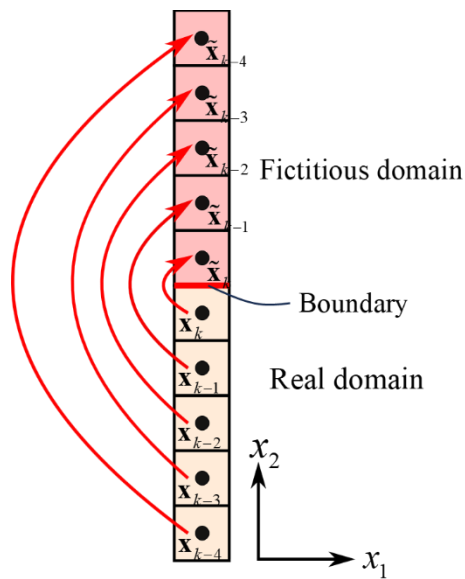


Figure 12. A set of points in the real and fictitious domains for computing the first order derivatives in a 1D model

For a boundary with a unit normal $\mathbf{n}^T = \{\pm 1, 0\}$ shown in Fig. 13, Eq. (5.29) simplifies to

$$\pm \left\{ \begin{array}{c} \frac{u_1(\tilde{\mathbf{x}}_\alpha, t) - u_1(\mathbf{x}_\alpha, t)}{\Delta x_{1\alpha}} \\ \frac{u_2(\tilde{\mathbf{x}}_\alpha, t) - u_2(\mathbf{x}_\alpha, t)}{\Delta x_{1\alpha}} \end{array} \right\} = \left\{ \begin{array}{c} \bar{u}_1^* \\ \bar{u}_2^* \end{array} \right\} \quad \text{with } \alpha = k, k-1, k-2, k-3, k-4 \quad (5.32)$$

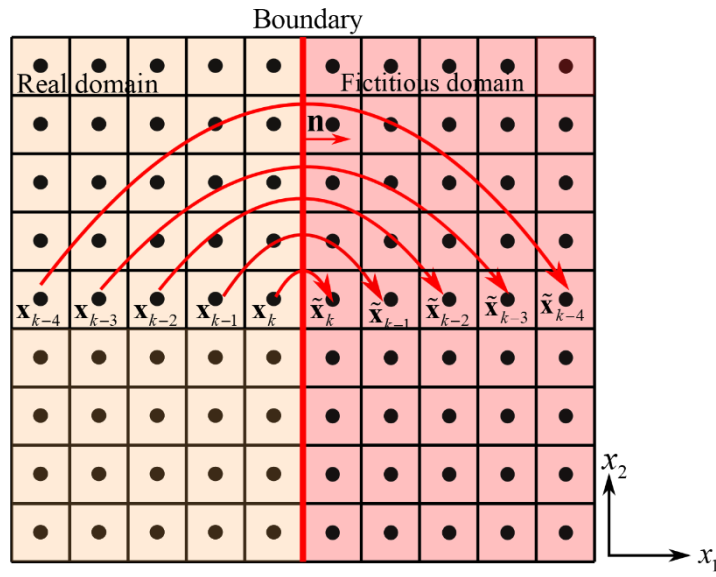


Figure 13. A set of points in the real and fictitious domains for computing the first order derivatives along the unit normal $\mathbf{n}^T = \{\pm 1, 0\}$ in a 2D model

For a 1D model with $u_2 = 0$ as shown in Fig. 14, Eq. (5.32) reduces to

$$\pm \frac{u_1(\tilde{\mathbf{x}}_\alpha, t) - u_1(\mathbf{x}_\alpha, t)}{\Delta x_{1\alpha}} = \bar{u}_1^* \quad \text{with } \alpha = k, k-1, k-2, k-3, k-4 \quad (5.33)$$

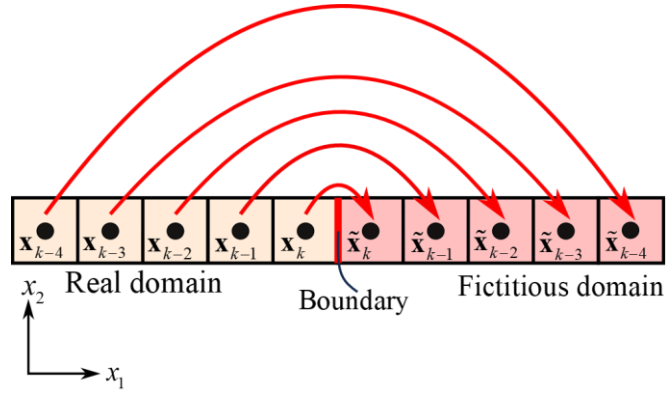


Figure 14. A set of points in the real and fictitious domains for computing the first order derivatives in a 1D model.

5.3.3 Traction boundary condition

As shown in Fig. 15, the traction, $\mathbf{T}^*(\bar{\mathbf{x}}_k, t)$ at point $\bar{\mathbf{x}}_k$ on the boundary with unit normal $\mathbf{n}_{(k)}$ is enforced by applying a distributed body load, $\mathbf{b}^*(\mathbf{x}_k)$ and $\mathbf{b}^*(\tilde{\mathbf{x}}_{(\alpha)})$ on points $\mathbf{x}_{(k)}$ and $\tilde{\mathbf{x}}_{(\alpha)}$, in the first layer of real and fictitious domains, respectively, as

$$\mathbf{b}^*(\mathbf{x}_k, t)\Delta x + \sum_{\alpha} \mathbf{b}^*(\tilde{\mathbf{x}}_{(\alpha)}, t)\Delta x = \mathbf{T}^*(\bar{\mathbf{x}}_k, t) \quad \text{with } \alpha = k, k-1, k-2, k-3, k-4 \quad (5.34)$$

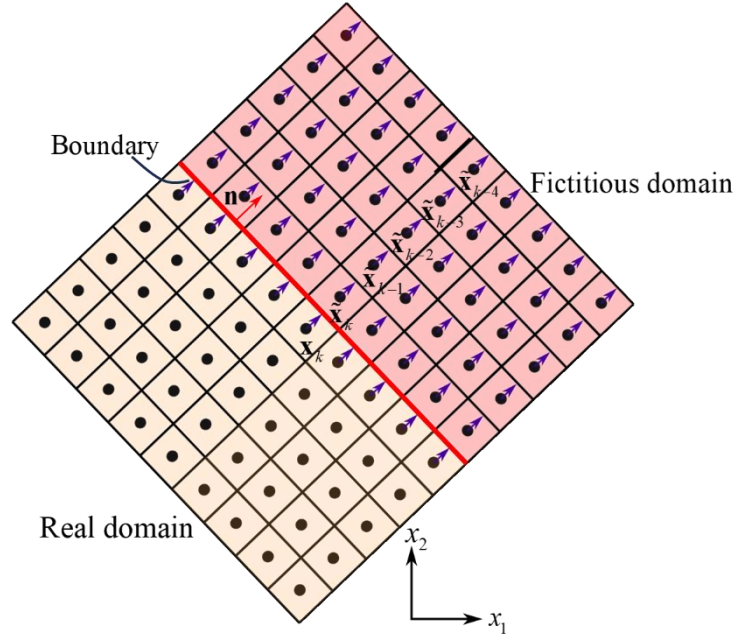


Figure 15. A set of points in the real and fictitious domains for applying the traction condition in the form of a body load along the boundary with unit normal \mathbf{n}

For uniform body load, $\mathbf{b}^*(\mathbf{x}_k) = \mathbf{b}^*(\tilde{\mathbf{x}}_{(\alpha)})$, Eq. (5.34) can be rewritten in component form as

$$\begin{cases} b_1^*(\mathbf{x}_k, t) \\ b_2^*(\mathbf{x}_k, t) \end{cases} = \begin{cases} b_1^*(\tilde{\mathbf{x}}_{(\alpha)}, t) \\ b_2^*(\tilde{\mathbf{x}}_{(\alpha)}, t) \end{cases} = \frac{1}{5\Delta x} \begin{cases} T_1^*(\bar{\mathbf{x}}_k, t) \\ T_2^*(\bar{\mathbf{x}}_k, t) \end{cases} \text{ with } \alpha = k, k-1, k-2, k-3, k-4 \quad (5.35)$$

5.3.4 Double traction boundary condition

The double traction condition at point $\bar{\mathbf{x}}_k$ on the boundary with unit normal \mathbf{n} , is enforced as

$$\ell^2 \left((\nabla \boldsymbol{\sigma}(\bar{\mathbf{x}}_{(k)}, t)) \mathbf{n} \right) \mathbf{n} = \bar{\mathbf{T}}^*(\bar{\mathbf{x}}_{(k)}, t) \quad (5.36)$$

In component form, this equation can be expressed as

$$\ell^2 \begin{bmatrix} \sigma_{11,1} n_1 + \sigma_{11,2} n_2 & \sigma_{12,1} n_1 + \sigma_{12,2} n_2 \\ \sigma_{21,1} n_1 + \sigma_{21,2} n_2 & \sigma_{22,1} n_1 + \sigma_{22,2} n_2 \end{bmatrix} \begin{Bmatrix} n_1 \\ n_2 \end{Bmatrix} = \ell^2 \begin{Bmatrix} \sigma_{11,1} n_1^2 + (\sigma_{11,2} + \sigma_{12,1}) n_1 n_2 + \sigma_{12,2} n_2^2 \\ \sigma_{21,1} n_1^2 + (\sigma_{21,2} + \sigma_{22,1}) n_1 n_2 + \sigma_{22,2} n_2^2 \end{Bmatrix} = \begin{Bmatrix} \bar{T}_1^* \\ \bar{T}_2^* \end{Bmatrix} \quad (5.37)$$

Using the linear elastic stress-strain relationship, Eq. (5.37) can be rewritten in terms of the strain components as

$$\ell^2 \begin{Bmatrix} (D_{11}\varepsilon_{11,1} + D_{12}\varepsilon_{22,1})n_1^2 + ((D_{11}\varepsilon_{11,2} + D_{12}\varepsilon_{22,2}) + D_{66}\varepsilon_{12,1})n_1n_2 + D_{66}\varepsilon_{12,2}n_2^2 \\ D_{66}\varepsilon_{21,1}n_1^2 + (D_{66}\varepsilon_{21,2} + (D_{21}\varepsilon_{11,1} + D_{22}\varepsilon_{22,1}))n_1n_2 + (D_{21}\varepsilon_{11,2} + D_{22}\varepsilon_{22,2})n_2^2 \end{Bmatrix} = \begin{Bmatrix} \bar{T}_1^* \\ \bar{T}_2^* \end{Bmatrix} \quad (5.38)$$

Invoking the kinematic relations, Eq. (5.38) can be rewritten in terms of the derivatives of displacement components as

$$\ell^2 \begin{Bmatrix} n_1^2 \begin{Bmatrix} D_{11}u_{1,11} + D_{12}u_{2,21} \\ D_{66}(u_{1,12} + u_{2,11}) \end{Bmatrix} + n_1n_2 \begin{Bmatrix} (D_{12}u_{2,22} + (D_{11} + D_{66})u_{1,21}) + D_{66}u_{2,11} \\ (D_{21}u_{1,11} + (D_{22} + D_{66})u_{2,12}) + D_{66}u_{1,22} \end{Bmatrix} \\ + n_2^2 \begin{Bmatrix} D_{66}(u_{2,21} + u_{1,22}) \\ D_{22}u_{2,22} + D_{21}u_{1,12} \end{Bmatrix} \end{Bmatrix} = \begin{Bmatrix} \bar{T}_1^* \\ \bar{T}_2^* \end{Bmatrix} \quad (5.39)$$

For a boundary with unit normal $\mathbf{n}^T = \{0, \pm 1\}$, this equation reduces to

$$\ell^2 \begin{Bmatrix} D_{66}(u_{2,12} + u_{1,22}) \\ D_{22}u_{2,22} + D_{21}u_{1,12} \end{Bmatrix} = \begin{Bmatrix} \bar{T}_1^* \\ \bar{T}_2^* \end{Bmatrix} \quad (5.40)$$

The second order derivatives appearing in Eq. (5.40) at point $\bar{\mathbf{x}}_k$ on the boundary can be approximated at point \mathbf{x}_k in the domain close to the boundary. The derivatives in the normal direction $\mathbf{n}^T = \{0, \pm 1\}$, i.e., $u_{1,22}$ and $u_{2,22}$ can be evaluated using a central finite difference approximation by considering a set of points in the real and fictitious domains shown in Fig 16 as

$$u_{1,22}(\mathbf{x}_k, t) = \frac{u_1(\tilde{\mathbf{x}}_\alpha) + u_1(\mathbf{x}_{\alpha-1}) - 2u_1(\mathbf{x}_k)}{(\Delta x_{2\alpha})^2} \quad (5.41)$$

and

$$u_{2,22}(\mathbf{x}_k, t) = \frac{u_2(\tilde{\mathbf{x}}_\alpha) + u_2(\mathbf{x}_{\alpha-1}) - 2u_2(\mathbf{x}_k)}{(\Delta x_{2\alpha})^2} \quad (5.42)$$

where $\Delta x_{2\alpha} = \tilde{x}_{2\alpha} - x_{2\alpha-1}$ and $\alpha = k, k-1, k-2, k-3, k-4$.

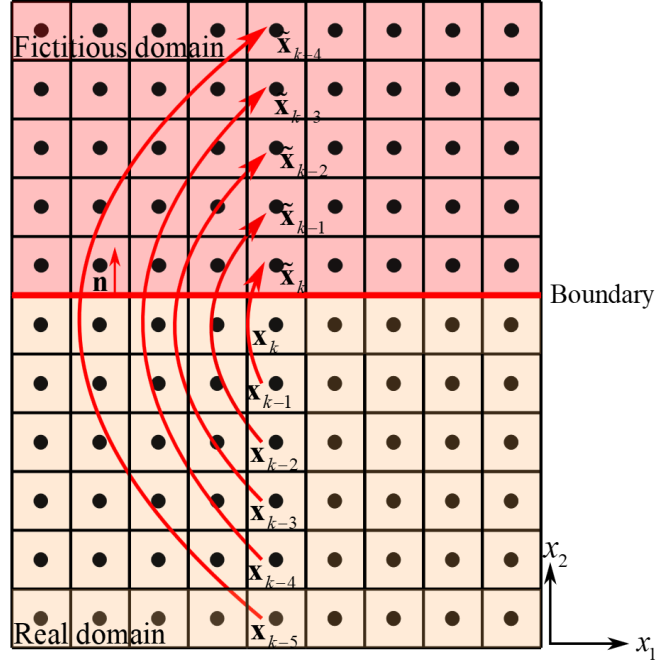


Figure 16. A set of points in the real and fictitious domains for approximating the second order derivatives in the direction of unit normal $\mathbf{n}^T = \{0, \pm 1\}$ in a nonlocal sense for a 2D model

The mixed second order derivatives in the direction of unit normal, $\mathbf{n}^T = \{0, \pm 1\}$, i.e., $u_{2,12}$ and $u_{1,12}$ are evaluated using a first order difference approximation of displacement gradients by considering a set of points in the real and fictitious domains shown in Fig 17 as

$$u_{2,12}(\mathbf{x}_k, t) = \frac{(u_2(\tilde{\mathbf{x}}_\beta) - u_2(\tilde{\mathbf{x}}_\alpha)) - (u_2(\tilde{\mathbf{x}}_{\beta-1}) - u_2(\tilde{\mathbf{x}}_{\alpha-1}))}{\Delta X_{1\beta\alpha} \Delta x_{2\alpha}} \quad (5.43)$$

and

$$u_{1,12}(\mathbf{x}_k, t) = \frac{(u_1(\tilde{\mathbf{x}}_\beta) - u_1(\tilde{\mathbf{x}}_\alpha)) - (u_1(\tilde{\mathbf{x}}_{\beta-1}) - u_1(\tilde{\mathbf{x}}_{\alpha-1}))}{\Delta X_{1\beta\alpha} \Delta x_{2\alpha}} \quad (5.44)$$

where $\Delta X_{1\beta\alpha} = x_{1\beta} - x_{1\alpha}$, $\alpha = k, k-1, k-2, k-3, k-4$ and $\beta = p, p-1, p-2, p-3, p-4$.

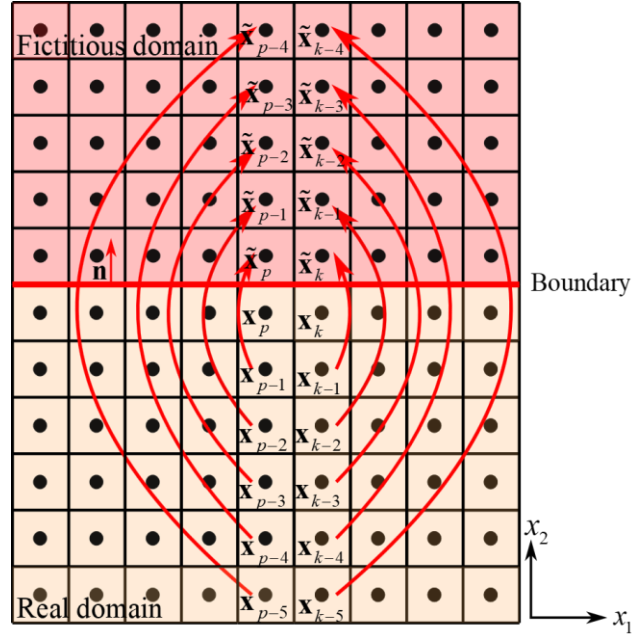


Figure 17. A set of points in the real and fictitious domains for approximating the second order mixed derivatives in the direction of unit normal $\mathbf{n}^T = \{0, \pm 1\}$ in a nonlocal sense for a 2D model

After substituting from Eqs. (5.41)-(5.44) into Eq. (5.40), the double traction condition is enforced in a nonlocal sense through the constraint equations as

$$\ell^2 D_{66} \left(\left(\frac{u_2(\tilde{\mathbf{x}}_\beta) - u_2(\tilde{\mathbf{x}}_\alpha) - u_2(\tilde{\mathbf{x}}_{\beta-1}) + u_2(\tilde{\mathbf{x}}_{\alpha-1})}{\Delta X_{1\beta\alpha} \Delta x_{2\alpha}} \right) + \left(\frac{u_1(\tilde{\mathbf{x}}_\alpha) + u_1(\mathbf{x}_{\alpha-1}) - 2u_1(\mathbf{x}_k)}{(\Delta x_{2\alpha})^2} \right) \right) = \bar{T}_1^* \quad (5.45)$$

and

$$\ell^2 \left(D_{22} \left(\frac{u_2(\tilde{\mathbf{x}}_\alpha) + u_2(\mathbf{x}_{\alpha-1}) - 2u_2(\mathbf{x}_k)}{(\Delta x_{2\alpha})^2} \right) + D_{21} \left(\frac{u_1(\tilde{\mathbf{x}}_\beta) - u_1(\tilde{\mathbf{x}}_\alpha) - u_1(\tilde{\mathbf{x}}_{\beta-1}) + u_1(\tilde{\mathbf{x}}_{\alpha-1})}{\Delta X_{1\beta\alpha} \Delta x_{2\alpha}} \right) \right) = \bar{T}_2^* \quad (5.46)$$

For a 1D model with $u_1 = 0$, Eq. (5.40) simplifies to

$$\ell^2 \begin{Bmatrix} D_{66} u_{2,12} \\ D_{22} u_{2,22} \end{Bmatrix} = \begin{Bmatrix} \bar{T}_1^* \\ \bar{T}_2^* \end{Bmatrix} \quad (5.47)$$

Using a set of points in the real and fictitious domains shown in Fig. 18 and after substituting from Eqs. (5.42) and (5.43) into Eq (5.47), the double traction condition is enforced in a nonlocal sense through the constraint equations as

$$\ell^2 \left\{ \begin{array}{l} D_{66} \left(\frac{u_2(\tilde{\mathbf{x}}_\beta) - u_2(\tilde{\mathbf{x}}_\alpha) - u_2(\tilde{\mathbf{x}}_{\beta-1}) + u_2(\tilde{\mathbf{x}}_{\alpha-1})}{\Delta X_{1\beta\alpha} \Delta x_{2\alpha}} \right) \\ D_{22} \left(\frac{u_2(\tilde{\mathbf{x}}_\alpha) + u_2(\mathbf{x}_{\alpha-1}) - 2u_2(\mathbf{x}_k)}{(\Delta x_{2\alpha})^2} \right) \end{array} \right\} = \begin{Bmatrix} \bar{T}_1^* \\ \bar{T}_2^* \end{Bmatrix} \quad (5.48)$$

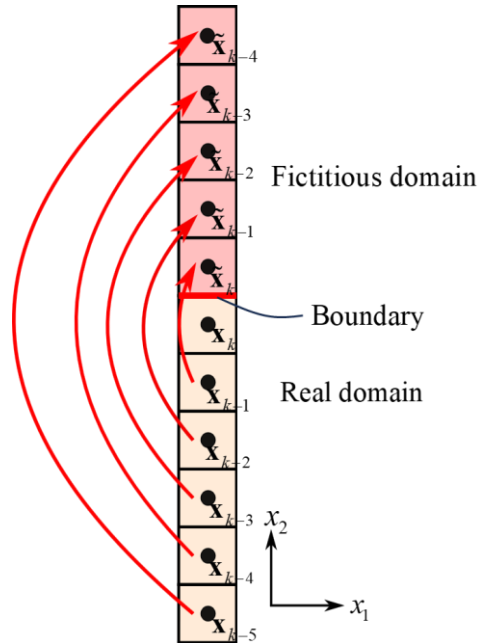


Figure 18. A set of points in the real and fictitious domains for computing the second order derivatives in a nonlocal sense for a 1D model

Similarly, the double traction conditions on a boundary with normal $\mathbf{n}^T = \{\pm 1, 0\}$, Eq. (5.39) reduces to

$$\ell^2 \left\{ \begin{array}{l} D_{11}u_{1,11} + D_{12}u_{2,21} \\ D_{66}(u_{1,21} + u_{2,11}) \end{array} \right\} = \begin{Bmatrix} \bar{T}_1^* \\ \bar{T}_2^* \end{Bmatrix} \quad (5.49)$$

The derivatives in the direction of unit normal $\mathbf{n}^T = \{\pm 1, 0\}$, i.e., $u_{1,11}$ and $u_{2,11}$ can be evaluated by using a central finite difference approximation by considering a set of points in the real and fictitious domains shown in Fig. 19 as

$$u_{1,11}(\mathbf{x}_k, t) = \frac{u_1(\tilde{\mathbf{x}}_\alpha) + u_1(\mathbf{x}_{\alpha-1}) - 2u_1(\mathbf{x}_k)}{(\Delta x_{1\alpha})^2} \quad (5.50)$$

and

$$u_{2,11}(\mathbf{x}_k, t) = \frac{u_2(\tilde{\mathbf{x}}_\alpha) + u_2(\mathbf{x}_{\alpha-1}) - 2u_2(\mathbf{x}_k)}{(\Delta x_{1\alpha})^2} \quad (5.51)$$

where $\Delta x_{1\alpha} = \tilde{x}_{1\alpha} - x_{1\alpha}$ with $\alpha = k, k-1, k-2, k-3, k-4$.

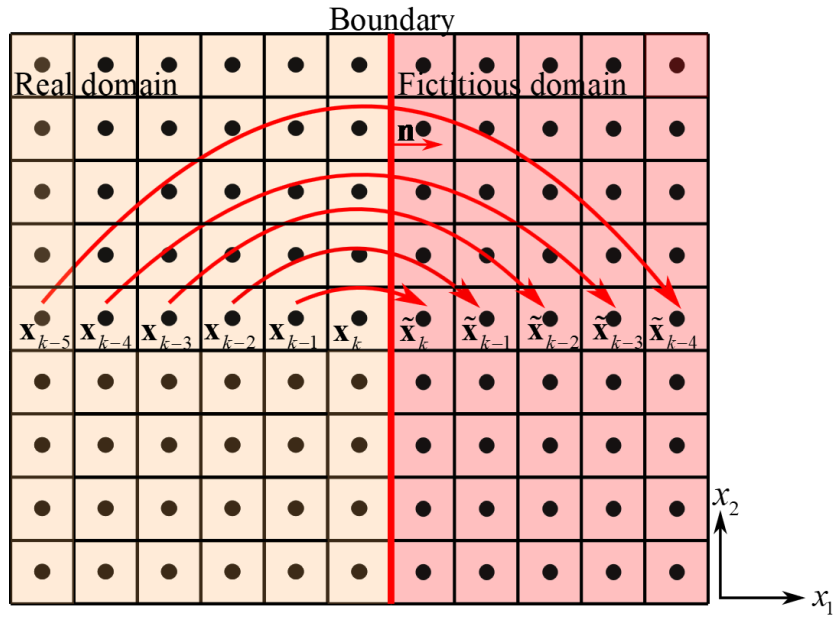


Figure 19. A set of points in the real and fictitious domains for approximating the second order derivatives in the direction of unit normal $\mathbf{n}^T = \{\pm 1, 0\}$ in a nonlocal sense for a 2D model

The mixed second order derivatives in the direction of unit direction, $\mathbf{n}^T = \{\pm 1, 0\}$, i.e., $u_{2,21}$ and $u_{1,21}$ are evaluated using a first order difference approximation of displacement gradients by considering a set of points in the real and fictitious domains shown in Fig. 20 as

$$u_{2,21}(\mathbf{x}_k, t) = \frac{(u_2(\tilde{\mathbf{x}}_\beta) - u_2(\tilde{\mathbf{x}}_\alpha)) - (u_2(\tilde{\mathbf{x}}_{\beta-1}) - u_2(\tilde{\mathbf{x}}_{\alpha-1}))}{\Delta X_{2\beta\alpha} \Delta x_{1\alpha}} \quad (5.52)$$

and

$$u_{1,21}(\mathbf{x}_k, t) = \frac{(u_1(\tilde{\mathbf{x}}_\beta) - u_1(\tilde{\mathbf{x}}_\alpha)) - (u_1(\tilde{\mathbf{x}}_{\beta-1}) - u_1(\tilde{\mathbf{x}}_{\alpha-1}))}{\Delta X_{2\beta\alpha} \Delta x_{1\alpha}} \quad (5.53)$$

where $\Delta X_{2\beta\alpha} = x_{2p} - x_{2k}$ with $\alpha = k, k-1, k-2, k-3, k-4$ and $\beta = p, p-1, p-2, p-3, p-4$.

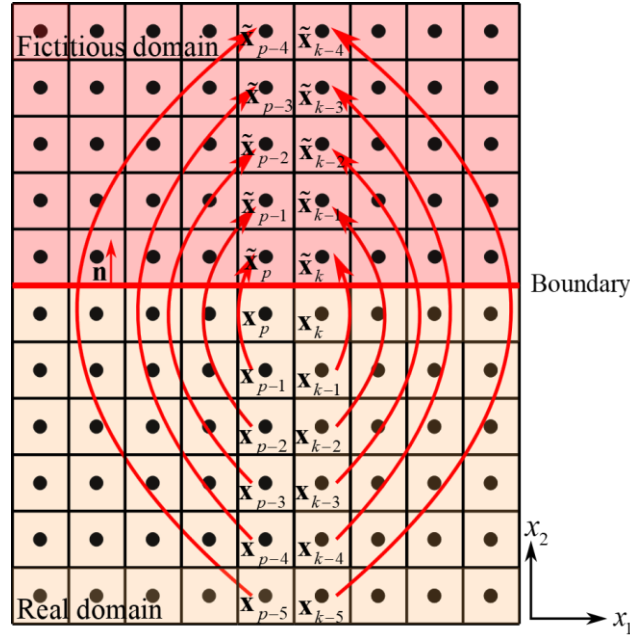


Figure 20. A set of domain and fictitious points for computing the mixed second order derivatives in the direction of unit normal $\mathbf{n}^T = \{\pm 1, 0\}$ in a nonlocal sense for a 2D model

After substituting from Eqs. (5.50)-(5.53) into Eq. (5.49), the double traction condition is enforced in a nonlocal sense through the constraint equations as

$$\ell^2 \left(D_{11} \left(\frac{u_1(\tilde{\mathbf{x}}_\alpha) + u_1(\mathbf{x}_{\alpha-1}) - 2u_1(\mathbf{x}_k)}{(\Delta x_{1\alpha})^2} \right) + D_{12} \left(\frac{(u_2(\tilde{\mathbf{x}}_\beta) - u_2(\tilde{\mathbf{x}}_\alpha)) - (u_2(\tilde{\mathbf{x}}_{\beta-1}) - u_2(\tilde{\mathbf{x}}_{\alpha-1}))}{\Delta X_{2\beta\alpha} \Delta x_{1\alpha}} \right) \right) = \bar{T}_1^* \quad (5.54)$$

and

$$\ell^2 D_{66} \left(\left(\frac{(u_1(\tilde{\mathbf{x}}_\beta) - u_1(\tilde{\mathbf{x}}_\alpha)) - (u_1(\tilde{\mathbf{x}}_{\beta-1}) - u_1(\tilde{\mathbf{x}}_{\alpha-1}))}{\Delta X_{2\beta\alpha} \Delta x_{1\alpha}} \right) + \left(\frac{u_2(\tilde{\mathbf{x}}_\alpha) + u_2(\mathbf{x}_{\alpha-1}) - 2u_2(\mathbf{x}_k)}{(\Delta x_{1\alpha})^2} \right) \right) = \bar{T}_2^* \quad (5.55)$$

For a 1D model with $u_2 = 0$, Eq. (5.49) simplifies to

$$\ell^2 \begin{Bmatrix} D_{11}u_{1,11} \\ D_{66}u_{1,21} \end{Bmatrix} = \begin{Bmatrix} \bar{T}_1^* \\ \bar{T}_2^* \end{Bmatrix} \quad (5.56)$$

Using a set of points in the real and fictitious domains shown in Fig. 21 and after substituting from Eqs. (5.50) and (5.53) into Eq (5.56), the double traction condition is enforced in a nonlocal sense through the constraint equations as

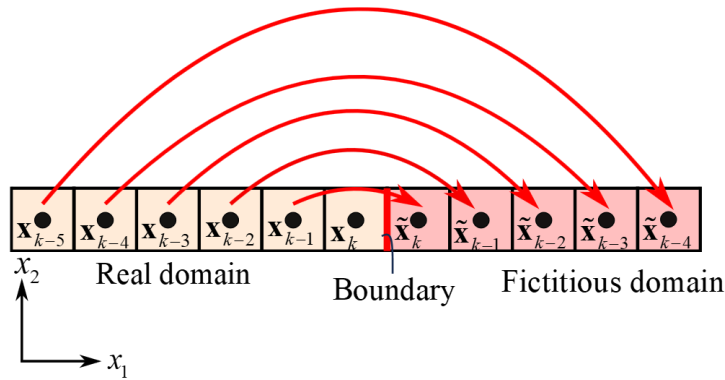


Figure 21. A set of points in the real and fictitious domains for computing the second order derivatives in a nonlocal sense for a 1D model

$$\ell^2 \begin{Bmatrix} D_{11} \left(\frac{u_1(\tilde{\mathbf{x}}_\alpha) + u_1(\tilde{\mathbf{x}}_{\alpha-1}) - 2u_1(\mathbf{x}_k)}{(\Delta x_{1\alpha})^2} \right) \\ D_{66} \left(\frac{(u_1(\tilde{\mathbf{x}}_\beta) - u_1(\tilde{\mathbf{x}}_\alpha)) - (u_1(\tilde{\mathbf{x}}_{\beta-1}) - u_1(\tilde{\mathbf{x}}_{\alpha-1}))}{\Delta X_{2\beta\alpha} \Delta x_{1\alpha}} \right) \end{Bmatrix} = \begin{Bmatrix} \bar{T}_1^* \\ \bar{T}_2^* \end{Bmatrix} \quad (5.57)$$

In the case of a curved boundary, the proposed approach is still valid since the unit normal of a material point on the curved boundary can be evaluated. In the case of a traction boundary condition, it is applied in the form of a distributed body load and can be decomposed into its components and directly implemented. In the case of a double traction, the components of the unit normal vector at a material point located on a curved boundary surface can be determined a priori. Therefore, the proposed approach is applicable to curved boundaries.

5.4 Numerical results

For the solution of the governing equations, an in-house research code is developed to implement PDSG for quasi-static analysis. The non-classical boundary conditions required for higher order PDSG models are imposed in the form of constraint equations using the fictitious layer approach. The accuracy of this implementation is first verified by considering the one-dimensional response of a microscale and nanoscale film under quasi-static loading due to tensile force and tangential displacement. Subsequently, the capability of the present approach is demonstrated by considering the two-dimensional response of a square nanoscale film with and without a crack under tensile force. The Young's modulus, Poisson's ratio, and density of the material are specified as $E = 1.0 \times 10^{-6}$ N/nm², $\nu = 0$ or $\nu = 0.333$, and $\rho = 1370$ kg/m³, respectively (Limkatanyu et al., 2022). All simulations, except the thin film subjected to tangential displacement, use the same material parameters and are performed for an elastic response under plane stress conditions.

The internal length scale parameter ℓ is a material property. Usually, its value is taken from experiments. In the PD framework, the value of ℓ in the strain gradient model is known a priori and the non-locality required for handling discontinuities is introduced through the horizon size $\delta = 5.015\Delta x$ as a function of discretization size. The PDSG predictions are validated against the analytical solutions to establish the efficacy of the discretization parameters and the convergence of the results.

5.4.1 Quasi-static PDSG model of CNT under tensile force

The differences between the analysis performed in section 4.4.1 and 5.4.1 are the imposition of the boundary conditions. Section 4.4.1 employs Lagrange multipliers to enforce the higher order boundary conditions, whereas section 5.4.1 uses finite difference techniques to determine constraint equations. As shown in Fig. 22, a carbon nano tube (CNT) is clamped at the left end and subjected to an axial tensile force, $F_0 = 100 \times 10^{-9}$ N on the right end. The length of CNT is specified as $L = 10$ nm. Its annular cross-sectional area is $A = \pi(r_o^2 - r_i^2)$ with $r_o = 1.17$ nm, $r_i = 1$ nm. The internal length parameter, ℓ is chosen as 0.5 and 2 nm. First, the CNT is modeled as a 1D solid bar as

shown in Fig. 22a with the same cross-sectional area. The inner and outer radii that define the tube are only used to calculate the cross-sectional area. The PDSG model of a bar and enforcement of non-classical boundary conditions are established against the analytical solution as the PD horizon approaches zero. The analytical solution to the equilibrium equation with SG elasticity, i.e., $\ell \neq 0$ concerns only 1D bar models. To establish the validity of the 2D PDSG model, the 1D solution is mimicked through a 2D model of a panel by enforcing zero displacement in the vertical direction along with the appropriate classical and non-classical boundary conditions on all four edges. Subsequently, the CNT is modeled as a 2D nanoscale carbon film as shown in Fig. 22b. The volume of the tube is equal between one and two-dimensional analyses. The film having a width of $W = 0.1$ nm has a thickness of $h = 11.5893$ nm. The thickness variable is neither necessary nor used in the 2D analysis. The grid spacing is specified as $\Delta x = L/100$. For the 1D model, the boundary conditions are applied on the left and right ends of the bar. Figure 23 shows the discretization of these models for 1D and 2D analyses. The real domain is extended on the left and right ends by fictitious regions with a size of δ .

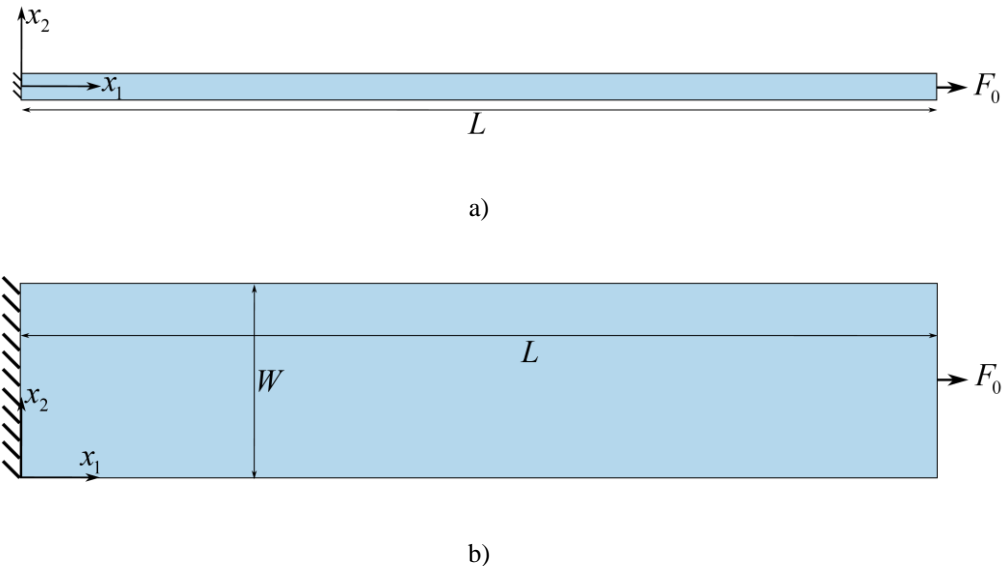


Figure 22. Carbon nanotube idealization as a nanoscale film for: a) one-dimensional analysis, and b) two-dimensional analysis

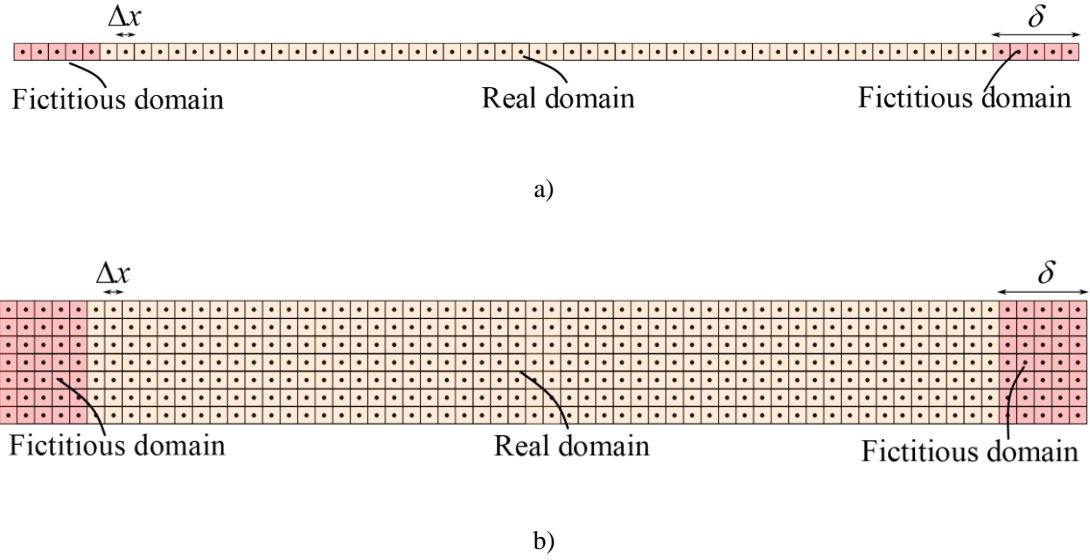


Figure 23. PD discretization with uniform grid spacing: a) 1D analysis, and b) 2D analysis

The classical boundary conditions are expressed in the form

$$u_1(x_1 = 0) = 0 \quad (5.58)$$

and

$$\sigma(x_1 = L) = E \left[\frac{\partial u_1(x_1 = L)}{\partial x_1} - \ell^2 \frac{\partial^3 u_1(x_1 = L)}{\partial x_1^3} \right] = \frac{F_0}{A} \quad (5.59)$$

The nonclassical boundary conditions can be specified as Limkatanyu et al. (2022)

$$\frac{\partial u_1(x_1 = L)}{\partial x_1} = 0 \quad (5.60)$$

and

$$E \ell^2 \frac{\partial^2 u_1(x_1 = 0)}{\partial x_1^2} = 0 \quad (5.61)$$

The displacement boundary condition, Eq. (5.58) is enforced through Eq. (5.26). The values of nodes in the fictitious region are specified directly as

$$u_1(\tilde{\mathbf{x}}_\alpha, t) = u_0 \text{ with } \alpha = k, k-1, k-2, k-3, k-4 \quad (5.62)$$

where m is the fictitious node number on the left edge with the unit normal $\mathbf{n}^T = \{-1, 0\}$ and $u_0 = 0$ is the imposed value of displacement. The displacement gradient condition, Eq. (5.60) is enforced through Eq. (5.29) as

$$u_1(\tilde{\mathbf{x}}_\alpha, t) = u_1(\mathbf{x}_\alpha, t) \text{ with } \alpha = k, k-1, k-2, k-3, k-4 \quad (5.63)$$

The real and fictitious node pairs are shown in Figs. 11 to 13.

On the right end, the tensile force in Eq. (5.59) is applied in the form of a distributed body load on the points in the real and fictitious regions as shown in Fig. 15. The distributed body load for *1D analysis* is computed as

$$b_{1(m)} = \frac{F_0}{5\Delta V} \text{ with } m = \mathbf{x}_k, \hat{\mathbf{x}}_\alpha \text{ and } \alpha = k, k-1, k-2, k-3, k-4 \quad (5.64)$$

where $F_0 = 100$ nN and $\Delta V = A\Delta x$ is the incremental volume of material points. The cross-sectional area of CNT is $A = 1.15893 \times 10^{-18}$ m².

The distributed body load for 2D analysis is computed as

$$b_{1(m)} = \frac{F_0}{5N_R\Delta V} \text{ with } m = \mathbf{x}_k, \hat{\mathbf{x}}_\alpha \text{ and } \alpha = k, k-1, k-2, k-3, k-4 \quad (5.57)$$

where $N_R = W/\Delta x$ denotes the number of PD points along the right edge and $\Delta V = h(\Delta x)^2$ is the incremental volume of material points. Traction free conditions lead to zero distributed body load; thus, they do not require the imposition of explicit additional constraints.

The double traction condition, Eq. (5.61) at the left edge is enforced as the constraint equation, Eq. (5.39) as

$$u_1(\tilde{\mathbf{x}}_\alpha, t) = u_1(\mathbf{x}_{\alpha-1}, t) - 2u_1(\mathbf{x}_\alpha, t) \quad \text{with } m = \mathbf{x}_k, \hat{\mathbf{x}}_\alpha \text{ and } \alpha = k, k-1, k-2, k-3, k-4 \quad (5.65)$$

the real and fictitious node pairs are shown in Figs. 10 to 15. This constraint equation is applied to all real and fictitious node pairs.

Figures 24a and 24b show the quasi-static response of CNT based on the PDSG and classical solutions for both 1D and 2D models for $\ell/\delta = 0, 10.0$ and 40.0 . Both the 1D and 2D PDSG predictions capture the analytical solutions as well as the increased strengthening effect along the length of the CNT for increasing ratio of ℓ/δ . This comparison establishes the validity of the implementation and enforcement of non-classical boundary conditions as the PD horizon approaches zero.

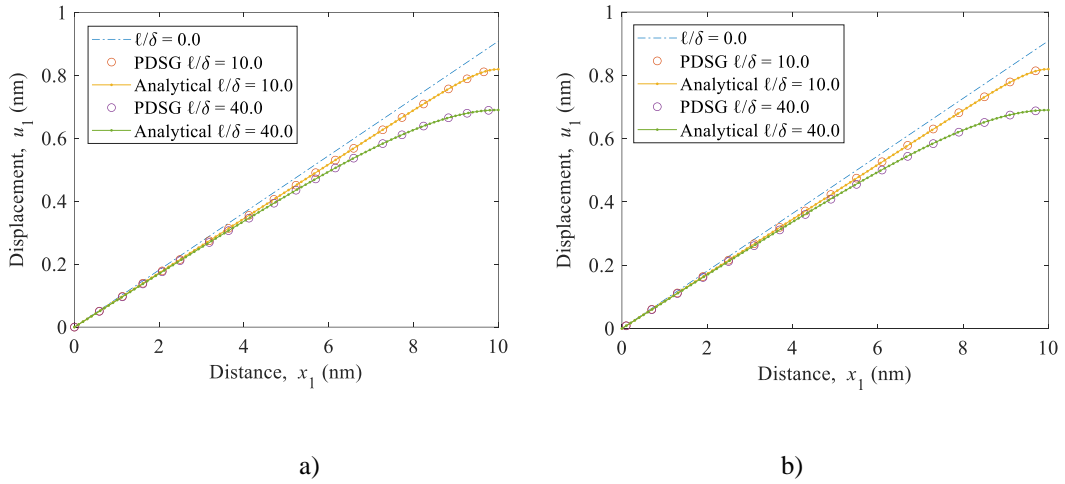


Figure 24. Comparison of PDSG prediction with analytical solution for horizontal displacement, u_1 for $\ell/\delta = 10.0$ and 40.0 : a) 1D model and, b) 2D model

5.4.2 PDSG model of a microscale film under tangential displacement

As shown in Fig. 25a, the rectangular film is clamped along the bottom end and subjected to tangential displacement constraint along the top end. The film shown in Fig. 25 has a length and width of $L = 0.5\mu\text{m}$ and $W = 0.125\mu\text{m}$, respectively. As shown in Fig. 25b, the film is discretized with uniform grid spacing of $\Delta x = 0.01\text{nm}$ resulting in 600 and 720 points in the real and fictitious regions, respectively. Shekarchizadeh et al. (2022) provided a 1D analytical solution with $\ell \neq 0$ under the assumption that the vertical displacement component is zero, i.e., $u_2(x_1, x_2) = 0$ and the horizontal

displacement is independent of x_1 , i.e., $u_1(x_1, x_2) = u_1(x_2)$. The material of the plate was assumed to be the same used by Shekarchizadeh et al. (2022) with the Young's modulus, $E = 400\text{MPa}$ Poisson's ratio, $\nu = 0.49$. The internal length parameter, ℓ is varied as $0.1\mu\text{m}$ and $0.3\mu\text{m}$. To compare the PDSG predictions with the analytical solution, the vertical displacement component is specified as zero i.e., $u_2(x_1, x_2) = 0$ at all PD points. Therefore, the horizontal displacement is uniform along the length in x_1 - direction and varies only along the width in x_2 -direction as $u_1(x_1, x_2) = u_1(x_2)$. The 1D solution is recovered with a 2D model by specifying the displacement component in the vertical direction as zero. The boundary conditions are applied on all four edges.

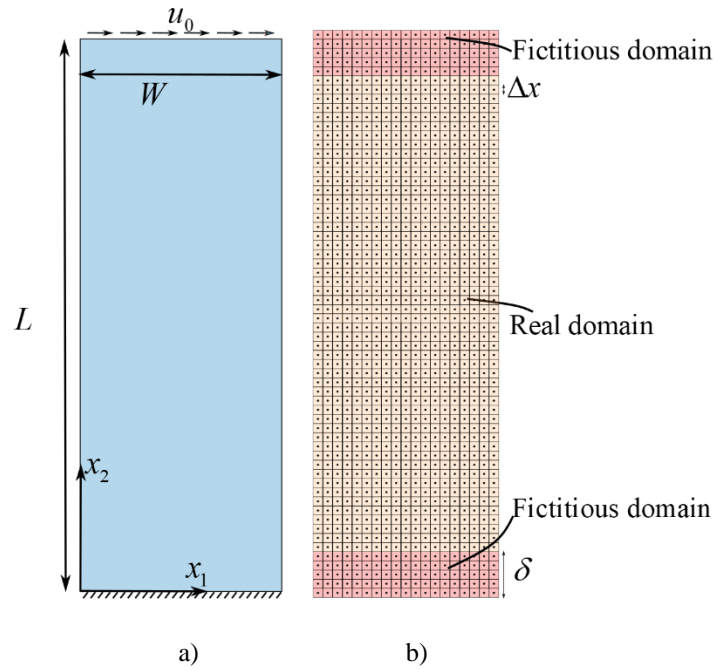


Figure 25. A rectangular microscale film subjected to tangential displacement constraint: a) Geometry and boundary conditions, and b) PD discretization

The classical boundary conditions are of the form

$$u_1(x_1, x_2 = 0) = 0 \quad (127) \quad (5.66)$$

and

$$u_1(x_1, x_2 = L) = u_0 \quad (128) \quad (5.67)$$

The nonclassical boundary conditions can be specified as Shekarchizadeh et al. (2022)

$$\frac{\partial u_1(x_1, x_2 = L)}{\partial x_2} = 0 \quad (129) \quad (5.68)$$

and

$$E\ell^2 \frac{\partial^2 u_1(x_1, x_2 = 0)}{\partial x_2^2} = 0 \quad (130) \quad (5.69)$$

The displacement boundary conditions, Eqs. (5.66) and (5.67) are applied on the fictitious points at the bottom boundary with $\mathbf{n}^T = \{0, -1\}$ and top boundary of the film with $\mathbf{n}^T = \{0, 1\}$ through Eq. (5.26).

The displacement gradient and double traction free conditions, Eq. (5.68) and (5.69) applied along the top edge and bottom edge of the film, respectively, cannot be enforced in the form of a constraint condition. This is due to the nature of ADR method used to compute the steady state solution. The first and second order cross derivatives cannot be guaranteed to be satisfied. Therefore, the Lagrange multiplier method described in section 4.4 and Appendix 1.4 is used to enforce both nonclassical boundary conditions.

Traction free conditions leading to zero distributed body load do not need to be enforced explicitly as additional constraints. For the purpose of simplification, the cross derivative of u_1 in Eq. (5.46) is disregarded, and thus, the constraint.

Figs. 26a and 26b show the PDSG predictions of deformed shapes due to the shear loading corresponding to the values of $\ell/\delta = 1.11$ and 3.32, respectively. As expected, the shear deformation is independent of horizontal direction and varies in the vertical direction.

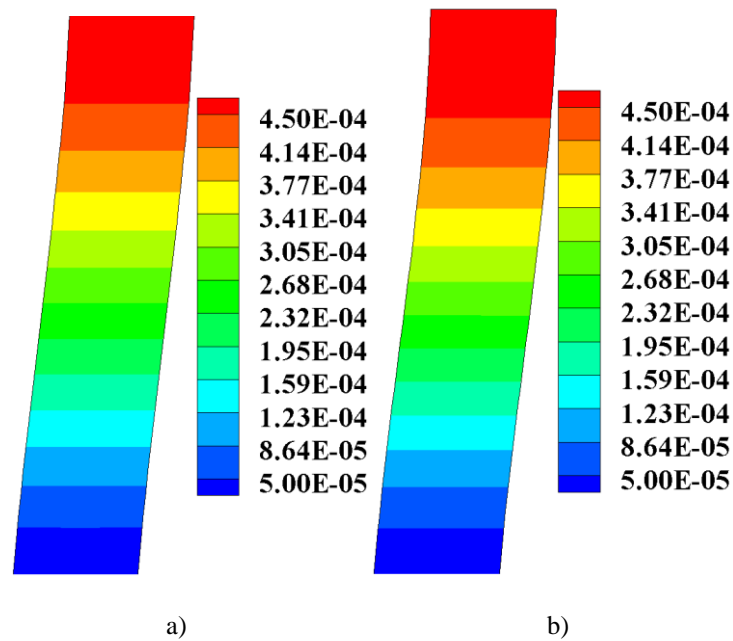


Figure 26. PDSG prediction of horizontal displacement (displacements scaled 100x), u_1 : a) $\ell/\delta = 1.11$ and b) $\ell/\delta = 3.32$

Fig. 27 shows the comparison of horizontal displacement from the PDSG prediction and analytical solution by Shekarchizadeh et al. (2022) for $\ell/\delta = 1.11$ and 3.32 along the vertical centerline of the film at $x_1 = 0.5W$. The PDSG predictions capture the analytical solution with a slight stiffening effect with the increasing values of ℓ/δ . The comparison of PDSG predictions against the analytical solution confirms the enforcement of non-classical boundary conditions as the PD horizon approaches zero. There is a slight deviation from the analytical solution towards the top of the plate in the case when $\ell/\delta = 1.11$ and near the bottom when $\ell/\delta = 3.32$.

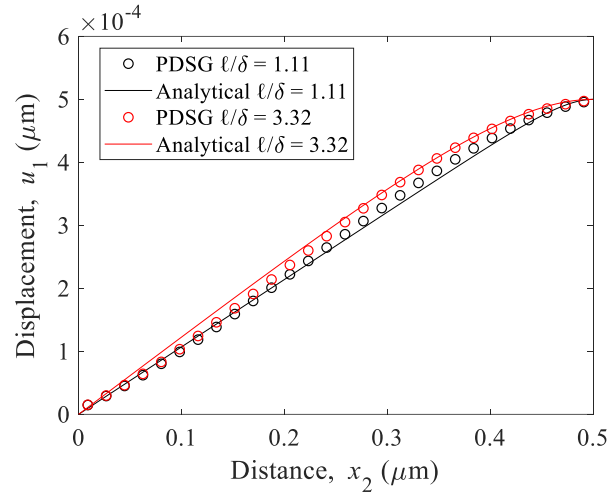


Figure 27. Comparison of PDSG and analytical solutions for horizontal displacement, $u_1(x_1 = 0.5W, x_2)$ along the x_2 axis for $\ell/\delta = 18$ and 36 .

5.4.3 PDSG model of a square nanoscale film with and without a crack

As shown in Fig. 28, the square film geometry is defined by its length $L = 10\text{nm}$, width $W = 1\text{nm}$. The initial crack length shown in Fig 28b is $2a = 2\text{nm}$. The tensile loading of $F_0 = 100 \times 10^{-9}\text{ N}$ is applied on the top and bottom edges of the film. The left and right edges of the film are free of tractions. The film is discretized with a grid spacing of $\Delta x = 0.25$ resulting in 1600 and 800 PD points in the real and fictitious regions, respectively. The discretization is achieved by considering the parameters from the 2D models recovering the 1D PDSG solutions as the PD horizon approaches zero. The initial crack is introduced by removing the PD bonds crossing the crack surfaces as shown in Fig. 29b.

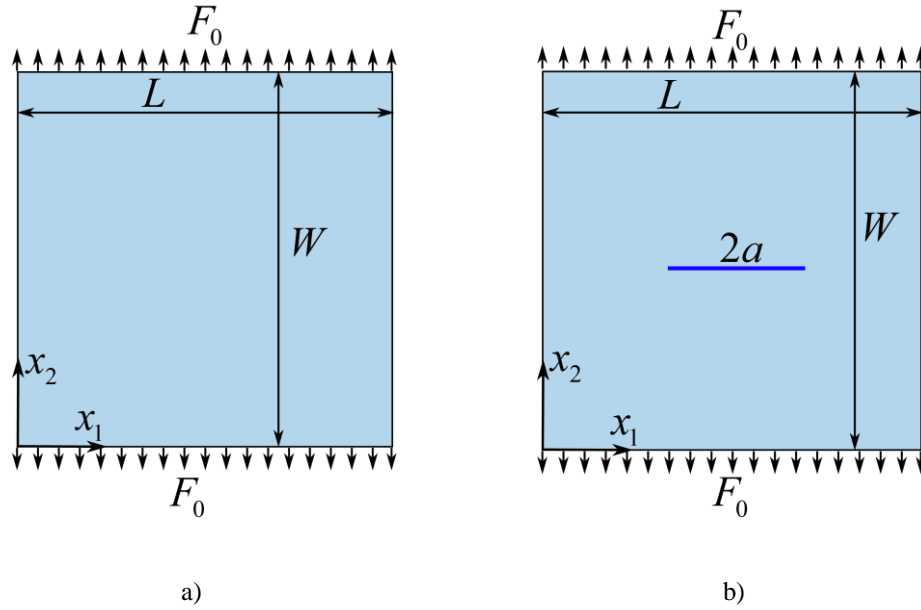


Figure 28. Geometry and loading of the square film under tension: a) without a crack, and b) with a central crack

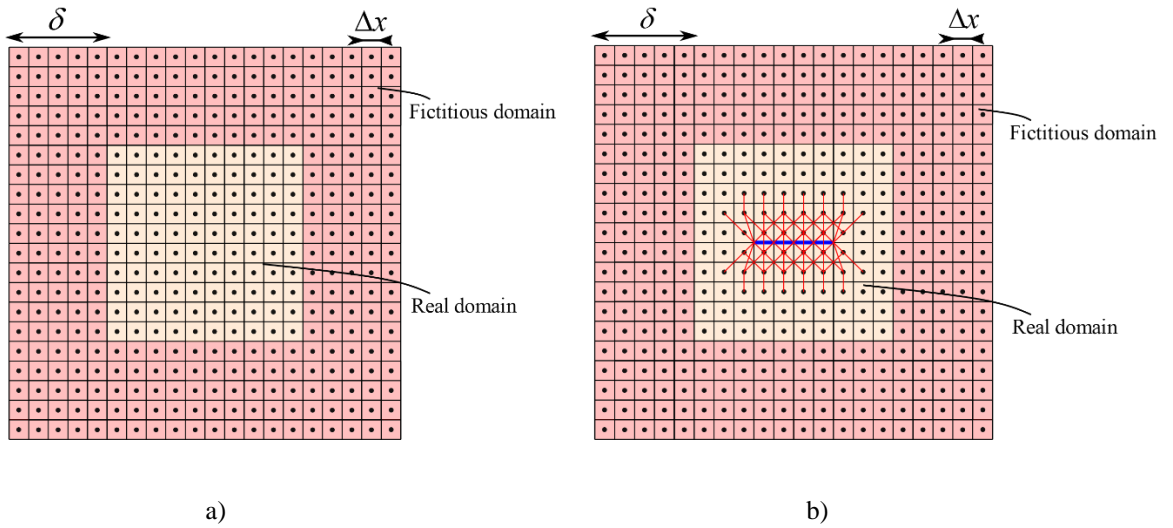


Figure 29. Discretization of the square film: a) without a crack, and b) with a central crack

Tensile loading is applied on the boundaries in the form of a distributed body load on the points in the real region close to the boundary and in the fictitious region. The body load is computed as

$$b_{2(m)} = \frac{F_0}{5N_R \Delta V} \text{ with } m = \mathbf{x}_k, \hat{\mathbf{x}}_\alpha \text{ and } \alpha = k, k-1, k-2, k-3, k-4 \quad (5.70)$$

where $N_R = W/\Delta x$ denotes the number of PD points along the top edge and the incremental volume of material point is $\Delta V = h(\Delta x)^2$.

Traction free conditions leading to zero distributed body load do not require additional constraints. The zero double traction on the top and bottom edges of the film are enforced by using the constraint equations, Eqs. (5.45) and (5.46) while disregarding the contribution from the cross derivative of u_1 and u_2 .

$$u_{1(m)}(\tilde{\mathbf{x}}_\alpha, t) = -u_1(\mathbf{x}_{\alpha-1}, t) + 2u_1(\mathbf{x}_\alpha, t) \quad \text{and } \alpha = k, k-1, k-2, k-3, k-4 \quad (5.71a)$$

and

$$u_{2(m)}(\tilde{\mathbf{x}}_\alpha, t) = -u_2(\mathbf{x}_{\alpha-1}, t) + 2u_2(\mathbf{x}_\alpha, t) \quad \text{and } \alpha = k, k-1, k-2, k-3, k-4 \quad (5.71b)$$

The real and fictitious node pairs are shown in Figs. 16 and 18. These constraint equations, Eq. (5.71a and 5.71b) are applied to all real and fictitious node pairs. The zero-displacement gradient conditions on the left and right edges of the film are enforced by using the constraint equation, Eq. (5.30).

$$u_1(\tilde{\mathbf{x}}_\alpha, t) = u_1(\mathbf{x}_\alpha, t) \quad \text{with } \alpha = k, k-1, k-2, k-3, k-4 \quad (5.72a)$$

and

$$u_2(\tilde{\mathbf{x}}_\alpha, t) = u_2(\mathbf{x}_\alpha, t) \quad \text{with } \alpha = k, k-1, k-2, k-3, k-4 \quad (5.72b)$$

These constraint equations are applied to all real and fictitious node pairs as shown in Figs. 11 to 14. In the absence of a crack, Fig. 30 shows the vertical displacement variation along the center line, $x_1 = 5\text{nm}$ of the film for varying values of ℓ/δ . It is observed that the displacements at the ends of the film are reduced, indicating a stiffening effect with an increase in ℓ/δ values.

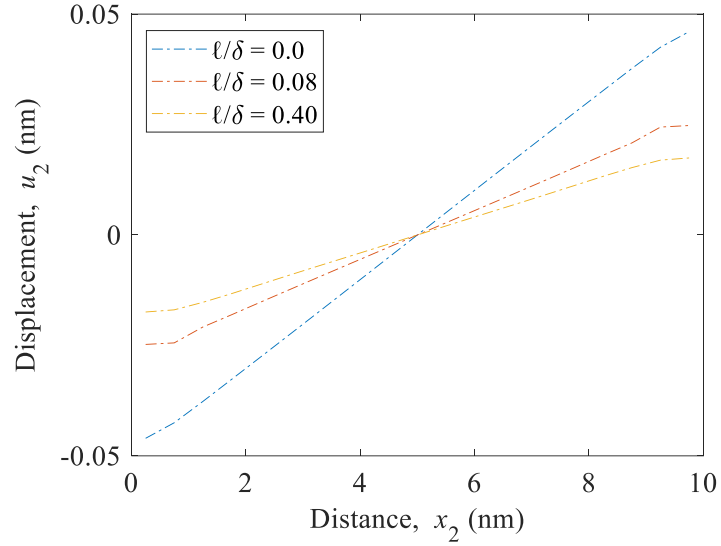


Figure 30. In the absence of a crack, the vertical displacement along the center line, $x_1 = 5.0\text{nm}$ for varying values of l/δ .

In the presence of a crack, Fig. 31 shows the PD predictions of vertical displacement contour variations for the film with different values of $l/\delta = 0.08$ and 0.40 . Figure 32 shows the vertical displacement variation of the film for varying values of l/δ along the center line $x_1 = 5\text{nm}$. Both the contour and vertical line displacement plots indicate that PDSG captures the discontinuity at the crack tip with reduced displacement values as the ratio of l/δ increases. Figure 33 shows the crack opening displacement of the film for varying values of l/δ which indicates that the magnitude of the crack opening displacement decreases due to the stiffening effect as the ratio of l/δ increases. Figure 34 shows the mesh convergence study performed for $\Delta x = 1.0, 0.5, 0.25, 0.125\text{ nm}$. Ultimately, the plate discretization that was chosen for analysis was 40×40 PD points in the real domain with 5 layers of fictitious material points in the surrounding.

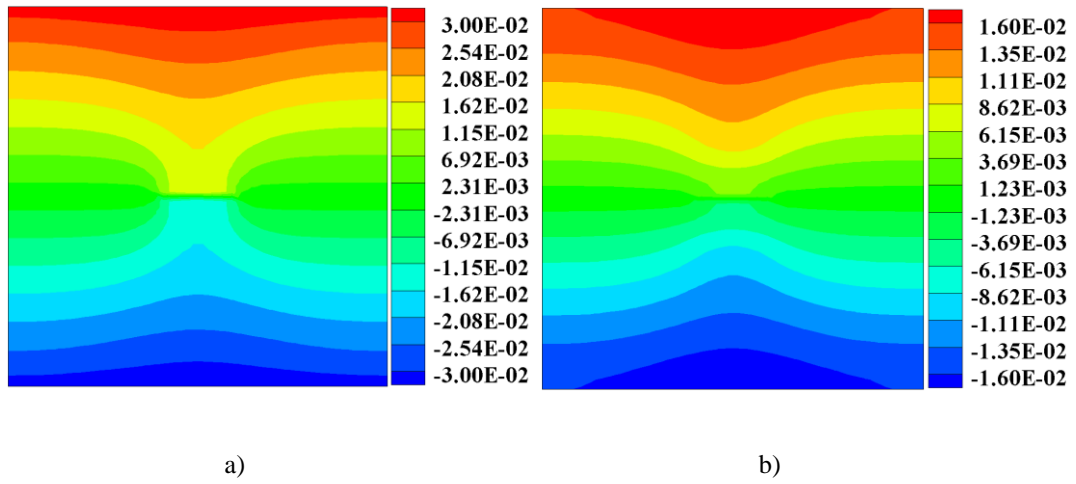


Figure 31. PDSG predictions of vertical displacement contour variations: a) $\ell/\delta = 0.08$, and b) $\ell/\delta = 0.40$

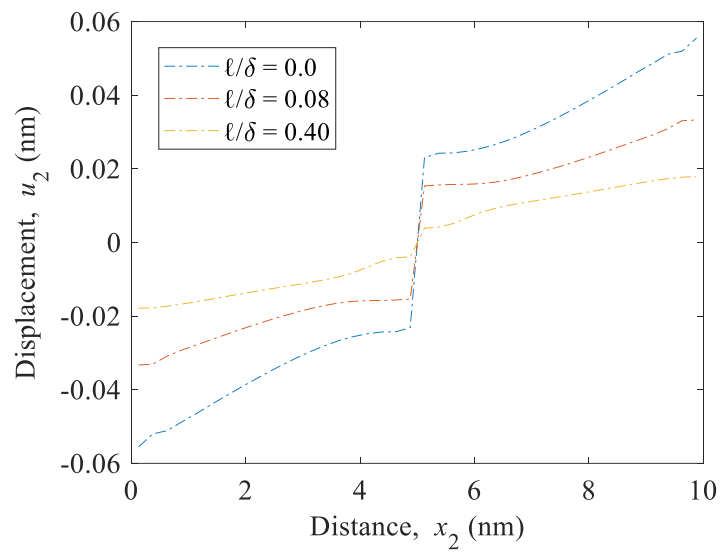


Figure 32. In the presence of a crack, displacement variation as a function of ℓ/δ : $u_2(x_1, x_2 = 5\text{nm})$

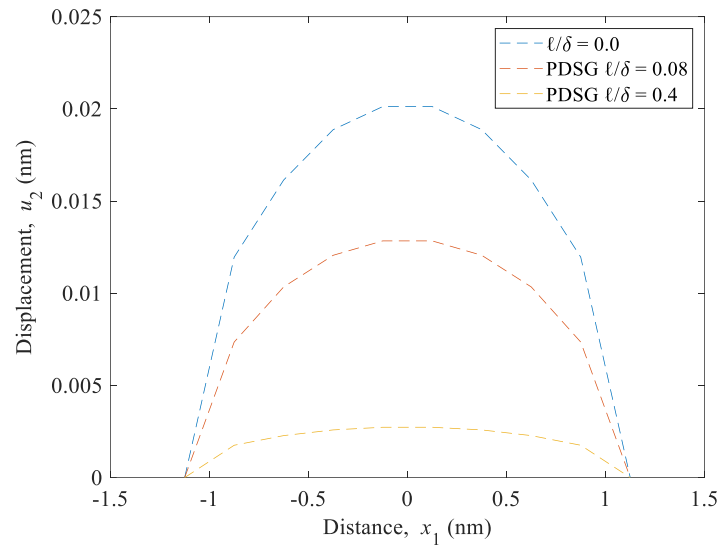


Figure 33. Reduction in crack opening displacement for increasing value of l/δ

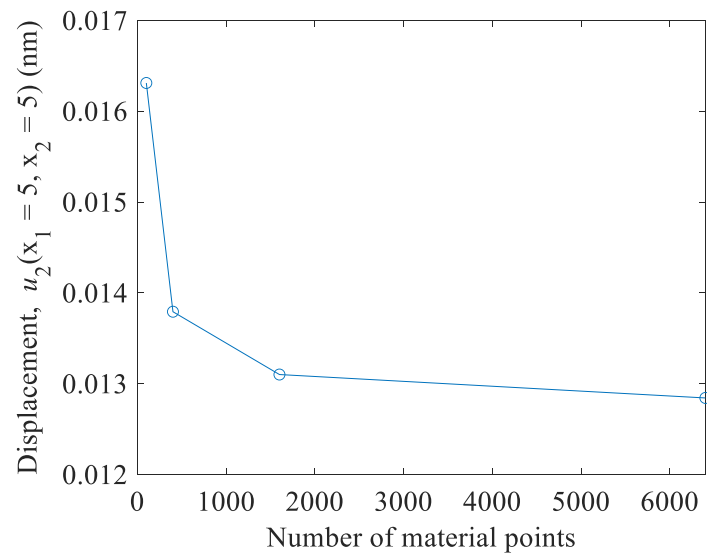


Figure 34. Mesh dependence study with constant l/δ ratio

6. CONCLUSIONS AND FUTURE WORK

6.1 Summary

Nature often emerges as the ultimate innovator, but our understanding of materials has significantly advanced through the fusion of material science, advanced fabrication techniques, computational modeling, and experimental characterization at the micro and nanoscales. Observations at these small scales have demonstrated size-dependent behavior, which is critical in systems like MEMS and NEMS. The interplay between intrinsic and extrinsic dimensions amplifies these effects, highlighting the importance of leveraging size-dependent behaviors for future advancements in material science and engineering.

The combination of PD and SGE provides a computational framework capable of multiscale analysis. It is accomplished by employing the PDDO to rewrite the Navier-like displacement equations with strain gradient in their integral form. This novel formulation of the internal force vector and force density vectors in terms of the PD functions is unprecedented. Unlike many existing non-classical theories, the PDSG model is valid in the presence of discontinuities such as cracks or material interfaces, allowing for damage initiation and propagation. This unified approach can accommodate fracture and crack propagation, as well as incorporate microstructural effects, leading to enhanced predictability and material modeling. Parameter identification remains a challenge, as both PD and SGE introduce their own length scale parameters, necessitating advanced experimental methods for accurate characterization.

The one-dimensional study demonstrates the initial capability of coupling SGE and PD theories. The classical form of the SGE equation of motion for a one-dimensional bar is a fourth-order partial differential equation, with boundary conditions consisting of two classical and two nonclassical types. The PDSG recovers the classical SGE solution for a CNT subjected to quasi-static loading, showing a stiffening effect as the internal length parameter increases. This effect is evidenced by decreased displacement along the bar length, especially near the ends, an outcome not captured by classical continuum mechanics. Additionally, the transient analysis of a 1D nano film under dynamic loading shows a noticeable phase shift in the frequency response compared to the point-wise solution.

Two-dimensional formulations for bond-based and ordinary state-based PD with strain gradient elasticity are presented. The PDSG displacement predictions accurately recover the analytical strain gradient solutions in the case of axial tension. The tangential displacement solution deviates slightly from the analytical solution. This discrepancy is likely due to the enforcement of boundary conditions when using the ADR method. The differences in boundary conditions stem from the directions in which the derivatives are taken. For the tangential case, the derivative must be taken in a direction perpendicular to the displacement direction. Consequently, these constraint equations cannot be directly enforced while using ADR, necessitating the use of Lagrange multipliers. This approach guided the solution closer to the analytical solution, albeit with some error. The quasi-static response of a 2D nano film with and without cracks subjected to tensile load demonstrates reduced displacement with increasing values of the internal length parameter.

In summary, the integration of PD and SGE offers a robust tool for modeling size-dependent effects in materials, particularly valuable for simulating the behavior of materials with defects or localized features at different length scales. This approach paves the way for future advancements in material science and engineering, emphasizing the importance of understanding and leveraging size-dependent behaviors.

6.2 Future work

This work demonstrates the capability of the PDSG model and there are many areas left to be explored. Only a few problems have been considered thus far. The future work identified as critical are listed below:

- Validation against experimental test data
 - Plate with a center hole under tension
 - Mode I crack propagation test
- Investigation of the two-dimensional version of the quasi-brittle problem considered by Hobbs et al. (2022).
 - This will involve investigating the choice of the internal length parameter brought in through SGE along with the peak load and post-peak failure response.

- Derivation of critical stretch in terms of PD horizon and SGE internal length parameter.
- Three-dimensional formulation and numerical implementation
 - To verify the three-dimensional formulation, an example problem will be considered where a rectangular prism is subjected to tension at both ends and free on all other surfaces.

APPENDICES

Appendix A: PDDO for a relative function

The derivation of the PD functions g_4^p , where p is the order of differentiation. The subscript of the PD functions indicates the order of Taylor series expansion used during construction. The relative change in a function, $u(x+\xi)-u(x)$ with fourth-order TSE and neglecting higher-order terms is constructed as

$$u(x+\xi)-u(x) = \xi \frac{\partial u(x)}{\partial x} + \frac{1}{2!} \xi^2 \frac{\partial^2 u(x)}{\partial x^2} + \frac{1}{3!} \xi^3 \frac{\partial^3 u(x)}{\partial x^3} + \frac{1}{4!} \xi^4 \frac{\partial^4 u(x)}{\partial x^4} + R_4(x) \quad (\text{A.1})$$

The relative distance between two points is defined as $\xi = x' - x$. Each term in Eq. (A.1) is multiplied by the PD functions, g_4^p and integrated over the domain of interaction, H_x , results in

$$\begin{aligned} \int_{H_x} (u(x+\xi)-u(x)) g_4^p(\xi) dV_{x'} &= \frac{\partial u(\mathbf{x})}{\partial x} \int_{H_x} \xi g_4^p(\xi) dV_{x'} + \frac{\partial^2 u(\mathbf{x})}{\partial x^2} \int_{H_x} \frac{1}{2!} \xi^2 g_4^p(\xi) dV_{x'} \\ &+ \frac{\partial^3 u(\mathbf{x})}{\partial x^3} \int_{H_x} \frac{1}{3!} \xi^3 g_4^p(\xi) dV_{x'} + \frac{\partial^4 u(\mathbf{x})}{\partial x^4} \int_{H_x} \frac{1}{4!} \xi^4 g_4^p(\xi) dV_{x'} \end{aligned} \quad (\text{A.2})$$

The orthogonality condition allows for the desired derivative to be extracted and is written as

$$\frac{1}{n!} \int_{H_x} \xi^n g_4^p(\xi) dV_{x'} = \delta_{np} \quad (\text{A.3})$$

The PD form of the derivatives can then be written as

$$\left\{ \begin{array}{c} \frac{\partial u(x)}{\partial x} \\ \frac{\partial^2 u(x)}{\partial x^2} \\ \frac{\partial^3 u(x)}{\partial x^3} \\ \frac{\partial^4 u(x)}{\partial x^4} \end{array} \right\} = \int_{H_x} (u(x+\xi)-u(x)) \left\{ \begin{array}{c} g_4^1(\xi) \\ g_4^2(\xi) \\ g_4^3(\xi) \\ g_4^4(\xi) \end{array} \right\} dV_{x'} \quad (\text{A.4})$$

The PD functions are constructed as a linear combination of polynomial basis functions as

$$g_4^p(\xi) = a_1^p w_1(|\xi|)\xi + a_2^p w_2(|\xi|)\xi^2 + a_3^p w_3(|\xi|)\xi^3 + a_4^p w_4(|\xi|)\xi^4 \quad (\text{A.5})$$

where a_q^p are the unknown coefficients and $w_q(|\xi|)$ are the specified weight functions. Invoking orthogonality results in a system of algebraic equations to determine the coefficients, a_q^p as

$$\mathbf{A}\mathbf{a} = \mathbf{b} \quad (\text{A.6})$$

with

$$\mathbf{A} = \int_{H_x} w(|\xi|) \begin{bmatrix} \xi^2 & \xi^3 & \xi^4 & \xi^5 \\ \xi^3 & \xi^4 & \xi^5 & \xi^6 \\ \xi^4 & \xi^5 & \xi^6 & \xi^7 \\ \xi^5 & \xi^6 & \xi^7 & \xi^8 \end{bmatrix} dV_{x'}. \quad (\text{A.7})$$

The weight functions in the quasi-static case are chosen as

$$w_1(|\xi|) = w_2(|\xi|) = w_3(|\xi|) = w_4(|\xi|) = e^{-(4|\xi|/\delta)^2} \quad (\text{A.8})$$

whereas the weight functions for the transient case are chosen as

$$w_1(|\xi|) = w_3(|\xi|) = \frac{\delta^2}{|\xi|^2} \quad \text{and} \quad w_2(|\xi|) = w_4(|\xi|) = \frac{\delta^3}{|\xi|^3}. \quad (\text{A.9})$$

The matrix of unknown coefficients is constructed as

$$\mathbf{a} = \begin{bmatrix} a_1^1 & a_2^1 & a_3^1 & a_4^1 \\ a_1^2 & a_2^2 & a_3^2 & a_4^2 \\ a_1^3 & a_2^3 & a_3^3 & a_4^3 \\ a_1^4 & a_2^4 & a_3^4 & a_4^4 \end{bmatrix} \quad (\text{A.10})$$

and the right-hand-side matrix, \mathbf{b} is defined as

$$\mathbf{b} = \begin{bmatrix} 1 & 0 & 0 & 0 \\ 0 & 2 & 0 & 0 \\ 0 & 0 & 12 & 0 \\ 0 & 0 & 0 & 24 \end{bmatrix}$$

(A.11)

Appendix B: One-dimensional analytical form of PD functions

The fourth order Taylor series expansion is written as

$$f(x + \xi) = f(x) + \xi \frac{\partial f(x)}{\partial x} + \frac{1}{2!} \xi^2 \frac{\partial^2 f(x)}{\partial x^2} + \frac{1}{3!} \xi^3 \frac{\partial^3 f(x)}{\partial x^3} + \frac{1}{4!} \xi^4 \frac{\partial^4 f(x)}{\partial x^4} + R_4(x) \quad (\text{B.1})$$

Each term is then multiplied by the PD function g_2^p where $p=1,2,3,4$ represents the order of differentiation considered.

$$\begin{aligned} \int_{H_x} f(x + \xi) g_4^p(\xi) dV_{x'} &= \int_{H_x} f(x) g_4^p(\xi) dV_{x'} + \frac{\partial f(\mathbf{x})}{\partial x} \int_{H_x} \xi g_4^p(\xi) dV_{x'} \\ &+ \frac{\partial^2 f(\mathbf{x})}{\partial x^2} \int_{H_x} \frac{1}{2!} \xi^2 g_4^p(\xi) dV_{x'} + \frac{\partial^3 f(\mathbf{x})}{\partial x^3} \int_{H_x} \frac{1}{3!} \xi^3 g_4^p(\xi) dV_{x'} + \frac{\partial^4 f(\mathbf{x})}{\partial x^4} \int_{H_x} \frac{1}{4!} \xi^4 g_4^p(\xi) dV_{x'} \end{aligned} \quad (\text{B.2})$$

The PD functions are constructed as a linear combination of polynomial basis functions as

$$g_4^p(\xi) = a_0^p w(|\xi|) + a_1^p w(|\xi|)\xi + a_2^p w(|\xi|)\xi^2 + a_3^p w(|\xi|)\xi^3 + a_4^p w(|\xi|)\xi^4 \quad (\text{B.3})$$

where a_q^p are the unknown coefficients and $w_q(|\xi|)$ are the specified weight functions. Invoking orthogonality results in a system of algebraic equations to determine the coefficients, a_q^p .

The weight function, $w(|\xi|)$, is chosen to be

$$w(|\xi|) = 1 \quad (\text{B.4})$$

Invoking the orthogonality condition as

$$\int_{H_x} \frac{1}{n!} \xi^n g_4^p(\xi) dV_{x'} = \delta_{n,p} \quad (\text{B.5})$$

or

$$\mathbf{Aa} = \mathbf{b} \quad (\text{B.6})$$

The shape matrix, \mathbf{A} , and known \mathbf{b} matrix to be constructed, respectively as

$$\mathbf{A} = \int_{-\delta}^{\delta} w(|\xi|) \begin{bmatrix} 1 & \xi & \xi^2 & \xi^3 & \xi^4 \\ \xi & \xi^2 & \xi^3 & \xi^4 & \xi^5 \\ \xi^2 & \xi^3 & \xi^4 & \xi^5 & \xi^6 \\ \xi^3 & \xi^4 & \xi^5 & \xi^6 & \xi^7 \\ \xi^4 & \xi^5 & \xi^6 & \xi^7 & \xi^8 \end{bmatrix} d\xi = \begin{bmatrix} 2\delta & 0 & \frac{2\delta^3}{3} & 0 & \frac{2\delta^5}{5} \\ 0 & \frac{2\delta^3}{3} & 0 & \frac{2\delta^5}{5} & 0 \\ \frac{2\delta^3}{3} & 0 & \frac{2\delta^5}{5} & 0 & \frac{2\delta^7}{7} \\ 0 & \frac{2\delta^5}{5} & 0 & \frac{2\delta^7}{7} & 0 \\ \frac{2\delta^5}{5} & 0 & \frac{2\delta^7}{7} & 0 & \frac{2\delta^9}{9} \end{bmatrix} \quad (\text{B.7})$$

and

$$\mathbf{b} = \begin{bmatrix} 1 & 0 & 0 & 0 & 0 \\ 0 & 1 & 0 & 0 & 0 \\ 0 & 0 & 2 & 0 & 0 \\ 0 & 0 & 0 & 12 & 0 \\ 0 & 0 & 0 & 0 & 24 \end{bmatrix} \quad (\text{B.8})$$

Solving for the PD coefficient matrix, $\mathbf{a} = \mathbf{A}^{-1}\mathbf{b}$ results in

$$\mathbf{a} = \begin{bmatrix} a_0^0 & a_1^0 & a_2^0 & a_3^0 & a_4^0 \\ a_0^1 & a_1^1 & a_2^1 & a_3^1 & a_4^1 \\ a_0^2 & a_1^2 & a_2^2 & a_3^2 & a_4^2 \\ a_0^3 & a_1^3 & a_2^3 & a_3^3 & a_4^3 \\ a_0^4 & a_1^4 & a_2^4 & a_3^4 & a_4^4 \end{bmatrix} = \begin{bmatrix} \frac{225}{128\delta} & 0 & -\frac{525}{32\delta^3} & 0 & \frac{2835}{16\delta^5} \\ 0 & \frac{75}{8\delta^3} & 0 & -\frac{315}{4\delta^5} & 0 \\ -\frac{525}{64\delta^3} & 0 & \frac{2205}{16\delta^5} & 0 & -\frac{14175}{8\delta^7} \\ 0 & -\frac{105}{8\delta^5} & 0 & \frac{525}{4\delta^7} & 0 \\ \frac{945}{128\delta^5} & 0 & -\frac{4725}{32\delta^7} & 0 & \frac{33075}{16\delta^9} \end{bmatrix} \quad (\text{B.9})$$

The elements of (B.9) and the weight function can then be combined to construct the PD functions from Eq. (B.3) and the end results are shown in Eqs. (3.39a-3.39e).

Appendix C: Two-dimensional analytical form of PD derivatives

Following a similar procedure described in Appendix A, the two-dimensional derivatives up to fourth order can be constructed as

$$\begin{pmatrix} \frac{\partial f(\mathbf{x})}{\partial x_1} \\ \frac{\partial f(\mathbf{x})}{\partial x_2} \end{pmatrix} = \int_{H_x} \left(w_1(|\xi|) \frac{4}{h\pi\delta^4} \begin{pmatrix} \xi_1 \\ \xi_2 \end{pmatrix} - w_3(|\xi|) \frac{4}{h\pi\delta^6} \begin{pmatrix} \xi_1^3 + \xi_1 \xi_2^2 \\ \xi_1^2 \xi_2 + \xi_2^3 \end{pmatrix} \right) (f(\mathbf{x} + \xi) - f(\mathbf{x})) dV_x, \quad (\text{C.1})$$

and

$$\begin{pmatrix} \frac{\partial^2 f(\mathbf{x})}{\partial x_1^2} \\ \frac{\partial^2 f(\mathbf{x})}{\partial x_2^2} \\ \frac{\partial^2 f(\mathbf{x})}{\partial x_1 \partial x_2} \end{pmatrix} = \int_{H_x} \left(w_2(|\xi|) \frac{15}{2h\pi\delta^6} \begin{pmatrix} 3\xi_1^2 - \xi_2^2 \\ -\xi_1^2 + 3\xi_2^2 \\ 2\xi_1 \xi_2 \end{pmatrix} + w_4(|\xi|) \frac{15}{2h\pi\delta^8} \begin{pmatrix} -3\xi_1^4 - \xi_1^2 \xi_2^2 + \xi_2^4 \\ \xi_1^4 - \xi_1^2 \xi_2^2 - 3\xi_2^4 \\ -2\xi_1^3 \xi_2 - 2\xi_1 \xi_2^3 \end{pmatrix} \right) (f(\mathbf{x} + \xi) - f(\mathbf{x})) dV_x, \quad (\text{C.2})$$

and

$$\begin{pmatrix} \frac{\partial^3 f(\mathbf{x})}{\partial x_1^3} \\ \frac{\partial^3 f(\mathbf{x})}{\partial x_2^3} \\ \frac{\partial^3 f(\mathbf{x})}{\partial x_1^2 \partial x_2} \\ \frac{\partial^3 f(\mathbf{x})}{\partial x_2^2 \partial x_1} \end{pmatrix} = \int_{H_x} \left(w_1(|\xi|) \frac{-8}{h\pi\delta^6} \begin{pmatrix} 3\xi_1 \\ 3\xi_2 \\ \xi_2 \\ \xi_1 \end{pmatrix} + w_3(|\xi|) \frac{8}{h\pi\delta^8} \begin{pmatrix} 9\xi_2^3 - 3\xi_1^2 \xi_2 \\ -3\xi_1^2 \xi_2 + 9\xi_2^3 \\ 11\xi_1^2 \xi_2 - \xi_2^3 \\ -\xi_1^3 + 11\xi_1 \xi_2^2 \end{pmatrix} \right) (f(\mathbf{x} + \xi) - f(\mathbf{x})) dV_x, \quad (\text{C.3})$$

and

$$\begin{pmatrix} \frac{\partial^4 f(\mathbf{x})}{\partial x_1^4} \\ \frac{\partial^4 f(\mathbf{x})}{\partial x_2^4} \\ \frac{\partial^4 f(\mathbf{x})}{\partial x_1^3 \partial x_2} \\ \frac{\partial^4 f(\mathbf{x})}{\partial x_2^3 \partial x_1} \\ \frac{\partial^4 f(\mathbf{x})}{\partial x_1^2 \partial x_2^2} \end{pmatrix} = \int_{H_x} \left(w_2(|\xi|) \frac{30}{h\pi\delta^8} \begin{pmatrix} -9\xi_1^2 + 3\xi_2^2 \\ 3\xi_1^2 - 9\xi_2^2 \\ -6\xi_1\xi_2 \\ -6\xi_1\xi_2 \\ -(\xi_1^2 + \xi_2^2) \end{pmatrix} + w_4(|\xi|) \frac{10}{h\pi\delta^{10}} \begin{pmatrix} 57\xi_1^4 - 42\xi_1^2\xi_2^2 - 3\xi_2^4 \\ -3\xi_1^4 - 42\xi_1^2\xi_2^2 + 57\xi_2^4 \\ 78\xi_1^3\xi_2 - 18\xi_1\xi_2^3 \\ -18\xi_1^3\xi_2 + 78\xi_1\xi_2^3 \\ -7\xi_1^4 + 82\xi_1^2\xi_2^2 - 7\xi_2^4 \end{pmatrix} \right) (f(\mathbf{x}+\xi) - f(\mathbf{x})) dV_x. \quad (\text{C.4})$$

With the choice of weight functions being $w_n(|\xi|) = \frac{\delta^{n+1}}{|\xi|^{n+1}}$, with $n=1,2,3,4$, the analytical form of the

function and vector operators corresponding to Eq. (2.13) can then be derived. The component form of

$\nabla(\nabla^2\theta)$ can be expressed as

$$\theta_{,ikk} \mathbf{e}_i = (\theta_{,111} + \theta_{,122}) \mathbf{e}_1 + (\theta_{,211} + \theta_{,222}) \mathbf{e}_2 \quad (\text{C.5})$$

Substituting the PD derivative representations as

$$\theta_{,ikk} \mathbf{e}_i = \left(-\frac{32\xi_1}{\pi\delta^6} + \frac{64\xi_1(\xi_1^2 + \xi_2^2)}{\pi\delta^8} \right) \mathbf{e}_1 + \left(-\frac{32\xi_2}{\pi\delta^6} + \frac{64\xi_2(\xi_1^2 + \xi_2^2)}{\pi\delta^8} \right) \mathbf{e}_2 \quad (\text{C.6})$$

Noticing that the Eq. (C.6) is expressed in terms of a dot product and a vector, it can be rewritten as

$$\nabla(\nabla^2\theta) = \int_H \left(-\frac{32}{\pi\delta^6} w_1(|\xi|) + \frac{64}{\pi\delta^8} w_3(|\xi|)(\xi \cdot \xi) \right) (\theta(\mathbf{x}+\xi) - \theta(\mathbf{x})) \xi dA_x. \quad (\text{C.7})$$

The component form of $\nabla\nabla^2(\nabla \cdot \mathbf{u})$ can be expressed as

$$u_{,j,jkka} \mathbf{e}_i = (u_{,1,1111} + u_{,1,1122} + u_{,2,1112} + u_{,2,1222}) \mathbf{e}_1 + (u_{,1,1112} + u_{,1,1222} + u_{,2,1122} + u_{,2,2222}) \mathbf{e}_2 \quad (\text{C.8})$$

Substituting for the PD derivative representations results in

$$\begin{aligned}
u_{j,jkkl} \mathbf{e}_i = & \left\{ \begin{aligned} & \left(-\frac{60(5\xi_1^2 - \xi_2^2)}{h\pi\delta^8} + \frac{100(5\xi_1^2 - \xi_2^2)(\xi_1^2 + \xi_2^2)}{h\pi\delta^{10}} \right) u_1 \\ & + 6 \left(-\frac{60\xi_1\xi_2}{h\pi\delta^8} + \frac{100\xi_1\xi_2(\xi_1^2 + \xi_2^2)}{h\pi\delta^{10}} \right) u_2 \end{aligned} \right\} \mathbf{e}_1 \\
& + \left\{ \begin{aligned} & 6 \left(-\frac{60\xi_1\xi_2}{h\pi\delta^8} + \frac{100\xi_1\xi_2(\xi_1^2 + \xi_2^2)}{h\pi\delta^{10}} \right) u_1 \\ & + \left(-\frac{60(5\xi_2^2 - \xi_1^2)}{h\pi\delta^8} + \frac{100(5\xi_2^2 - \xi_1^2)(\xi_1^2 + \xi_2^2)}{h\pi\delta^{10}} \right) u_2 \end{aligned} \right\} \mathbf{e}_2
\end{aligned} \tag{C.9}$$

For derivation purposes the integration over the family is implied. Noticing that the Eq. (C.9) is expressed in terms of dot and dyadic products, it can be rewritten as

$$\begin{aligned}
u_{j,jkkl} \mathbf{e}_i = & -\frac{18 \times 20}{h\pi\delta^8} \begin{bmatrix} \xi_1^2 & \xi_1\xi_2 \\ \xi_1\xi_2 & \xi_2^2 \end{bmatrix} \begin{Bmatrix} u_1 \mathbf{e}_1 \\ u_2 \mathbf{e}_2 \end{Bmatrix} + \frac{3 \times 20}{h\pi\delta^8} \begin{bmatrix} (\xi \cdot \xi) & 0 \\ 0 & (\xi \cdot \xi) \end{bmatrix} \begin{Bmatrix} u_1 \mathbf{e}_1 \\ u_2 \mathbf{e}_2 \end{Bmatrix} \\
& + \frac{30 \times 20}{h\pi\delta^{10}} \begin{bmatrix} \xi_1^2 & \xi_1\xi_2 \\ \xi_1\xi_2 & \xi_2^2 \end{bmatrix} (\xi \cdot \xi) \begin{Bmatrix} u_1 \mathbf{e}_1 \\ u_2 \mathbf{e}_2 \end{Bmatrix} - \frac{5 \times 20}{h\pi\delta^{10}} \begin{bmatrix} (\xi \cdot \xi)^2 & 0 \\ 0 & (\xi \cdot \xi)^2 \end{bmatrix} \begin{Bmatrix} u_1 \mathbf{e}_1 \\ u_2 \mathbf{e}_2 \end{Bmatrix}
\end{aligned} \tag{C.10}$$

Finally, the gradient of the Laplacian of a vector can be written as

$$\nabla \nabla^2 (\nabla \cdot \mathbf{u}) = \int_{H_x} \left(\begin{aligned} & -\frac{36 \times 10}{\pi\delta^8} w_2(|\xi|) (\xi \otimes \xi) + \frac{6 \times 10}{\pi\delta^8} w_2(|\xi|) (\xi \cdot \xi) \\ & + \frac{60 \times 10}{\pi\delta^{10}} w_4(|\xi|) (\xi \cdot \xi) (\xi \otimes \xi) - \frac{10 \times 10}{\pi\delta^{10}} w_4(|\xi|) (\xi \cdot \xi)^2 \end{aligned} \right) (\mathbf{u}(\mathbf{x} + \xi) - \mathbf{u}(\mathbf{x})) dA_x. \tag{C.11}$$

The biharmonic operator operating on a vector, $\mathbf{u}(\mathbf{x})$, can be expressed as

$$\nabla^4 \mathbf{u}(\mathbf{x}) = \left(\frac{\partial^4}{\partial x_1^4} + 2 \frac{\partial^4}{\partial x_1^2 \partial x_2^2} + \frac{\partial^4}{\partial x_2^4} \right) \mathbf{u}(\mathbf{x}) \tag{C.12}$$

Substituting for the corresponding PD derivatives as

$$\nabla^4 \mathbf{u}(\mathbf{x}, \xi) = \int_{H_x} \left(\frac{-240}{\pi\delta^8} w_2(|\xi|) (\xi \cdot \xi) + \frac{400}{\pi\delta^{10}} w_4(|\xi|) (\xi \cdot \xi)^2 \right) (\mathbf{u}(\mathbf{x} + \xi) - \mathbf{u}(\mathbf{x})) dA_x. \tag{C.13}$$

Equation (2.13) can then be expressed in its nonlocal integral form as

$$\begin{aligned}
\mathbf{L}(\mathbf{x}, \boldsymbol{\xi}) = & \ell^2 \int_H \left(-\frac{32}{\pi\delta^6} w_1(|\boldsymbol{\xi}|) + \frac{64}{\pi\delta^8} w_3(|\boldsymbol{\xi}|)(\boldsymbol{\xi} \cdot \boldsymbol{\xi}) \right) (\boldsymbol{\theta}(\mathbf{x} + \boldsymbol{\xi}) - \boldsymbol{\theta}(\mathbf{x})) \boldsymbol{\xi} \\
& + \mu \left(\begin{aligned} & -\frac{240}{h\pi\delta^8} w_2(|\boldsymbol{\xi}|)(\boldsymbol{\xi} \cdot \boldsymbol{\xi}) + \frac{400}{h\pi\delta^{10}} w_4(|\boldsymbol{\xi}|)(\boldsymbol{\xi} \cdot \boldsymbol{\xi})^2 \\ & -\frac{36 \times 20}{h\pi\delta^8} \frac{\delta^3}{|\boldsymbol{\xi}|^3} (\boldsymbol{\xi} \otimes \boldsymbol{\xi}) + \frac{6 \times 20}{h\pi\delta^8} w_2(|\boldsymbol{\xi}|)(\boldsymbol{\xi} \cdot \boldsymbol{\xi}) \\ & + \frac{60 \times 20}{h\pi\delta^{10}} w_4(|\boldsymbol{\xi}|)(\boldsymbol{\xi} \cdot \boldsymbol{\xi})(\boldsymbol{\xi} \otimes \boldsymbol{\xi}) - \frac{10 \times 20}{h\pi\delta^{10}} w_4(|\boldsymbol{\xi}|)(\boldsymbol{\xi} \cdot \boldsymbol{\xi})^2 \end{aligned} \right) (\mathbf{u}(\mathbf{x} + \boldsymbol{\xi}) - \mathbf{u}(\mathbf{x})) dA_{\mathbf{x}}. \tag{C.14}
\end{aligned}$$

For a material point with a symmetric domain of interaction and substituting for $w_n(|\boldsymbol{\xi}|)$, the internal force vector can be simplified to

$$\mathbf{L}(\mathbf{x}, \boldsymbol{\xi}) = \ell^2 \int_{H_{\mathbf{x}}} \left(\begin{aligned} & \left(-\frac{32}{h\pi\delta^4} \frac{1}{|\boldsymbol{\xi}|} + \frac{64}{h\pi\delta^4} \frac{1}{|\boldsymbol{\xi}|} \frac{(\boldsymbol{\xi} \cdot \boldsymbol{\xi})}{|\boldsymbol{\xi}|^2} \right) (\boldsymbol{\theta}(\mathbf{x} + \boldsymbol{\xi}) - \boldsymbol{\theta}(\mathbf{x})) \frac{\boldsymbol{\xi}}{|\boldsymbol{\xi}|} \\ & + \mu \left(\frac{480}{h\pi\delta^5} \frac{(\boldsymbol{\xi} \otimes \boldsymbol{\xi})}{|\boldsymbol{\xi}|^2} \frac{(\mathbf{u}(\mathbf{x}') - \mathbf{u}(\mathbf{x}))}{|\boldsymbol{\xi}|} + \frac{80}{h\pi\delta^5} \frac{(\mathbf{u}(\mathbf{x}') - \mathbf{u}(\mathbf{x}))}{|\boldsymbol{\xi}|} \right) \end{aligned} \right) dA_{\mathbf{x}}. \tag{C.15}$$

Splitting the internal force vector as

$$\mathbf{L}^{PD SG} = \int_{H_{\mathbf{x}}} (\mathbf{t}^{SG}(\mathbf{x}) - \mathbf{t}^{SG}(\mathbf{x}')) dV_{\mathbf{x}}. \tag{C.16}$$

Results in the following force density vectors $\mathbf{t}^{SG}(\mathbf{x})$ and $\mathbf{t}^{SG}(\mathbf{x}')$ as

$$\mathbf{t}^{SG}(\mathbf{x}) = a \frac{32}{h\pi\delta^4} \frac{1}{|\boldsymbol{\xi}|} \boldsymbol{\theta}(\mathbf{x}) \frac{\boldsymbol{\xi}}{|\boldsymbol{\xi}|} + \mu \left(\frac{240}{h\pi\delta^5} \frac{(\boldsymbol{\xi} \otimes \boldsymbol{\xi})}{|\boldsymbol{\xi}|^2} \frac{(\mathbf{u}(\mathbf{x}') - \mathbf{u}(\mathbf{x}))}{|\boldsymbol{\xi}|} + \frac{40}{h\pi\delta^5} \frac{(\mathbf{u}(\mathbf{x}') - \mathbf{u}(\mathbf{x}))}{|\boldsymbol{\xi}|} \right) \tag{C.17}$$

and

$$\mathbf{t}^{SG}(\mathbf{x}') = a \frac{32}{h\pi\delta^4} \frac{1}{|\boldsymbol{\xi}|} \boldsymbol{\theta}(\mathbf{x}') \frac{\boldsymbol{\xi}'}{|\boldsymbol{\xi}'|} + \mu \left(\frac{240}{h\pi\delta^5} \frac{(\boldsymbol{\xi} \otimes \boldsymbol{\xi})}{|\boldsymbol{\xi}|^2} \frac{(\mathbf{u}(\mathbf{x}) - \mathbf{u}(\mathbf{x}'))}{|\boldsymbol{\xi}|} + \frac{40}{h\pi\delta^5} \frac{(\mathbf{u}(\mathbf{x}) - \mathbf{u}(\mathbf{x}'))}{|\boldsymbol{\xi}|} \right) \tag{C.18}$$

Appendix D: Lagrange multiplier method for enforcing boundary conditions

Dirichlet type boundary conditions can be enforced directly without the need of special treatment. Neumann type or more complex boundary conditions require special care to properly enforce them at each time step. These more complex boundary conditions can be enforced using the Lagrange multiplier method by Carpenter et al. (1991) which ensures the compatibility by relating the displacements at time t_{n+1} with Lagrange multipliers at time t_n . The incremental equation of motion is modified as

$$\mathbf{M}\ddot{\mathbf{u}}_n = \mathbf{F}(\mathbf{u}_n) + \mathbf{b}_n + \mathbf{G}_{n+1}^T \lambda_n \quad (\text{D.1})$$

The constraint condition is written as

$$\mathbf{G}_{n+1} \mathbf{u}_{n+1} + \boldsymbol{\eta}_{n+1} = 0 \quad (\text{D.2})$$

in which, \mathbf{M} is the lumped mass matrix, \mathbf{u} is the displacement vector, $\ddot{\mathbf{u}}$ is the acceleration vector, \mathbf{F} is the force vector, \mathbf{G}_{n+1} is the constraint vector, and λ_n is the unknown Lagrange multiplier. The known constraint parameter, $\boldsymbol{\eta}$ provides information related to the boundary condition, such as the applied traction or strain. The displacement vector \mathbf{u}_{n+1} is broken down into two parts as

$$\mathbf{u}_{n+1} = \mathbf{u}_{n+1}^* + \mathbf{u}_{n+1}^c \quad (\text{D.3})$$

where \mathbf{u}_{n+1}^* , is the displacement vector determined by the explicit time integration without the contribution from the Lagrange multiplier correction. The vector \mathbf{u}_{n+1}^c is the corrected displacement vector which is determined by applying the boundary conditions using Lagrange multipliers. The equation for the Lagrange multiplier can be expressed as

$$\lambda_n = \left(\Delta x^2 \mathbf{G}_{n+1} \mathbf{M}^{-1} \mathbf{G}_{n+1}^T \right)^{-1} \left(\mathbf{G}_{n+1} \mathbf{u}_{n+1}^* + \boldsymbol{\eta}_{n+1} \right) \quad (\text{D.4})$$

The corrected displacement vector is determined as

$$\mathbf{u}_{n+1}^c = -\Delta x^2 \mathbf{M}^{-1} \mathbf{G}_{n+1}^T \lambda_n \quad (\text{D.5})$$

The imposition of multiple boundary conditions at the same location may require Gauss-Seidel iterative approach (Carpenter et al. (1991)). It is worth noting that the lowest order boundary condition is enforced first. The boundary conditions given by Eqs. (4.31) and (4.32) can be constructed nearly identically with $\eta_{n+1} = 0$. The displacement vector associated with the family members of material point k is defined as

$$\mathbf{v}_{(k)} = \{u_{(1)} \quad u_{(2)} \quad \cdots \quad u_{(N_{(k)})} \quad u_{(k)}\}^T \quad (\text{D.6})$$

The last element of Eq. (D.6) is the displacement of the point of interest, $u_{(k)}$. The parameter $N_{(k)}$ is the number of family members of material point, k , with $k = 1, K+1$. The discrete form of these equations with constant cross-sectional area, A , and grid spacing, Δx , can be written as

$$\sum_{j=1}^{N_{(k)}} (u_{(j)} - u_{(k)}) g_4^q(\xi_{(k)(j)}) A \Delta x = \sum_{j=1}^{N_{(k)}} u_{(j)} g_4^q(\xi_{(k)(j)}) - u_{(k)} \sum_{j=1}^{N_{(k)}} g_4^q(\xi_{(k)(j)}) = 0 \quad (\text{D.7})$$

where $q = 1, 2$ depending on the derivative order of the boundary condition. Expanding Eq. (D.7) allows for the extraction of the constraint vector as

$$\mathbf{G}_{n+1} = \left\{ g_4^q(\xi_{(k)(1)}) \quad \cdots \quad g_4^q(\xi_{(k)(N_{(k)})}) \quad - \sum_{j=1}^{N_{(k)}} g_4^q(\xi_{(k)(j)}) \right\} \quad (\text{D.8})$$

Equation (D.8) can then be used for the boundary conditions given by Eqs. (4.31) and (4.32) for the material point, k , with $k = 1, K+1$. The number of elements in \mathbf{G}_{n+1} is $N_{(k)} + 1$. The boundary condition expressed in Eq. (4.30) can be constructed in its discrete form as

$$\begin{aligned} & \sum_{j=1}^{N_{(k)}} (u_{(j)} - u_{(k)}) g_4^1(\xi_{(k)(j)}) A \Delta x - \ell^2 \sum_{j=1}^{N_{(k)}} (u_{(j)} - u_{(k)}) g_4^3(\xi_{(k)(j)}) A \Delta x \\ & = \sum_{j=1}^{N_{(k)}} (u_{(j)} g_4^1(\xi_{(k)(j)}) - \ell^2 u_{(j)} g_4^3(\xi_{(k)(j)})) - u_{(k)} \sum_{j=1}^{N_{(k)}} (g_4^1(\xi_{(k)(j)}) - \ell^2 g_4^3(\xi_{(k)(j)})) = \frac{F}{EA^2 \Delta x} \end{aligned} \quad (\text{D.9})$$

In the case of quasi-static loading, the constraint parameter is nonzero as $\eta_{n+1} = \frac{\mathbf{F}}{EA^2 \Delta x}$. In the case of dynamic loading this parameter is set to zero to satisfy the traction free condition. Expanding Eq. (D.9) allows for the extraction of the constraint vector as

$$\mathbf{G}_{n+1} = \left\{ g_4^1(\xi_{(k)(1)}) - \ell^2 g_4^3(\xi_{(k)(1)}) \quad \cdots \quad g_4^1(\xi_{(k)(N_k)}) - \ell^2 g_4^3(\xi_{(k)(N_k)}) \quad - \sum_{j=1}^{N_{(1)}} \left(g_4^1(\xi_{(k)(j)}) - \ell^2 g_4^3(\xi_{(k)(j)}) \right) \right\} \quad (\text{D.10})$$

This equation can then be used to enforce the boundary condition given by Eq. (4.30) at the material point $k = K + 1$. Equations (D.8) and (A.10) are substituted into Eq. (D.4), which is then substituted into (D.5) to calculate the corrected displacements associated with the family members of the boundary point. The corrected displacements are then added to the corresponding displacements provided by the initial displacement vector found from explicit time integration.

Appendix E: Acronyms

ADR: Adaptive Dynamic Relaxation

BB: Bond-Based

CCM: Classical Continuum Mechanics

CNT: Carbon Nanotube

MEMS: Micro-ElectroMechanical System

NEMS: Nano-ElectroMechanical System

OSB: Ordinary State-Based

PD: Peridynamics

PDDO: Peridynamic Differential Operator

PDE: Partial Differential Equation

PDSG: Peridynamics with Strain Gradient

SED: Strain Energy Density

SG: Strain Gradient

SGE: Strain Gradient Elasticity

SWCNT: Single-Walled Carbon Nanotube

TSE: Taylor Series Expansion

BIBLIOGRAPHY

- Aifantis, E. C. (1992). On the role of gradients in the localization of deformation and fracture. *International Journal of Engineering Science*, 30(10), 1279-1299.
- Alibert, J. J., Seppecher, P., & Dell'Isola, F. (2003). Truss modular beams with deformation energy depending on higher displacement gradients. *Mathematics and Mechanics of Solids*, 8(1), 51-73.
- Al-Rub, R. K. A. (2004). *Material length scales in gradient-dependent plasticity/damage and size effects: theory and computation*. Louisiana State University and Agricultural & Mechanical College.
- Al-Rub, R. K. A., & Voyiadjis, G. (2004). Determination of the material intrinsic length scale of gradient plasticity theory. *International Journal for Multiscale Computational Engineering*, 2(3).
- Altan, S. B., & Aifantis, E. C. (1992). On the structure of the mode III crack-tip in gradient elasticity. *Scripta Metallurgica et Materialia*, 26(2), 319-324.
- Askes, H., & Aifantis, E. C. (2002). Numerical modeling of size effects with gradient elasticity-formulation, meshless discretization and examples. *International Journal of Fracture*, 117, 347-358.
- Askes, H., Morata, I., & Aifantis, E. C. (2008). Finite element analysis with staggered gradient elasticity. *Computers & Structures*, 86(11-12), 1266-1279.
- Bazilevs, Y., Behzadinasab, M., & Foster, J. T. (2022). Simulating concrete failure using the Microplane (M7) constitutive model in correspondence-based peridynamics: Validation for classical fracture tests and extension to discrete fracture. *Journal of the Mechanics and Physics of Solids*, 166, 104947.
- Bazant, Z. P. (1999). Size effect on structural strength: a review. *Archive of applied Mechanics*, 69, 703-725.
- Carpenter, N. J., Taylor, R. L., & Katona, M. G. (1991). Lagrange constraints for transient finite element surface contact. *International journal for numerical methods in engineering*, 32(1), 103-128.

- Chan, W., & Chen, H. (2023). Modeling material length-scale effect using the second-order peridynamic material correspondence model. *International Journal of Engineering Science*, 189, 103877.
- Chen, C. Q., Shi, Y., Zhang, Y. S., Zhu, J., & Yan, Y. J. (2006). Size dependence of Young's modulus in ZnO nanowires. *Physical review letters*, 96(7), 075505.
- Chen, H., & Chan, W. (2020). Higher-order peridynamic material correspondence models for elasticity. *Journal of Elasticity*, 142(1), 135-161.
- Damodharan, J. (2021). Nanomaterials in medicine—An overview. *Materials Today: Proceedings*, 37, 383-385.
- Dell'Isola, F., Lekszycki, T., Pawlikowski, M., Grygoruk, R., & Greco, L. (2015). Designing a light fabric metamaterial being highly macroscopically tough under directional extension: first experimental evidence. *Zeitschrift für angewandte Mathematik und Physik*, 66, 3473-3498.
- Deng, S., Liu, J., & Liang, N. (2007). Wedge and twist disclinations in second strain gradient elasticity. *International journal of solids and structures*, 44(11-12), 3646-3665.
- Eringen, A. C. (1972). Linear theory of nonlocal elasticity and dispersion of plane waves. *International Journal of Engineering Science*, 10(5), 425-435.
- Feizi, S., Cooksley, C. M., Nepal, R., Psaltis, A. J., Wormald, P. J., & Vreugde, S. (2022). Silver nanoparticles as a bioadjuvant of antibiotics against biofilm-mediated infections with methicillin-resistant *Staphylococcus aureus* and *Pseudomonas aeruginosa* in chronic rhinosinusitis patients. *Pathology*, 54(4), 453-459.
- Gao, X. L., & Ma, H. (2010). Solution of Eshelby's inclusion problem with a bounded domain and Eshelby's tensor for a spherical inclusion in a finite spherical matrix based on a simplified strain gradient elasticity theory. *Journal of the Mechanics and Physics of Solids*, 58(5), 779-797.

- Gao, X. L., & Park, S. (2007). Variational formulation of a simplified strain gradient elasticity theory and its application to a pressurized thick-walled cylinder problem. *International Journal of Solids and Structures*, *44*(22-23), 7486-7499.
- Georgiadis, H. G., Vardoulakis, I., & Velgaki, E. (2004). Dispersive Rayleigh-wave propagation in microstructured solids characterized by dipolar gradient elasticity. *Journal of Elasticity*, *74*, 17-45.
- Gourgiotis, P. A., & Georgiadis, H. (2009). Plane-strain crack problems in microstructured solids governed by dipolar gradient elasticity. *Journal of the Mechanics and Physics of Solids*, *57*(11), 1898-1920.
- Greer, J. R., & De Hosson, J. T. M. (2011). Plasticity in small-sized metallic systems: Intrinsic versus extrinsic size effect. *Progress in Materials Science*, *56*(6), 654-724.
- Hobbs, M., Dodwell, T., Hattori, G., & Orr, J. (2022). An examination of the size effect in quasi-brittle materials using a bond-based peridynamic model. *Engineering Structures*, *262*, 114207.
- Khakalo, S., & Niiranen, J. (2017). Gradient-elastic stress analysis near cylindrical holes in a plane under bi-axial tension fields. *International Journal of Solids and Structures*, *110*, 351-366.
- Kilic, B., & Madenci, E. (2010). An adaptive dynamic relaxation method for quasi-static simulations using the peridynamic theory. *Theoretical and Applied Fracture Mechanics*, *53*(3), 194-204.
- Lam, D. C., Yang, F., Chong, A. C. M., Wang, J., & Tong, P. (2003). Experiments and theory in strain gradient elasticity. *Journal of the Mechanics and Physics of Solids*, *51*(8), 1477-1508.
- Lazar, M., Maugin, G. A., & Aifantis, E. C. (2006). Dislocations in second strain gradient elasticity. *International Journal of Solids and Structures*, *43*(6), 1787-1817.
- Liebold, C., & Müller, W. H. (2015). Applications of strain gradient theories to the size effect in submicro-structures incl. experimental analysis of elastic material parameters. *Bull. TICMI*, *19*(1), 45-55.

- Liebold, C., & Müller, W. H. (2016). Applications of higher-order continua to size effects in bending: Theory and recent experimental results. *Generalized Continua as Models for Classical and Advanced Materials*, 237-260.
- Limkatanyu, S., Sae-Long, W., Mohammad-Sedighi, H., Rungamornrat, J., Sukontasukkul, P., Imjai, T., & Zhang, H. (2022). Static and free vibration analyses of single-walled carbon nanotube (SWCNT)–substrate medium systems. *Nanomaterials*, 12(10), 1740.
- Liu, M. Q., & Gao, X. L. (2013). Strain gradient solution for the Eshelby-type polygonal inclusion problem. *International Journal of Solids and Structures*, 50(2), 328-338.
- Madenci, E., Oterkus, E., Madenci, E., & Oterkus, E. (2014). Coupling of the peridynamic theory and finite element method. *Peridynamic theory and its applications*, 191-202.
- Madenci, E., Barut, A., & Dorduncu, M. (2019). *Peridynamic differential operator for numerical analysis* (Vol. 10, pp. 978-983). Berlin: Springer International Publishing.
- Madenci, E., Barut, A., & Futch, M. (2016). Peridynamic differential operator and its applications. *Computer Methods in Applied Mechanics and Engineering*, 304, 408-451.
- Madenci, E., Roy, P., & Behera, D. (2022). *Advances in peridynamics* (No. 307395). Berlin: Springer International Publishing.
- Maranganti, R., & Sharma, P. (2007). A novel atomistic approach to determine strain-gradient elasticity constants: Tabulation and comparison for various metals, semiconductors, silica, polymers and the (ir) relevance for nanotechnologies. *Journal of the Mechanics and Physics of Solids*, 55(9), 1823-1852.
- Mindlin, R. D. (1964). Micro-structure in linear elasticity. *Archive for rational mechanics and analysis*, 16, 51-78.
- Mindlin, R. D. (1965). Second gradient of strain and surface-tension in linear elasticity. *International journal of solids and structures*, 1(4), 417-438.

- Mindlin, R. D., & Eshel, N. (1968). On first strain-gradient theories in linear elasticity. *International Journal of Solids and Structures*, 4(1), 109-124.
- Niiranen, J., Khakalo, S., Balabanov, V., & Niemi, A. H. (2016). Variational formulation and isogeometric analysis for fourth-order boundary value problems of gradient-elastic bar and plane strain/stress problems. *Computer Methods in Applied Mechanics and Engineering*, 308, 182-211.
- Polyzos, D., & Fotiadis, D. I. (2012). Derivation of Mindlin's first and second strain gradient elastic theory via simple lattice and continuum models. *International Journal of Solids and Structures*, 49(3-4), 470-480.
- Rahali, Y., Giorgio, I., Ganghoffer, J. F., & Dell'Isola, F. (2015). Homogenization à la Piola produces second gradient continuum models for linear pantographic lattices. *International Journal of Engineering Science*, 97, 148-172.
- Ru, C. Q., & Aifantis, E. (1993). A simple approach to solve boundary-value problems in gradient elasticity. *Acta Mechanica*, 101(1), 59-68.
- Sepecher, P., Alibert, J. J., & Isola, F. D. (2011, September). Linear elastic trusses leading to continua with exotic mechanical interactions. In *Journal of Physics: Conference Series* (Vol. 319, No. 1, p. 012018). IOP Publishing.
- Shan GuoBin, S. G., Yan, S., Tyagi, R. D., Surampalli, R. Y., & Zhang, T. C. (2009). Applications of nanomaterials in environmental science and engineering.
- Shekarchizadeh, N., Abali, B. E., & Bersani, A. M. (2022). A benchmark strain gradient elasticity solution in two-dimensions for verifying computational approaches by means of the finite element method. *Mathematics and Mechanics of Solids*, 27(10), 2218-2238.
- Silling, S. A. (2000). Reformulation of elasticity theory for discontinuities and long-range forces. *Journal of the Mechanics and Physics of Solids*, 48(1), 175-209.

- Silling, S. A., & Askari, E. (2005). A meshfree method based on the peridynamic model of solid mechanics. *Computers & structures*, 83(17-18), 1526-1535.
- Silling, S. A., & Lehoucq, R. B. (2010). Peridynamic theory of solid mechanics. *Advances in applied mechanics*, 44, 73-168.
- Silling, S. A., Epton, M., Weckner, O., Xu, J., & Askari, E. (2007). Peridynamic states and constitutive modeling. *Journal of elasticity*, 88, 151-184.
- Vardoulakis, I., Exadaktylos, G., & Aifantis, E. (1996). Gradient elasticity with surface energy: mode-III crack problem. *International Journal of Solids and Structures*, 33(30), 4531-4559.
- Voyiadjis, G. Z., & Al-Rub, R. K. A. (2005). Gradient plasticity theory with a variable length scale parameter. *International Journal of solids and structures*, 42(14), 3998-4029.
- Wolfram Research, Inc., Mathematica, Version 13.2, Champaign, IL (2022).
- Wu, Y., Markmann, J., & Lilleodden, E. T. (2023). On the consequences of intrinsic and extrinsic size effects on the mechanical response of nanoporous Au. *Materials & Design*, 232, 112175.
- Zhang, X., & Sharma, P. (2005). Inclusions and inhomogeneities in strain gradient elasticity with couple stresses and related problems. *International Journal of Solids and Structures*, 42(13), 3833-3851.
- Zhu, T. T., Bushby, A. J., & Dunstan, D. J. (2008). Materials mechanical size effects: a review. *Materials Technology*, 23(4), 193-209.